HYBRID ELECTRIC REGIONAL AIRCRAFT DESIGN WITH OPTIMAL POWER MANAGEMENT

CONCEPTION D'UN AVION HYBRIDE-ÉLECTRIQUE RÉGIONAL AVEC GESTION DE LA PUISSANCE OPTIMALE

A Thesis Submitted to the Division of Graduate Studies
of the Royal Military College of Canada
by

Stewart J. Reid, B.ASc.

In Partial Fulfillment of the Requirements for the Degree of
Master of Applied Science in Aeronautical Engineering

March, 2022

Acknowledgements

I would like to give my thanks to Dr. Ruben E. Perez, for his tutelage throughout my time at RMC. His patience throughout my undergraduate and graduate theses and his leadership under the uncertainty of the pandemic will not be forgotten. My gratitude is extended also to Dr. Jansen, Ryley, Ankit and all the other members past and present of the lab, whose advice and support was essential to success. Last but not least my family, whose continuous support of my pursuits could never be substituted.

Abstract

Reid, Stewart James. M.A.Sc. Royal Military College of Canada, May 2022. *Hybrid Electric Regional Aircraft Design with Optimal Power Management.* Supervised by Ruben E. Perez, B.Eng., M.A.Sc., Ph.D., P.Eng., Associate Professor.

The aviation industry has continuously improved its efficiency over the last decade with innovations in technology, design and operation. Further improvements are becoming more difficult as current technology reaches maximum maturity and efficiency. Electrification of road vehicles is predicted to completely replace combustion engines in vehicles. As the efficiency and reliability of electric batteries and motors improve, so does the case for electric propulsion systems in aircraft. Jet fuel carries 61 times more energy than batteries for the same weight, making complete replacement of fuel challenging. Hybrid electric propulsion, where both fuel and batteries are used to power propulsion systems could be feasible and improve fuel efficiency. Hybrid electric powertrains use electric power to reduce the power demands from the combustion engine. Electric batteries are discharged and charged during the operation based on when extra power is needed or available.

A unique aircraft design method is proposed that includes optimized power management which determines when and how much battery charge should be used, in both discharge and charge to reduce overall fuel consumption. Regional aircraft typically fly the shortest routes of a commercial airline fleet. These short routes have wider variations in power, which is where hybrid electric powertrains are the most beneficial. The hybrid electric aircraft design method finds that a hybrid electric regional aircraft, at current technology levels, could achieve similar fuel performance to current regional aircraft. This result is in contrast of the current literature, which anticipates significant improvements to battery energy density and electric motor efficiency to achieve similar fuel performance results.

Keywords: aircraft conceptual design, sustainable aviation, hybrid electric propulsion, optimization

Résumé

Reid, Stewart James M.A.Sc. , Mai 2022. *Conception d'un avion hybride-électrique régional avec gestion de la puissance optimale.* Supervisé par Ruben E. Perez, B.Eng., M.A.Sc., Ph.D., P.Eng., Professeur adjoint.

L'indsutrie d'aviation a amélioré le rendement au fil de la décennie avec l'innovation de la technologie, le conception et l'opération. Les améliorations futures deviennent plus difficiles à mesure que la technologie actuelle attient son rendement maximale. On prédit que l'électrification de la voiture va remplacer toutes les voitures à moteurs de combustion. À mesure que le rendement et la fiabilité des batteries et des moteurs électriques s'améliorent, il en va de même pour les systèmes de propulsion électriques dans les avions. Le carburant contient 61 fois plus d'énergie que les batteries pour le même poids, ce qui rend difficile le remplacement complet du carburant. La propulsion électrique hybride, qui utilise le carburant et les batteries pour alimenter les systèmes de propulsion, pourrait être réalisable et améliorer le rendement énergétique. Les groupes de motopropulseurs électriques hybrides utilisent l'énergie électrique pour réduire les demandes de puissance d'un moteur à combustion. Les batteries électriques sont déchargées et chargées pendant le fonctionnement en fonction du moment où une alimentation supplémentaire est nécessaire ou disponible.

Une méthode de conception d'avion unique est proposée qui inclut une gestion optimisée de la puissance qui détermine quand et la combien de charge de la batterie doit être utilisée, à la fois en décharge et en charge pour réduire la consommation totale de carburant. Les avions régionaux empruntent généralement les itinéraires les plus courts d'une flotte de compagnies aériennes commerciales. Ces trajets courts ont des variations de puissance plus importantes, là où les groupes motopropulseurs électriques hybrides sont les plus avantageux. La méthode de conception d'avions hybride-électrique montre qu'un avion régional électrique hybride, aux niveaux technologiques actuels, pourrait atteindre des performances de carburant similaires à celles des avions régionaux actuels. Ce résultat contraste avec la littérature actuelle, qui prévoit des améliorations significatives de la densité d'énergie de la batterie et de l'efficacité du moteur électrique pour obtenir des résultats de performance de carburant similaires.

Mots-clés: conception conceptuelle de l'avion, aviation durable, propulsion hybride-électrique, optimisation

Contents

Acknowledgements ii

Abstract iii

Résumé iv

List of Tables viii

List of Figures ix

Nomenclature xii

1 Introduction 1
- 1.1 Research Objectives . . . 6
- 1.2 Thesis Layout . . . 7
- 1.3 Contributions . . . 8

2 Literature Review 9
- 2.1 Hybrid Electric Powertrain Design . . . 9
- 2.2 Hybrid Electric Aircraft Design . . . 11
- 2.3 Concluding Remarks on the State-of-the-Art . . . 15

3 Propulsion and Hybrid Electric Component Models 16
- 3.1 Conventional Components . . . 16
  - 3.1.1 Turboprop/Turboshaft Engine . . . 17
  - 3.1.2 Variable Pitch Propeller . . . 21
  - 3.1.3 Turboprop Propulsion Model Validation . . . 22
- 3.2 Electrical Components . . . 23
  - 3.2.1 Lithium-Ion Battery . . . 24
    - 3.2.1.1 Battery Data . . . 25
    - 3.2.1.2 Battery Cell Discharge . . . 26
    - 3.2.1.3 Battery Pack Design . . . 27
    - 3.2.1.4 Battery Cell Charge . . . 28
  - 3.2.2 Electric Motor/Generator . . . 28
    - 3.2.2.1 Geometric Model . . . 30

3.2.3 Power Management and Distribution 30

4 Regional Aircraft Design **32**
4.1 Aircraft Configuration Model 32
4.1.1 Hybrid Electric Configuration 33
4.2 Blown-Wing Model 34
4.3 Design Mission Profile 35
4.4 Component Weight Models 36
4.5 Mission and Weight Sizing Method 36
4.6 Weight & Field Length Model Validation 38
4.7 Payload-Range Model Validation 39
4.8 Regional Design Mission Requirements 41

5 Hybrid Electric Mission Performance Analysis **44**
5.1 Power Management Optimization Problem 45
5.2 Power Management Test Cases 48
5.2.1 Single Stop Design Mission 49
5.2.2 Double Stop Design Mission 53

6 Aircraft Design Optimization **57**
6.1 Aircraft Design Variables and Constraints 57
6.2 Nested Hybrid Electric Aircraft Design Problem Formulation . 59
6.3 Next-Gen Turboprop Aircraft 61
6.4 Retro-fit Powertrain Design 65
6.5 Next-Gen Hybrid Electric Aircraft design 67
6.6 Next-Gen Hybrid Electric Aircraft with Generator Redundancy 71
6.7 Results Overview 73
6.8 Weight Sizing in Hybrid Electric Propulsion Design 75
6.9 Results Comparison to Hybrid Electric Design Literature . . . 77

7 Conclusions and Recommendations **79**
7.1 Conclusions 80
7.2 Recommendations for Future Work 80

Bibliography **82**

Appendices **87**

A Additional Component Data **88**
A.1 Propeller Data 88
A.2 Battery Data 88

A.3 Component Weight Equations 88

B Additional Regional Aircraft Model Data **91**
B.1 Feasible Wing & Landing Gear Combinations 91
B.2 In-Service Aircraft Model Data 91
B.3 Regional Aircraft Weight Modelling 93

C Regional Aircraft Design Solution Data **95**
C.1 Retrofit Supplemental Data 95
C.2 Next-Gen Hybrid Electric Aircraft Power Management Data . . 97
C.3 Next-Gen Hybrid Electric Aircraft With Redundant Generators Supplemental Data 99
C.4 Final Results Table 101

List of Tables

4.1 T_{set} settings for standard mission profile. 36
4.2 Turboprop and electric component weight models. Equations requiring multiple lines are included in the Appendix. 37
4.3 Comparison of aircraft model to aircraft specifications. 39

5.1 G_{set} settings for HEAC mission profile. For a single stop mission there are 24 points in total. 47
5.2 Hybrid electric powertrain and mission design parameters for test case. 48
5.3 Comparison of single-stop weight sizing and mission performance . 51
5.4 Comparison of double-stop sizing mission performance 54

6.1 Aircraft design variables 58
6.2 Aircraft design constraints 59
6.3 Next-Gen turboprop aircraft solution 62
6.4 Turboprop aircraft KPI comparison. 63
6.5 Comparison of in-service aircraft and their hybrid electric retrofit equivalents. 66
6.6 Next-Gen HEAC solution 68
6.7 KPI comparison of Next-Gen turboprop and HEAC. 69
6.8 KPI comparison of HEAC with and without redundant generators. 72
6.9 Comparable HEAC design studies 77
6.10 Electric component sizing inputs and HEAC weight ratios 78

A.1 LCO battery details. Prices current as of June 2017. [29] 89

B.1 Feasible wing and landing gear combinations 91

C.1 ATR Retrofit Hybrid Electric Aircraft Solution 95
C.2 Q400 Retrofit Hybrid Electric Aircraft Solution 95
C.3 SAAB 2000 Retrofit Hybrid Electric Aircraft Solution 95
C.4 Next-Gen hybrid electric aircraft solution with generator redundancy 101

List of Figures

1.1 Emissions projections 2
1.2 Hybrid electric powertrain power flow diagram. 5
1.3 Electric propulsion architectures for aircraft [8]. 6

2.1 HEV sales 1999-2019 [12] 10
2.2 Onion plots showing effect of hybridization of power and energy . . 12

3.1 Turboprop propulsion system. 17
3.2 Power hooks for a PW127M-equivalent turboshaft engine. Engine throttle shown from $G_{\text{set}} : [0.5, 1.0]$. 19
3.3 Fuel flow rate for a PW127M-equivalent turboshaft engine. Engine throttle shown from $G_{\text{set}} : [0.5, 1.0]$. 20
3.4 Propeller disk efficiency model. Minimum and maximum disk loading (k) range denoted with dash and dash-dot line respectively [24]. 21
3.5 Thrust Map @ $T_{\text{set}} = 1.0$. 22
3.6 Turboprop thrust and fuel flow model comparison to BADA data [26]. 23
3.7 Hybrid electric propulsion system and powertrain. 24
3.8 LCO battery data at $T = 15$ °C [29]. 25
3.9 C-rate of battery model at different constant power discharges . . 27
3.10 Electric motor model shown for $P_{\text{max}} = 2750\,\text{shp}$ 29

4.1 Conventional turboprop aircraft configuration. 33
4.2 Hybrid electric aircraft configuration. 34
4.3 Standard Mission Profile 35
4.4 Sizing method including design mission performance and weight convergence. Dashed lines denote data-only connectors. 38
4.5 Payload-range diagram with fixed OEW,MTOW,MPLW,MFW to aircraft specification 40
4.6 Payload-range diagram with *pyACDT* weight method 41
4.7 Qantas regional route network daily passenger demand data from 2019. 43

5.1 Positive feedback loop caused by increases in OEW 45
5.2 Optimization history for power management test cases. 49

5.3 Power management solution for an ATR 72 aircraft on a single-stop design mission. 50
5.4 Segment performance comparison of power management solution of the single stop mission to the baseline turboprop aircraft. 52
5.5 Power management solution for an ATR 72 aircraft on a double-stop design mission. 53
5.6 Segment performance comparison of double stop power management solution to the baseline turboprop aircraft. 56

6.1 Nested optimization of HEAC sizing. Dashed line denotes a data-only connector. 60
6.2 Next-Gen turboprop 61
6.3 Comparison of turboprop aircraft by segment for KPI. 64
6.4 Next-Gen HEAC geometry 68
6.5 Comparison of Next-Gen aircraft solutions as a turboprop and hybrid electric propulsion, by segment for key performance metrics. . 70
6.6 Redundant generator geometry in the tail section. Each turboshaft engine has its own electric generator. 71
6.7 Turboshaft weight sizing, specific power included. 73
6.8 Overview of regional aircraft solutions. 74
6.9 Propulsion components weight sizing. 76

A.1 Turboprop inlet blockage correction [25]. 88
A.2 Polynomial fit model. Model extended to $C = 0.01/\text{h}$. 89
A.3 Voltage curve fit for discharge rates at $SOC = 90\%$. Curve fitting using $f(x) = ae^{-\frac{x}{b}+c}$. Used to determine voltage shift for low C-rates. 90
A.4 Voltage at constant power discharge in the battery model 90

B.1 In-service regional turboprop configurations. All dimensions in feet. 92

C.1 ATR 72 retro-fit power management 96
C.2 Q400 retro-fit power management 96
C.3 SAAB retro-fit power management 97
C.4 Comparison of ATR 72 aircraft configuration as a turboprop and hybrid electric propulsion 98
C.5 Comparison of Q400 aircraft configuration as a turboprop and hybrid electric propulsion 99
C.6 Comparison of SAAB 2000 aircraft configuration as a turboprop and hybrid electric propulsion by segment for key performance metrics. 100
C.7 HEAC power management solution 101

C.8 Hybrid electric aircraft with redundant generators geometry. . . . 102
C.9 HEAC-RG power management solution 103
C.10 Comparison of hybrid electric aircraft solutions with and without redundant generators by segment for key performance metrics. . . 104
C.11 Overview of regional aircraft solutions. 105

Nomenclature

$\text{Æ}R$	Aspect Ratio	[-]
b	Span	[ft]
C	Normalized Battery Current / C-rate	[1/hr]
c	Chord	[ft]
C_i	Electric Motor Coefficients $i : 0 : 3$	[-]
D	Diameter	[ft]
D	Drag	[lb]
F_b	Blockage Correction Factor	[-]
g	Generalized Constraint	
H	Hybridization	[-]
h	Altitude	[ft]
I	Current	[A]
J	Advance Ratio	[-]
k	Propeller Disk Loading	[shp/(slug ft)]
L	Electric Motor Length	[in]
M	Mach Number	[-]
P	Power	[shp]
Q	Torque	[ft-lb]
R	Mission Range	[nmi]
T	Temperature	[°C]
T	Thrust	[lb]

t	Time	[hr]
V	Velocity	[kts]
V	Voltage	[V]
W	Weight	[lb]

Subscripts

a	Available
bl	Blown Wing Area
cell	Battery cell
clean	Clean wing without blown effects.
climb	Climb operation attribute
cruise	Cruise operation attribute
des	Sizing Design Variable
E	Energy
eng	Engine Speed
f	Fuel
h	at Altitude, h
ht	Horizontal Tail
ia	Engine Incidence Angle
i	Initial Value/Guess
in	Inner Wing segment
L	Motor Losses
main	Main Mission Phase
max	Maximum Variable Value
m	Battery Pack Parallel Dimension
n	Battery pack series dimension

nom	Nominal rating
ops	Operation Design Variable
out	Outer Wing Segment
pack	Battery Pack
pay	Payload
P	Power
prop	Propeller Speed
r	Root of Lifting Surface
set	Thrust or Power setting in the propulsion or generator system.
ta	Engine Toe–in Angle
t	Thickness to Chord ratio of Lifting Surface
vt	Vertical Tail
w	Wing
x	Design Variable
x	Longitude coordinate
y	Latitude coordinate
z	Elevation coordinate

Greek Symbols

α	Angle of Attack	[°]
η	Efficiency	[-]
Γ	Dihedral	[°]
Λ	Sweep	[°]
λ	Taper Ratio	[-]
λ_j	Aspect Ratio of propeller flow for j^{th} propeller	[-]
ω	Rotational Speed	[min^{-1}]

ρ	Air Density	[slug/ft^3]
σ	Air Density Ratio	[-]
θ	Air Temperature Ratio	[-]

Dimensionless Groups

C_D	Drag Coefficient
C_i	Electric Motor Map Parameters $i : \{0, 3\}$
C_L	Lift Coefficient
C_l	Roll Moment Coefficient
C_n	Yaw Moment Coefficient

Acronyms

pyACDT	Aircraft Design Tool in Python	
ATR	Avions de transport régional	
BSFC	Brake Specific Fuel Consumption	[lb/(shp×hr)]
CORSIA	Carbon Ofssetting and Reduction Scheme for International Aviation	
DFW	Design Fuel Weight	[lb]
DHC	DeHavilland Canada	
DOC	Direct Operating Costs	
DOD	Depth of Discharge	[-]
FDPSO	Feasible Directions Particle Swarm Optimizer	
FF	Fuel Flow	[lb/hr]
FL	Flight Level	[100ft]
FR	Ferry Range	[nmi]
HEAC	Hybrid Electric Aircraft (sky)	
HEP	Hybrid Electric Powertrain	

HEV	Hybrid Electric Vehicle (road)	
IATA	International Air Transport Association	
ICAO	International Civil Aviation Organization	
ICE	Internal Combustion Engine	
IPCC	Iternational Panel on Climate Change	
LE	Leading Edge	
MAC	Mean Aerodynamic Chord	[-]
MFPR	Maximum Fuel-Payload Range	[nmi]
MFW	Maximum Fuel Weight	[lb]
MLG	Main Landing Gear Configuration	[-]
MTOW	Maximum Takeoff Weight	[lb]
MZFW	Maximum Zero Fuel Weight	[lb]
NG	Next-Generation / Clean Sheet Design	
OEW	Operational Empty Weight	[lb]
OML	Outer Mold Line	
pmf	Battery Pack Mass Factor	[-]
PRE	Payload Range Efficiency	[nmi×lb/lb]
RG	Redundant Generators	
RPK	Revenue Passenger Kilometres	
SAAB	Svenska Aeroplan AB	
SAF	Sustainable Aviation Fuel	
SL	Sea Level	
SOA	State of the Art	
SOC	State of Charge	[-]
ssl	Static Sea Level conditions	

STOL Short Take-off and Landing

TAS True Airspeed

TLR Technology Level Readiness

TOW Takeoff Weight ..... [lb]

TP Turboprop

TSFC Thrust Specific Fuel Consumption ..... [lb/(lb×hr)]

UNFCCC UNited Nations Convention on Climate Change

VTOL Vertical Take-off and Landing

1 Introduction

In pursuit of mitigating the effects of increasing global temperatures, the United Nations Framework Convention on Climate Change (UNFCCC) set a goal of limiting the global average temperature rise to 1.5°C at the Paris Climate Accords in 2015. To achieve this goal, the Intergovernmental Panel on Climate Change (IPCC) released a report from their 2018 conference assessing that emissions would have to reduce by 45% by 2030 and "net zero" by 2050 [1].

Aviation emissions have been consistently around 2% of global emissions over the last decade as revenue passenger kilometres (RPKs) doubled from 2006 to 2019 [2]. The business model of airlines has necessitated reducing fuel burn and emissions to reduce direct operating costs (DOC). Fuel efficiency in commercial aviation has increased by 54% from 1990 to 2019 and by 22.8% from 2009 to 2019 [3]. These efficiency gains have originated from both technology and operational factors. Inherently as engineering systems improve in performance efficiency, future performance gains require incrementally larger engineering investments to deliver gains. Over the last decade, aviation fuel efficiency has improved by 2.1% per year, meeting the goals set out by the the International Civil Aviation Organization (ICAO), a UN specialized agency, and the International Air Transport Association (IATA), a trade organization of airlines, who set goals of 2% and 1.5% respectively [2, 4].

Beyond 2020, ICAO has set the goal of limiting emissions to 2005 levels (called carbon-neutral growth), while IATA has set the goal of reducing emissions to 50% of the 2005 level. Both organizations agree that current efficiency improvement forecasts, based on aircraft replacement and operational changes, will soon reduce the rate of efficiency improvement to below 1.5% per year. The loss in efficiency improvement rate and strong expectations for RPKs to compound by 4.5–4.8% per year suggests that current technology will not achieve the aviation industry's climate goals of at least carbon-neutral growth by 2050. Figure 1.1a projects the timing and emissions effects of different factors set out in the IATA Roadmap to 2050 plan. The plan is reliant on sustainable aviation fuel (SAF) and radical technology to implement reductions from 2005 levels. Similarly the ICAO projection is shown in Figure 1.1b shows

the reliance on SAF as and Carbon Offsetting and Reduction Scheme for International Aviation (CORSIA), a carbon emissions market to offset emissions from international flights with investment into carbon reduction projects.

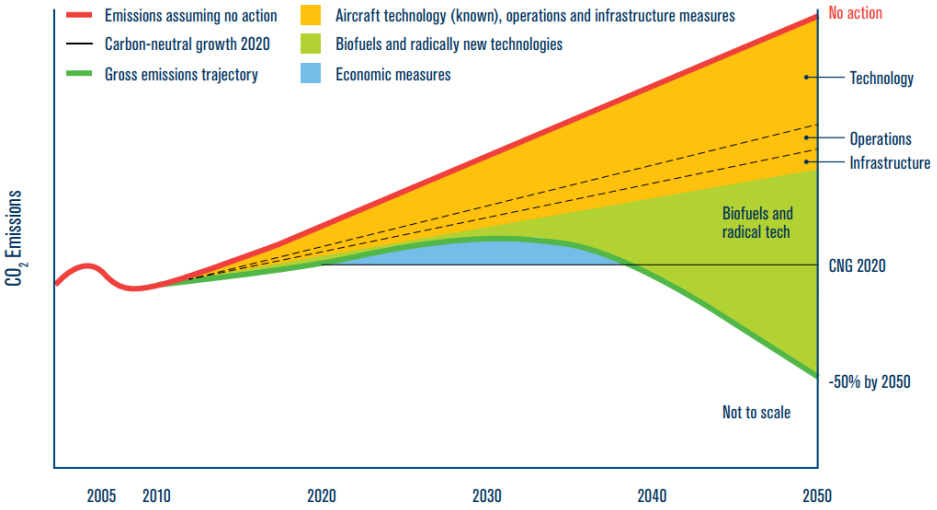

(a) IATA [2]

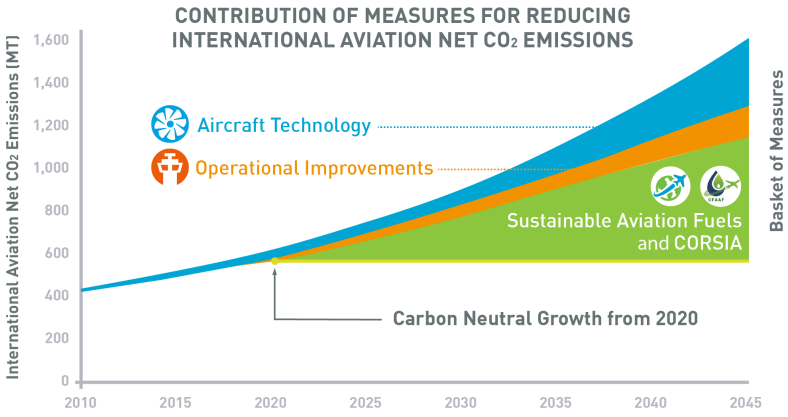

(b) ICAO [4]

Figure 1.1: Emissions projections

IATA has suggested two categories of technologies for future market consideration: evolutionary and revolutionary technologies. Evolutionary technologies, which are expected to be implemented before 2030 include Laminar Flow Control devices and Ultra High Bypass Turbofans. Revolutionary technologies are further classified into novel airframe configurations, revolutionary materials

and structures and revolutionary propulsion architectures [2]. While the first generation of revolutionary technologies are expected to have low efficiency improvements over evolutionary concepts, they are expected to have greater potential efficiency.

Among the revolutionary technologies proposed, electrification of aircraft propulsion appears to have the following system benefits:

- Feasibility of implementation into current aircraft design conventions and airport infrastructure.
- Potential to reduce maintenance costs (using lower maintenance electric motors).
- Technology Level Readiness (TLR) and research and development synergies with other transportation sectors (electric and hybrid electric in road vehicles and rail).
- Integration with conventional aero-propulsive systems and minimal changes to flight handling and envelope.
- Short range efficiency leading to route network operational efficiencies.

Electrification of aircraft is already occurring, with More Electric Aircraft (MEA) and All Electric Aircraft (AEA) reducing or replacing hydraulic and pneumatic driven flight-critical equipment with electric alternatives. Bleed-air and mechanical power extraction of the engine core is replaced by a single gearbox and alternator. This change allows significant reductions in secondary power loads on propulsive engines and in turn higher propulsive efficiencies. MEA concepts are in use on the Boeing 787 and Airbus A380 aircraft to improve fuel efficiency [5].

To date, development of aircraft propulsion electrification has occurred on general aviation airframes, the commercial market for these aircraft and any market growth due to electrification remains small. Regional aircraft appear to be a suitable platform for the first generation of electric aircraft propulsion for commercial viability and potential to improve market growth. Regional aircraft typically fly domestic routes, the emissions of which are excluded from CORSIA but included in many national carbon pricing schemes, including in Canada and the European Union. The profitability of these regional operations is typically low and will face significant economic pressure with the added costs of carbon pricing. These routes are however a vital transportation method of people and goods for remote communities, this is especially true in Canada's north [6].

Regional aircraft typically fly short ranges at subsonic speeds utilizing turboprop engines, that is: a turboshaft engine connected to a propeller via reduction gearbox. The turboprop engines for regional aircraft are sized based on maximum power requirements at the top of climb and short takeoff and landing (STOL) performance. Cruise power requirements for regional turboprop aircraft are significantly less than the maximum power requirements of climb and STOL. A hybrid-electric powertrain has the potential of fulfilling the maximum power requirements with less power generation by utilizing the reversibility of energy in electrochemical batteries. A regional aircraft with an optimally designed powertrain and mission could achieve superior fuel performance compared to a regional turboprop aircraft.

Hybrid electric powertrains (HEP) can be classified into architectures based on their connections between power inputs (generator), outputs (engine), and irreversible (fuel) and reversible (battery) energy stores. Internal Combustion Engines (ICE) can output power, while electric motors can both input and output power. Figure 1.2 shows the possible routings of energy and power to meet a load requirement in a hybrid electric powertrain. Figure 1.3 shows six generalized architectures considered for electric propulsion in aviation, adopted from common architectures in electric and hybrid electric vehicles (HEV). The key differences between HEV and hybrid electric aircraft will be the lack of mechanical clutching and limited to no regenerative braking in aircraft. These abilities are key to the architectures and performance in HEV. The following will introduce the reader to the architectures and qualitatively assess the benefits and drawbacks of each.

Hybrid electric architectures can be divided into three groups: parallel, turboelectric and series hybrid electric. Parallel architectures place both an electric motor and an ICE onto the propulsor shaft, akin to a MEA. The difference between parallel architectures and MEA is the expectation that at some point during operation the electric motor produces power to the shaft, boosting or replacing the ICE output to maximize efficiency. The ICE has to be designed for two, sometimes competing, objectives of mechanical and propulsive efficiency. As well, hybrid electric powertrains require integration of larger electric motors into propulsive ICE than typical of MEA, increasing the propulsion system complexity. This complexity may limit the design space and hybridization of power (hybridization of power being the proportion of the power load being fulfilled by an electric motor).

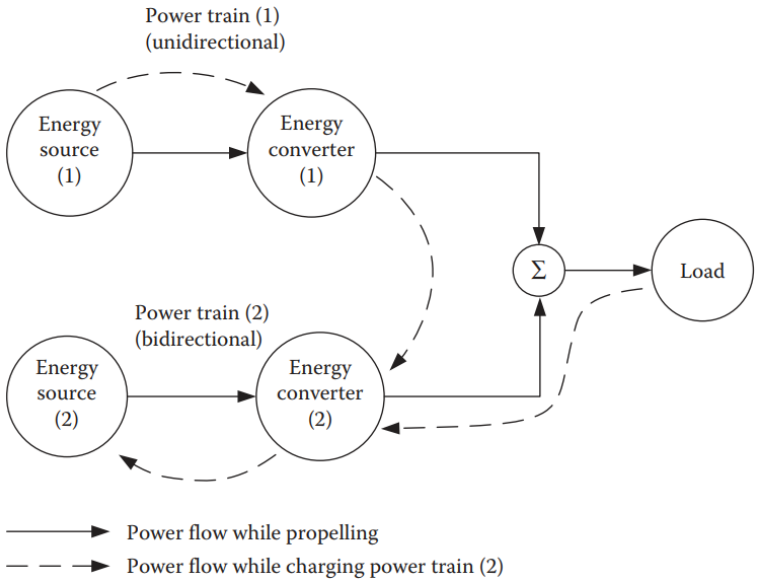

Figure 1.2: Hybrid electric powertrain power flow diagram. Energy source (1) is irreversible, akin to fuel and energy source (2) is reversible, akin to a battery [7].

The turboelectric architecture uses an ICE that produces excess power which is converted to electricity via a generator and transferred to other propulsive units with electric motor outputs. Partial turboelectric architecture uses the ICE as both a propulsor and power output (similar to parallel hybrid electric). Turboelectric architectures uses only fuel as an energy source and thus do not include the reversibility of electrical energy.

The series architecture uses an ICE and electric generator to produce power for propulsive units with electric motors, similar to a turboelectric. Electric energy produced by the generator can be stored in a battery. Series architecture allows for the instantaneous power demands of the propulsors to be partially decoupled from the energy generation. Series architecture uses electric motors and ICE as single purpose units (either mechanical or propulsive power) and remove the requirement for the ICE location to be determined by its aero-propulsive considerations. This research has chosen to focus on the series architecture due to the wide operating modes, propulsive layouts possible and wide hybridization of power possible with this architecture.

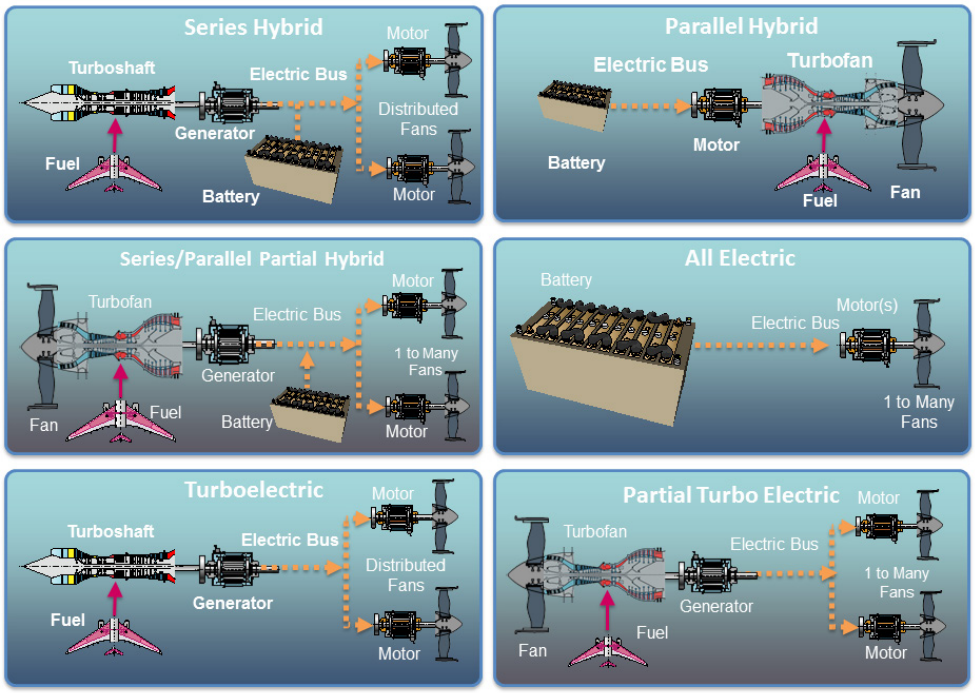

Figure 1.3: Electric propulsion architectures for aircraft [8].

1.1 Research Objectives

The main objective of this research is to implement an aircraft sizing method to regional hybrid electric aircraft. The sizing method will combine the aircraft aerostructure, propulsion and design mission sizing. The aircraft sizing will also identify the optimal power management to reduce fuel weight sizing. The following modelling and optimization objectives will be addressed to investigate the regional hybrid electric aircraft design problem:

- Develop a regional turboprop aircraft configuration model within the *pyACDT* codebase [9]. The aircraft model will be consistent with transport regulations and conventional design practices. This model must match within reason the performance of in-service aircraft configurations.

- Build the following electric component models for performance, geometry and weight, within the *pyACDT* codebase:
  - Electric motors/generators.
  - Battery packs.
  - Associated management and distributions systems.
- Develop a mission power management model for hybrid electric powertrains.
- Develop a coupled aircraft and mission sizing optimization for clean hybrid-electric aircraft.

1.2 Thesis Layout

The next chapters of this dissertation is organized as follows. Chapter 2 reviews previous work on hybrid electric powertrains in road vehicles and aircraft. Chapters 3 to 5 develop the design and performance models, sizing and optimization methods for hybrid electric aircraft analysis. The development of these models start from the smallest to largest system, with each chapter building upon the systems introduced previously. Chapter 3 presents the methods used in this research to model propulsion systems and hybrid electric powertrain components, how they are combined and validated. Chapter 4 introduces the current conventions used in regional turboprop aircraft design and conventional design mission sizing. Chapter 5 presents how hybrid electric aircraft mission performance is assessed using the energy reversibility of batteries. An optimization method is shown using the hybrid electric mission analysis method to minimize fuel consumption in the mission sizing. Chapter 6 culminates the build-up of all the previously introduced sub-systems into aircraft design optimization. The component and aircraft models are optimally designed using the mission sizing and optimization models. The results maximize the aircraft efficiency considering optimal design and power management. Chapter 7 presents the conclusions from this System of systems design investigation and contains future recommendations for further research into this topic.

1.3 Contributions

The contributions in this study include:

- A propulsion system analysis using hybrid electric or conventional turboprop components.
- A regional turboprop aircraft configuration using either hybrid electric or turboprop propulsion systems.
- An optimization method for power management of hybrid electric missions.
- A novel approach to hybrid electric aircraft sizing, using optimized power management.
- An analysis of hybrid electric aircraft, comparing their performance to current regional turboprop aircraft and the performance of new turboprop aircraft.

2 Literature Review

Aircraft conceptual design studies are inherently multidisciplinary due to the dependencies between the many aircraft systems. Performance analysis methods of aircraft further increases the complexity of the aircraft analysis by including many possible objectives, missions sizes and regulatory operational requirements. This chapter does not review literature for all the systems and disciplines present and is limited to the two key considerations in this design study. The first section covers hybrid powertrain literature from sources in the aviation and automotive fields. The second section covers regional aircraft design. The third section covers literature that includes both of these systems as hybrid electric aircraft design studies.

2.1 Hybrid Electric Powertrain Design

Hybrid electric powertrain (HEP) development outside of the aerospace industry has been ongoing in the automotive sector for some time. The technology was first proposed to combat rising oil prices in the 1970's [10]. Starting in the 2000's hybrid electric vehicles (HEV) have been in series production (see Figure 2.1). The HEV can exist in many more architectures than in a hybrid electric aircraft (HEAC). HEV typically are in a partial series/parallel architecture, which are known as complex architectures [11]. The mechanical power output of an ICE and HEV load are significantly lower, allowing for one or multiple clutches and planetary gears to provide more power modes. Furthermore ICE can be shut down and restarted using battery power with ease. In an aircraft where the conventional engine is a turboshaft, frequent clutching on the order of 1 000 shp and easy restarting are not possible and/or economical due to the weight and maintenance requirements of these systems.

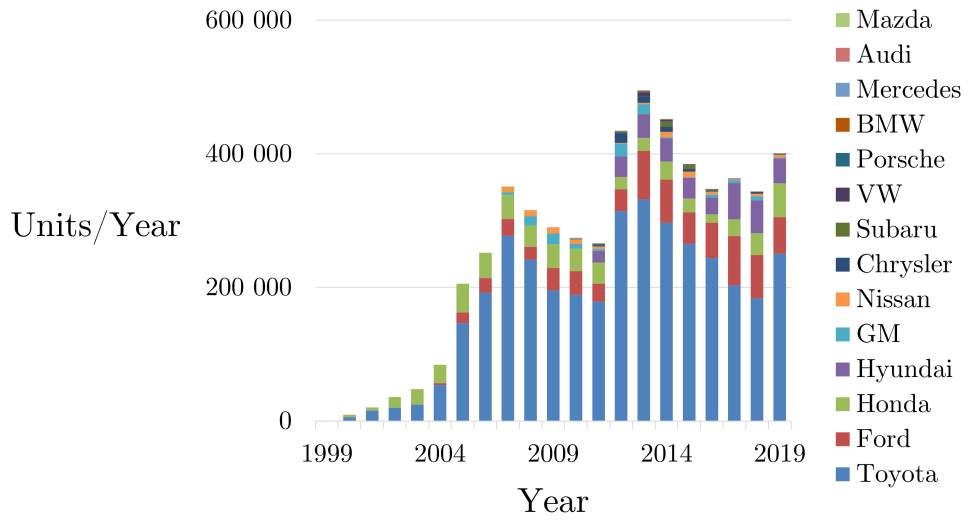

Figure 2.1: HEV sales 1999-2019 [12]

More recent efforts in HEV design have addressed the problem of plant and control optimization. The HEP can change in architecture and sizing of components. The control optimization can be configured to focus on switching of power modes dependent on the architecture and the power split between energy sources. HEV are tested using design cases which are statistical representations of typical loading conditions of automobiles. Compared to aircraft load cases, automobile load cases require significant variation in acceleration and deceleration. The optimal control strategy has to consider power output and power input to the HEP by harvesting energy from regenerative braking. In contrast HEAC are not expected to have any significant or reliable energy harvesting capabilities to be certifiable to aircraft industry standards. HEV powertrain design is typically limited to architecture and/or gearing design with a fixed ICE, electric motor and battery pack sizes [13].

While HEP have shown potential in their applications to cars and will continue to develop, the fully electric car market has outgrown the HEV. Primarily, the wide variation in driving power requirements and little to no ability to predict future power requirements in HEV driving missions provide low fuel efficiency gains over ICE alternatives. Additionally, most driving mission ranges and vehicle weights are within the capabilities of electric battery energy and power respectively.

Alternatively, aircraft follow predictable mission profiles with predictable power requirements. This predictability may lead to a more optimized HEP design and operation, producing worthwhile fuel efficiency improvements over ICE alternatives. Aircraft performance is, however much more weight-sensitive than vehicles. Increases in aircraft weight requires more aerodynamic lift for an aircraft to stay aloft and as a byproduct of increased lift, induced drag. To maintain airspeed, thrust has to be equal to drag, so when aircraft weight increases, thrust requirements increase in-turn. Thrust requirements increasing over the mission result in higher fuel consumption over the mission, requiring more fuel weight. The feedback effect of aircraft weight resulting in aircraft fuel weight leads to the minimization of weight of all components in aircraft design to reduce overall fuel consumption.

2.2 Hybrid Electric Aircraft Design

Aircraft design studies take many forms, with a wide ranging list of valid assumptions to choose from. As such it is uncommon for two aircraft design studies to have a mirrored approach. With some exceptions, this review of hybrid electric aircraft (HEAC) studies is limited to studies where independent variables from two of the following are included:

- Hybrid electric powertrain (HEP);
- Aircraft aerodynamic surfaces/outer mould line (OML);
- Aircraft design mission; and
- Power scheduling .

The work published by Bauhaus-Luftfahrt from 2015-2018 was developing HEAC models for a 180 seat transport aircraft using parallel HEP. Early work aimed to modify sizing methodologies and figures of merit for development to combine the fuel and electric energy source [14]. In HEP design, hybridization of power and energy (H_P and H_E) are commonly used metrics which define the split of power and energy between electric and conventional systems. Hybridization can be defined as used in the mission or the nominal capacity as the system is designed. This study [14] used fixed H_P settings for cruise and climb flight segments and designed battery and fuel weights to converge accordingly. Results showed a potential of a 9-13% reduction in block fuel while adding 5100-8400kg of batteries and 3.5-6 MW of electric motor power. Technology assumptions in this work included high-temperature superconducting motors at 20kW/kg and 1-1.5kW/kg batteries.

Work by Isikveren *et al.* [15] introduced an activation ratio (ϕ): the power control ratio of the two energy sources. The activation ratio is determined by algebraic solutions of the weight sizing based on energy and power densities and associated hybridization ratios for the mission. The onion plot shown in Figure 2.2 stated that low H_P and H_E produce improvements in air range (area fenced above with dashed line).

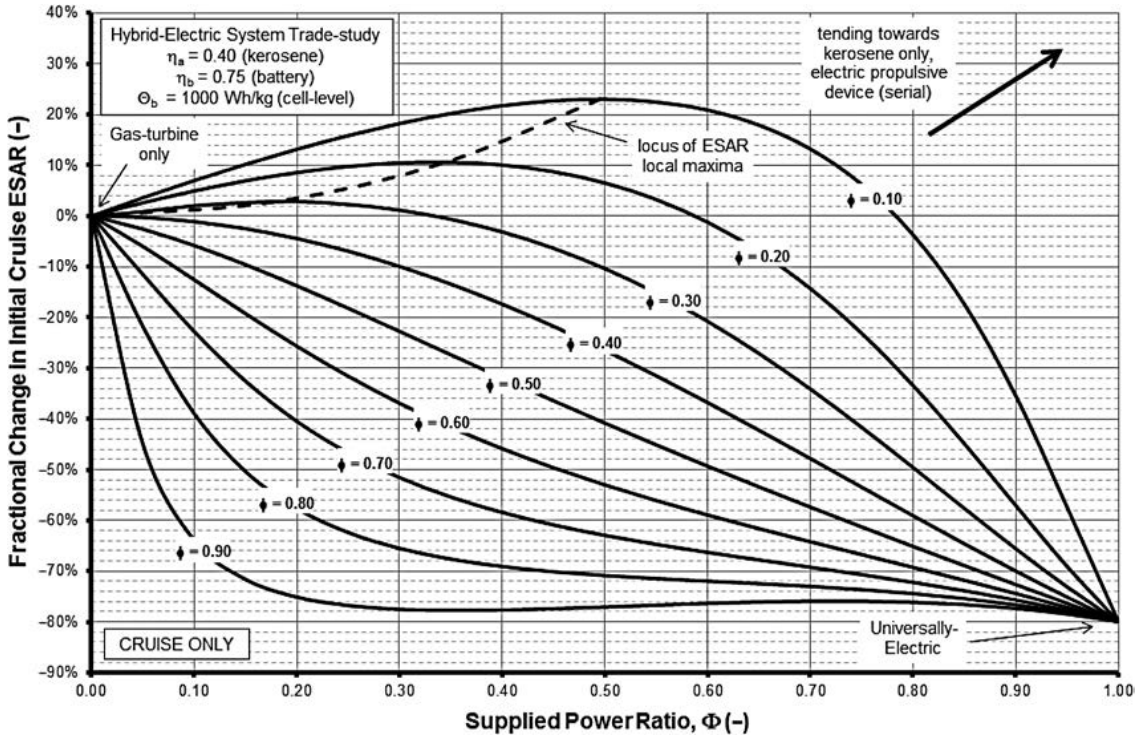

Figure 2.2: Onion plots showing effect of hybridization of power and energy ($H_P < 50\%$ and $H_E < 30\%$) shown in the contours and x-axis respectively. Y-axis denotes the change in energy specific air range (ESAR) vs. baseline [15].

Later work by Pornet *et al.* [16] introduced throttle dependent thrust specific fuel consumption ($TSFC$, with dimensions of fuel flow rate per unit of thrust) from *GasTurb* [17] which increased the fidelity of mission analysis for the variations in $TSFC$ with throttle (up to 34% at a single altitude and Mach flight condition). A new figure of merit was used to combine the operational costs differences between energy sources, cost specific air range (COSAR), measures

the cost per nautical mile of the design. This concept had independent combustion and electric propulsors (summing to 4 pylon-mounted fans) and wing and horizontal tail span extensions dependent on H_P.

The work by Isikveren and Pornet showed the potential for HEAC to improve fuel efficiency with low hybridization requirements. This shows promise for electric batteries which supply much lower power than turboshafts and store energy at a much lower density than jet fuel.

Finger [18] investigated aircraft sizing methodologies for HEAC in two architectures (parallel and series) and aircraft in four platforms (general aviation, unmanned surveillance, VTOL and STOL) and compared them to the baseline conventional powertrain performance. The performance methodology was based on a peak power shaving approach to electric sizing. Peak power shaving combines the power output of the conventional and electric systems when power requirements are at their maximum, typically at takeoff and the top of climb. Peak power shaving reduces the sizing of the conventional components by reducing their maximum power requirements, at the cost of adding electrical components. For each platform and architecture, four optimization objectives were compared (Maximum takeoff weight, primary energy/fuel, operational and production cost). Optimization was performed varying power loading (P/W), wing loading (W/S) and H_P, with H_E being determined explicitly using the other parameters and a fixed design mission. Optimal results for the STOL aircraft show that for both series and parallel architectures achieve small reductions in P/W and large increases in W/S for all objective scenarios with respect to the conventional solution. H_E in any scenario or architecture was $< 7.7\%$.

The HEP considered a fixed power management plan over the mission with no charging capability. While this plan allows for a closed formulation of energy sizing providing all design evaluations with feasible power management it also means that batteries provide only a secondary fuel source at a lower specific energy which, considering the strong performance penalties of weight, is unlikely to provide a better-than-alternatives solution. The aircraft OML was fixed in all platforms, meaning that the design optimization was a retro-fit rather than a clean sheet, leading to increases in wing-loading and in turn, drag. Gains in energy efficiency from peak power shaving would be lost to reductions in aerodynamic performance. Furthermore while more complex turboshaft and electric motor efficiency models were represented, in the optimal sizing loop, they were simplified to fixed efficiencies. This meant that the

power shaving strategy did not account for the increased fuel consumption at high throttle settings. The results show how sub-system component performance and weight are combined and applied to aircraft propulsion systems but did not use sufficient variability in design or planning to attain maximum utility from these components.

Work by Zamboni [19] developed methodologies for sizing regional HEAC with distributed propulsion systems and tip-mounted propellers. Distributed propulsion systems use many propulsors to blow a significant portion of the wing in the aim to improve C_L, allowing for reduced wing chord which then increases aspect ratio (which then leads to improved aerodynamic efficiency). Distributed propulsion is also claimed to have several system benefits including: more favourable weight distribution and allowance for thrust-based control, reducing the size of tail control surfaces. Tip-mounted propellers are expected to reduce the intensity of wing-tip vortices. Electric motors are stated since the enabler of this new aero-propulsive method as they have higher specific power than ICEs. Using an ATR 72-600 as a reference aircraft, parallel architecture are investigated with two propulsors each with a turboshaft and electric motor. A distributed parallel/series architecture uses two turboshafts with electric motors as propulsors and generators for a distributed set of propulsors driven by electric motors. Parameter sweeps of the architectures was shown for H_E in both climb and cruise. Results showed fuel mass improvement is more sensitive to H_E in climb compared to cruise. Results also showed that there is a break-even level of H_E in both climb and cruise. Generally if H_E is below 30% in either climb or cruise then the fuel mass increases. Designs for each architecture increase MTOW between 11-25% with batteries taking up to 17% of MTOW. Three level of technologies were assessed, a conservative, optimistic and futuristic scenarios for batteries, electric motors and distribution systems. The most conservative scenario assumes a battery specific energy of 500Wh/kg. Furthermore sizing electrical energy based on constant H_E for mission segments does not allow for effective use of the battery based on the thrust lapse and fuel consumption changes of turboprop engines with altitude. A low H_E in a segment leads to large batteries since they are drained slowly for a long time.

Some HEAC studies have considered optimal control of an aircraft with a HEP [20, 21]; these often are done on a fixed aircraft OML and fixed powertrain design. Nakka [22] implemented direct transcription method to co-design the plant and control of a series HEP on an MQ-9 Reaper. Control variables were the stator outlet temperature, electric motor and turboshaft power out-

puts and aircraft C_L. System design variables included: battery pack dimensions, electric motor design dimensions, current limits of the electric motors and generators, turboshaft pressure ratio and stator outlet temperature limit. State variables for the optimal control were altitude, velocity, flight path angle, battery state of charge (SOC), fuel and total mass. Optimal control results showed a steep discharge of the battery through climb with a charge in the early portion of the cruise segment and discharging to the minimum SOC through descent. This power management scheme and HEP design is physically intuitive and practical, however there is no performance comparison to the baseline MQ-9 aircraft.

2.3 Concluding Remarks on the State-of-the-Art

There are significant regulatory and integration hurdles with HEP's in aircraft propulsion, but before those issues can be explored, conceptual design studies need to find if a performance benefit exists that is worth pursuing, so that there is motivation for solving the regulation and integration problems. With the exception of the work by Nakka, aircraft design studies to date have not achieved the level of component performance detail and power management in design methodologies implemented by the automotive research community for HEV, which are a more mature technology, product and market. These methodologies seek significantly more variability in design and operation modelling than is typically included in conceptual aircraft design, where only the very top-level requirements and inputs are considered. Additionally, technology weight, energy, power and efficiency must all be evident in technology available at the time of concept. Aircraft certification is incredibly averse to unproven and new (to the industry) technologies.

Finally, a design roadmap to technology maturity of HEP in aircraft must consider the performance envelope of mature propulsion technology. If the performance improvement potential of current technology and hybrid electric technology are similar, much more significant incentives are required to encourage adoption.

3 Propulsion and Hybrid Electric Component Models

This chapter focuses on the power, efficiency and capacity modelling of components specific to turboprop and electric propulsion aircraft. The performance models presented have operational dependence, as opposed to simpler models with fixed efficiencies. Operational dependence leads to improved performance estimations and the capability to design components and operations in unison for better overall optimality. Weight models for these components is discussed in Section 4.4, since it they are more pertinent to configuration management than operational performance. These propulsion and powertrain models are additions to the array of aircraft sub-system models already included in the aircraft design analysis toolbox, *pyACDT* [9].

When modelling propulsion components and especially electric components, estimations on the performance of state-of-the-art (SOA) technology is a critical assumption. If component performance considers hypothetical future technology levels, aircraft design results will be harder to validate and limited by the conditional performance of the components used. The parametric performance models used here are validated against available data sources or embed performance data into their regressions, wherever possible.

3.1 Conventional Components

Both conventional turboprop and HEAC require independent propeller and engine models. These allows engines to be configured as either turboshaft power generators (to be combined with an electric generator/motor) or as turboprop engines (to be combined with a reduction gearbox and propeller). This interchangeability of models extends to the propeller model as well, so as to be independent of power sources. Engine and propeller models also have to be capable of continuous scalability for a wide range of design and operational possibilities. The desire for continuous scalability and computational efficiency leads to parametric models.

Figure 3.1 shows the organization of propulsion sub-systems and the flow of power between sub-systems. The inputs of the weight and efficiency models for each sub-system are defined below each block. The inputs are defined as either design or operational inputs (referred to as x_{des} and x_{ops} respectively). The turboshaft sub-system includes a reduction gearbox. The output power and rotational speed of the turboshaft sub-system is defined at the output of the gearbox. Validation of the turboprop model occurs at a propulsion system level, as publicly available performance data of propulsion sub-systems are not available. Fuel systems are modelled as lossless systems with weight dependent on the aircraft design (des) and sizing methods (x_{ops}).

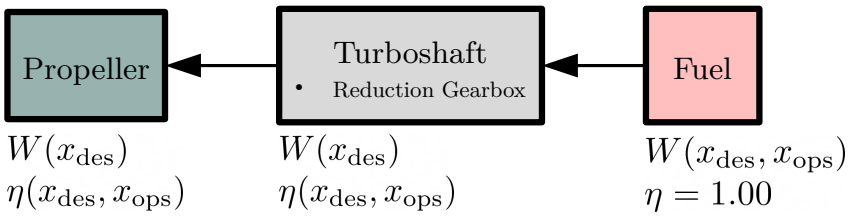

Figure 3.1: Turboprop propulsion system.

3.1.1 Turboprop/Turboshaft Engine

The following model is implemented for turboshaft engines to estimate fuel consumption of the engine and its dependence on operation including throttle setting and atmospheric conditions using the turboprop engine model from Mattingly [23]. Equations 3.1 and 3.2 show the parametric engine power and brake specific fuel consumption (BSFC) models considering altitude and Mach conditions. Equation 3.3 shows the turboshaft throttle setting (G_{set}) correction of BSFC. Equation 3.5 shows the same throttle setting (T_{set}) correction for turboprop engines which corrects TSFC.

$$P_h = P_{\text{ssl}} \left(k_0 \sigma^{k_1} - k_2\right) M^{k_3} \tag{3.1}$$

$$\text{BSFC}_h = \left(c_0 + c_1 M\right) \theta^{c_2} \tag{3.2}$$

$$\text{BSFC}_{h,\text{set}} = \text{BSFC}_h \left[\frac{0.1}{G_{\text{set}}} + \frac{0.24}{G_{\text{set}}^{0.8}} + 0.66 G_{\text{set}}^{0.8} + \left(0.1 M \left(\frac{1}{G_{\text{set}}} - G_{\text{set}}\right)\right)\right] \tag{3.3}$$

$$\text{TSFC}_h = \frac{\text{BSFC}_h P_h}{T} \tag{3.4}$$

$$\text{TSFC}_{h,\text{set}} = \text{TSFC}_h \left[\frac{0.1}{T_{\text{set}}} + \frac{0.24}{T_{\text{set}}^{0.8}} + 0.66 T_{\text{set}}^{0.8} + \left(0.1 M \left(\frac{1}{T_{\text{set}}} - T_{\text{set}}\right)\right)\right] \tag{3.5}$$

The resulting performance model in Figure 3.2 for a PW127M at FL150 for a range of Mach numbers is showing the parametric sweeps of altitude and Mach. Lines denote the G_{set} effect on power and fuel consumption based on the Equation 3.3 as well as the G_{set} at which minimum BSFC is achieved. Figure 3.3 shows the same data as fuel flow rate for the same sweeps in operational conditions.

The contrasts between the BSFC and fuel flow plots, especially altitude dependence, show the need to consider the opportunity costs of power generation in a turboshaft engine. Increasing altitude lowers both BSFC and available power, batteries maybe able to both boost higher altitude power available and transfer the excess power capacity from low to high altitudes. Alternatively batteries maybe used at low altitudes where BSFC is higher and then re-charged at higher altitudes where BSFC is lower. All of these potential strategies are dependent on the power requirements of the mission, which are primarily defined by the weight and mission profile of the aircraft.

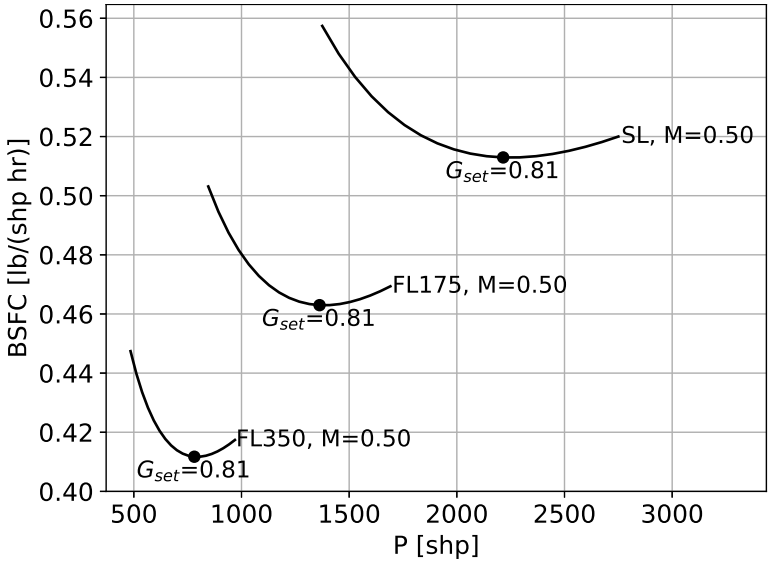

(a) Altitude dependence

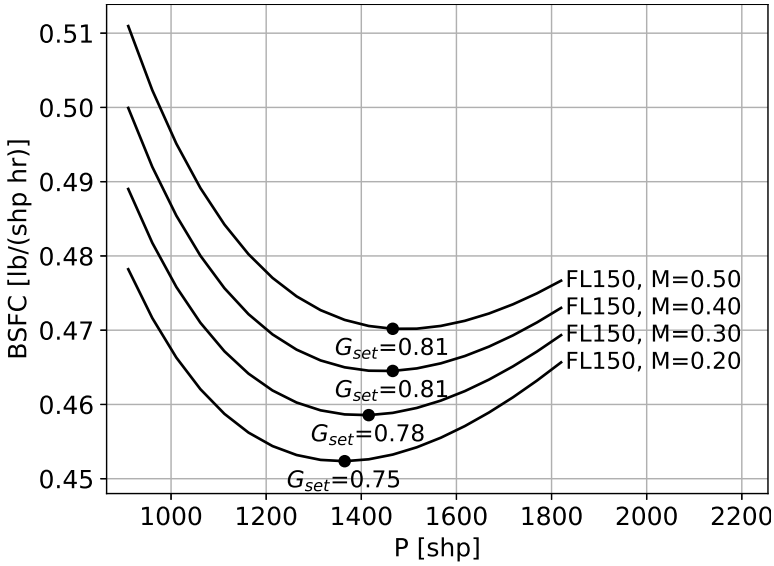

(b) Mach dependence

Figure 3.2: Power hooks for a PW127M-equivalent turboshaft engine. Engine throttle shown from $G_{\text{set}} : [0.5, 1.0]$.

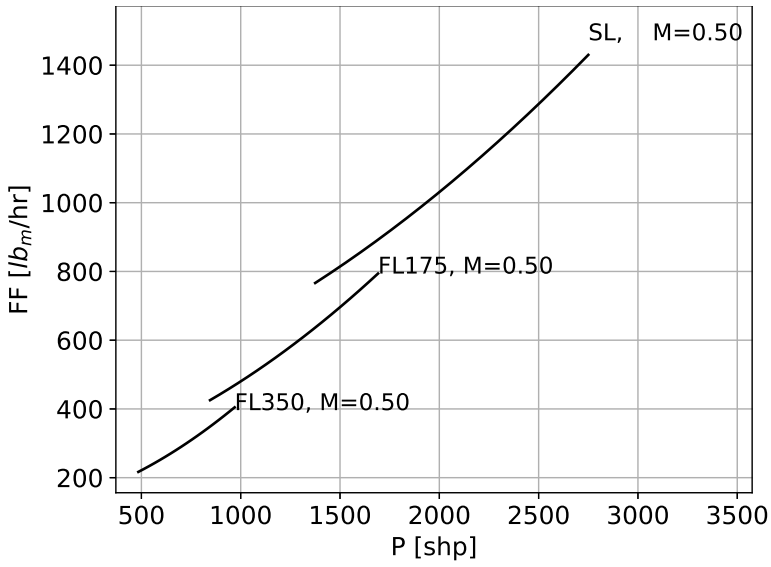

(a) Altitude dependence

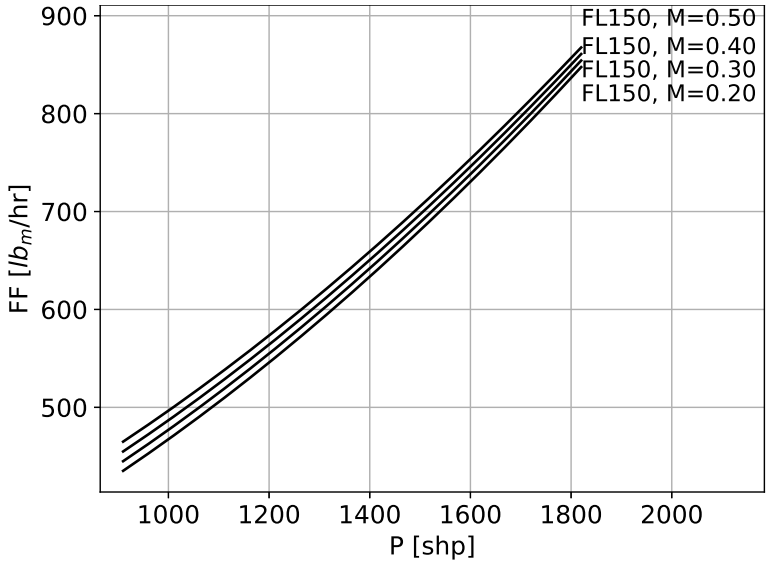

(b) Mach dependence

Figure 3.3: Fuel flow rate for a PW127M-equivalent turboshaft engine. Engine throttle shown from $G_{\text{set}} : [0.5, 1.0]$.

3.1.2 Variable Pitch Propeller

To calculate propeller efficiency (η_{prop}) and thrust (T) an interpolation of data presented by Scholz [24] is used and shown in Figure 3.4. The dataset is representative of the SOA in variable pitch propellers used in regional aircraft. Turboprop inlet blockage correction (F_b) are accounted for using data from Hamilton Standard [25] for scoop inlets and is shown in Figure A.1. The nominal propeller speed (at ssl conditions) is determined as a function of the nominal power of the engine and is shown in Equation 3.6. This equation comes from a review of engine power and propeller speeds of in-service aircraft with a conservative estimate of engine torque. Equation 3.7 augments propeller speed to roughly match the optimal advance ratio (J) operating point considering the air density ratio (σ) at the operation condition. Equation 3.9 and 3.10 determine propeller thrust given propeller power at altitude (P_h), throttle setting (T_{set}), propeller efficiency and inlet blockage. This model will be used for both propellers on turboprop engines and electric motors.

$$\omega_{\text{ssl}}[\text{rpm}] = 33500 {P_{\text{ssl}}}^{-0.4} \tag{3.6}$$

$$\omega_h = \omega_{\text{ssl}} \left(w_0 + w_1 M\right) \sigma \tag{3.7}$$

$$J = \frac{V_{\text{TAS}}}{\omega_h D_p} \tag{3.8}$$

$$k = \frac{P_h}{\rho A_p} \tag{3.9}$$

$$T = P_h \, T_{\text{set}} \, \eta_{\text{prop}}(V_{\text{TAS}}, k) \, F_b(J) \tag{3.10}$$

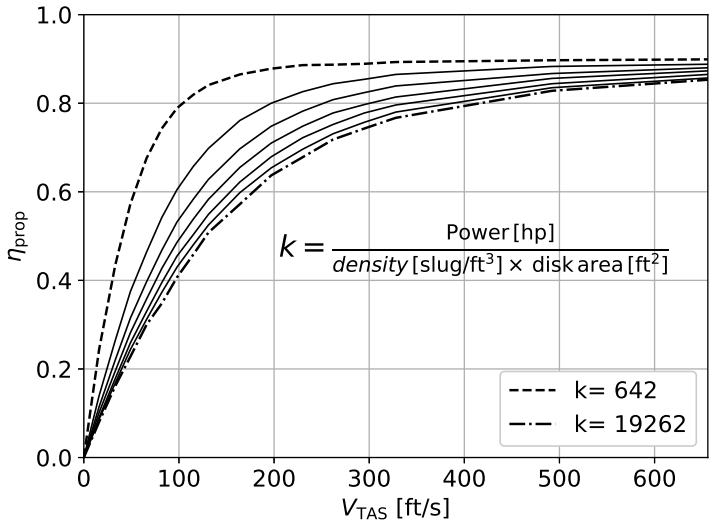

Figure 3.4: Propeller disk efficiency model. Minimum and maximum disk loading (k) range denoted with dash and dash-dot line respectively [24].

3.1.3 Turboprop Propulsion Model Validation

A thrust map for a turboprop engine is shown in Figure 3.5. This map combines the engine model using Equation 3.1, 3.2, 3.4, 3.5 and propeller model using Equation 3.6 to 3.10. Engine thrust is flat-rated up to Mach 0.1 which is consistent with models by Mattingly [23].

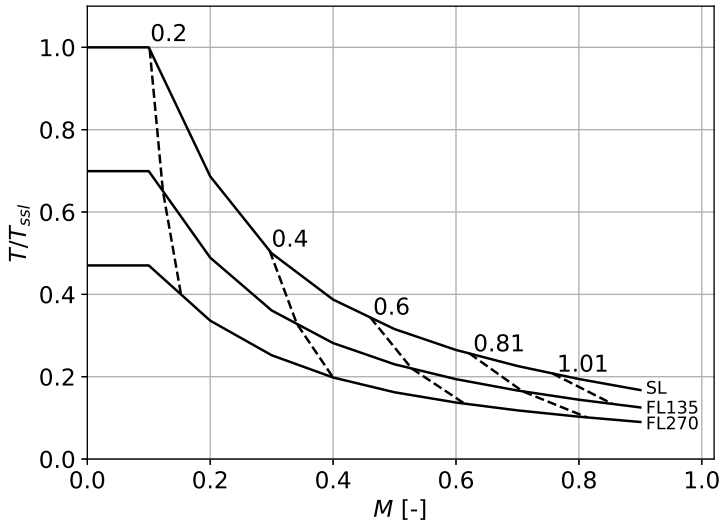

Figure 3.5: Thrust Map @ $T_{\text{set}} = 1.0$. Solid lines denote constant h, dashed lines denote constant TSFC. Map shown for a turboprop propulsion model with $P_{ssl} = 2750$ shp and $D_p = 13.5$ ft

The combined component thrust model was calibrated and validated by comparing to the EUROCONTROL Base of Aircraft data (BADA [26]). BADA is a database of in-service aircraft performance models used for research and development in air traffic management. The BADA performance datasets are developed in partnership with aircraft manufacturers and therefore provide the best performance reference available. Climb profiles of aircraft in the database provide thrust available and fuel flow rate, which can be used as a benchmark for the turboprop propulsion model. Figure 3.6 shows thrust and fuel flow rates for the ATR72-600 and DeHavilland Canada Dash 8 Q400 compared to model equivalent turboprop models. The thrust profiles match well for both aircraft performance datasets with fuel flow rate matching within the limitation of the parametric model.

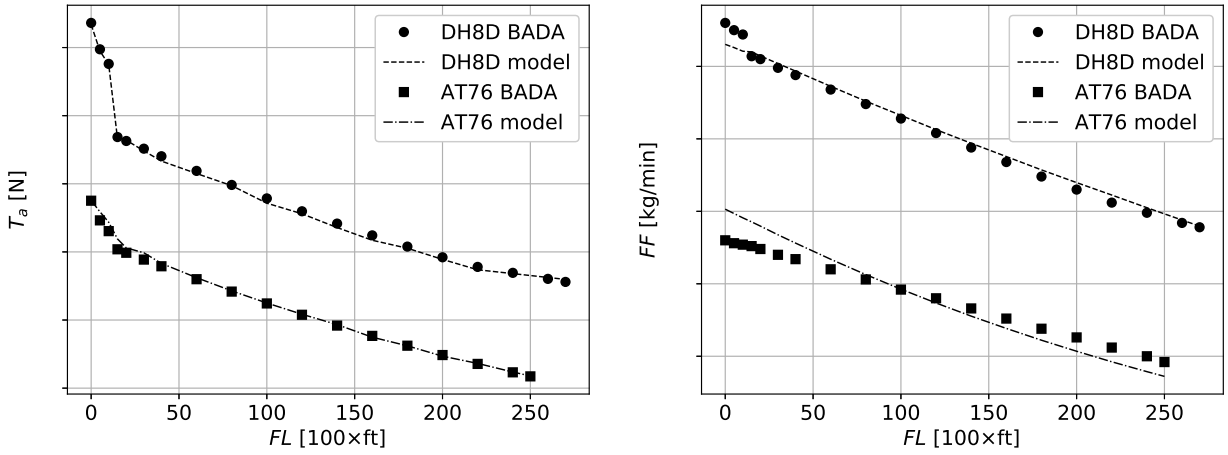

(a) Thrust available

(b) Fuel flow

Figure 3.6: Turboprop thrust and fuel flow model comparison to BADA data [26]. DH8D and AT76 engine models at P_{ssl} of 5100 shp and 2750 shp respectively.

3.2 Electrical Components

The electrical components modelled and shown in the following analysis will be limited to the battery cells and pack, electric motor/generator and wire distribution. These components will be included in addition to auxiliary, non-propulsion electrical equipment already included in aircraft weight estimation. The exception to this is the auxilliary power unit (APU), which is removed since it is replaced by the electric generator. The battery and electric motors will be inherited and modified from previous work. The electric cabling model is entirely adopted from Stuckl [27]. Aluminum core cables for DC power (2 poles, 2 cables each) are designed from the generator to each propulsor, passing through the location of the battery pack as well. This determines the mass, center of gravity and transmission power losses for the wire. While other components exist in a hybrid electric drivetrain (rectifiers, inverters, cooling, electrical bus, switching, circuit breakers, etc.) these components typically have fixed efficiency values and high specific power. This means that this auxilliary equipment efficiency and weight is not dependent on operation and that the impact on operational empty weight (OEW) is comparatively low. Thus these auxilliary equipment will not be considered in the electrical system sizing in this design study.

Figure 3.7 shows the organization of sub-systems and power flow in the hybrid electric propulsion model (the powertrain, including propeller). The propeller, turboshaft and fuel models are inherited and are identical to the conventional turboprop propulsion system. The turboshaft engine uses the same BSFC model which will inherently include reduction gearbox losses, even though a reduction gearbox will not be required in a generator. A trade-off between completely independent and interchangeable sub-system models and adherence to verifiable system performance data has to be made, given the limited availability and fidelity of performance data. This trade-off also leans to a more conservative performance model than reality, with a lower efficiency and specific weight.

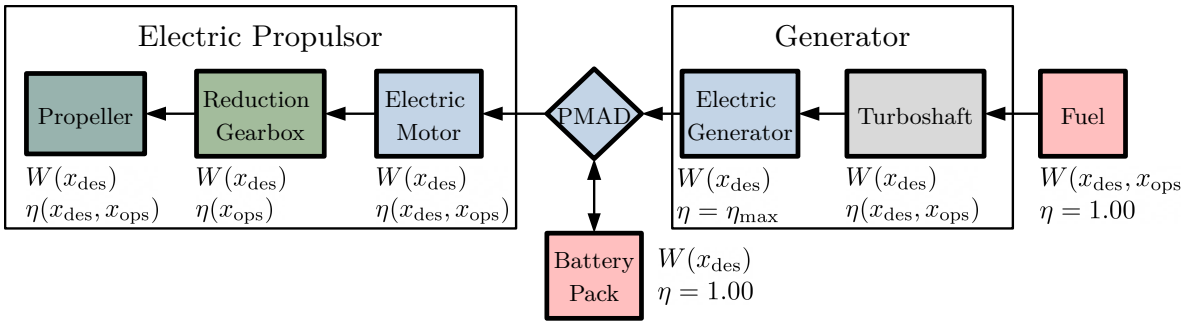

Figure 3.7: Hybrid electric propulsion system and powertrain.

A reduction gearbox is modelled independently between the electric motor and propeller in the electric propulsor. This gearbox allows matching of the peak efficiency speed of the electric motor and the propeller. The power management and distribution system (PMAD) is not modelled for weight or efficiency, since it is included as an auxiliary system, as described above. The PMAD exists in the hybrid electric performance model to manage the power output of the generator and the output or input of the battery pack. This management and distribution will be discussed in more detail in Section 3.2.3.

3.2.1 Lithium-Ion Battery

The lithium-ion battery model developed for this study is heavily influenced by the work of Vratny [28]. Battery discharge data for a Lithium cobalt oxide (LCO) is the basis of the battery cell [29]. Table A.1 in the Appendix shows detailed engineering data for the battery. The battery has a measured specific energy of 195Wh/kg. While this is not the most advanced lithium-ion battery

(Nickel manganese cobalt/NMC cells have a specific energy of 224 Wh/kg [29]), it is representative of the current capabilities of lithium-ion batteries. The expected specific energy of battery cells in 2030 is 275-320Wh/kg. This expectation is however further reduced by the added mass of the battery pack (to be discussed in Sections 3.2.1.3 and 4.4). While future battery cells are predicted to improve, the performance of current batteries in terms of energy and weight, is close to the end of the maturity of this technology. Other battery prototypes, not using lithium-ion chemistries, have been proposed but also come with significant penalties in reliability and economic lifecycle, as well a lack of publicly available performance data.

3.2.1.1 Battery Data

The data shown in Figure 3.8 shows the discharge voltage for the battery cell as depth of discharge (DOD), which is the opposite of the state of charge (SOC) as shown in Equation 3.11.

$$\text{DOD} = 1 - \text{SOC} \tag{3.11}$$

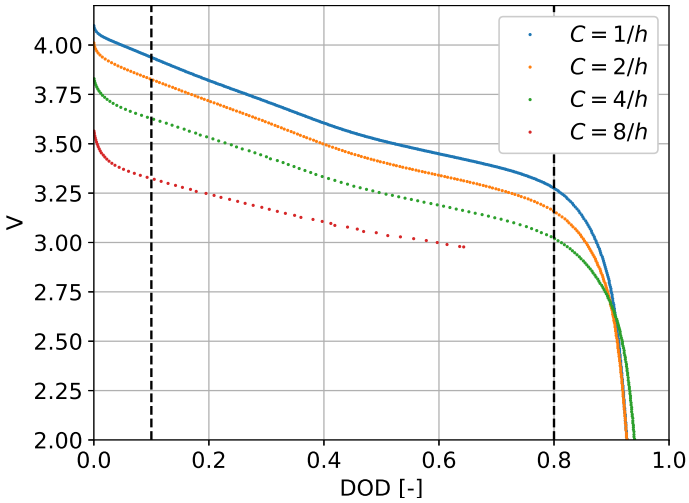

Figure 3.8: LCO battery data at $T = 15$ °C [29]. Dashed lines show charge limits implemented in the model. Battery data and implemented polynomial fit model.

The discharge voltage is shown at 4 discharge rates, known as C-rates. C-rates are the output current normalized to the capacity of the cell. This battery has a nominal capacity of 2.5 Ah, so the nominal current (I_{nom}) is 2.5 A,

which is equivalent to a C-rate of 1C. At a discharge rate of 1C, the battery capacity will be drained in 1 hour, at a discharge rate of 2C (equivalent to 5 A) the battery will be discharged in 0.5 hour. The C-rate is the derivative of the DOD and a negative C-rate charges the battery, decreasing the DOD and increasing the SOC. The battery tests completed by Barkholtz for this data were completed at four constant C-rates within the rated battery temperature and capacity limits. The 8C rate shown in Figure 3.8 does not discharge the battery completely due to the temperature constraints.

The Barkholtz battery tests were completed at ambient temperatures in 5°C increments from 5°C to 35°C. To simplify modelling, the data at 15 °C was used for the battery model, where the widest operating capability existed. This design decision was made under the assumption that these ambient conditions, which are close to the cabin conditions, could be well regulated. The battery data also provides an estimate of the limitations of batteries under continuous electrical load. The upper bounds on discharge rate are set considering the most extreme discharge scenario where the battery is discharged continuously. Thus any discharge rate within this performance model, for any time period is considered valid and not capable of causing a critical battery thermal problem.

To limit battery performance to more practical usage, the discharge range is limited. It can be seen in Figure 3.8 that outside the dashed lines the voltage change of the battery is non-linear, operating the battery in this area will reduce the cycle life of the battery and impact the battery economics. As such, the battery charge is limited to 90% to 20% SOC, giving any battery an effective capacity of 70% (1.75Ah).

3.2.1.2 Battery Cell Discharge

To interpolate the battery data, an 8^{th}-order polynomial is fit to each C-rate. For each battery discharge, the battery cell provides a constant power output (P_{cell}) for a prescribed time period (T). The final SOC (SOC_f) from the initial SOC (SOC_i) is determined by first-order integration of discharge over time, as shown in Equation 3.12.

$$SOC_f = SOC_i - \int_0^T C_{cell}(P_{cell}, SOC)dt \tag{3.12}$$

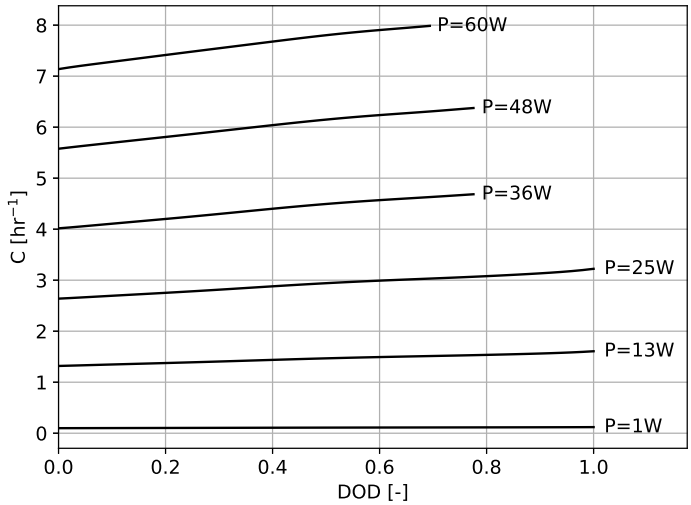

Figure 3.9: C-rate of battery model at different constant power discharges

C_{cell} is interpolated from the polynomials in Figure 3.9 given the P_{cell} required and the current SOC. Note that at low SOC where data are not available for 8C, 4C is the maximum discharge rating, this limits the power available from the battery. Discharge rates below 1C are common but not included in the battery dataset. To model discharge rates below 1C, additional discharge curves were added to the dataset using the discharge curve at 1C as a profile and shifting the curve up based on an extrapolation of the voltages at SOC=90%. This extrapolation is shown in the Appendix.

3.2.1.3 Battery Pack Design

In high power applications like automotive vehicles and aircraft, battery cells are arranged in packs. These packs typically are arranged into groups, called modules, to reduce the severity of a thermal runaway event. Within each module, battery cells are arranged in an $n \times m$ array, with n cells in series and m cells in parallel [28]. The operating voltage of the pack is $V_{cell} \times n$ and the operating current of the pack is $I_{nom} \times C_{cell} \times m$. Battery packs weigh more than the sum of the weight of the cells, due to the structures protecting the cells, fire-resistant materials and power management and distribution systems. To account for these additional components, an added pack mass factor of 30% is added to the weight of the cells, this is consistent with the state of the art pack masses in electric vehicles. The weight model for battery packs will be introduced in Section 4.4.

3.2.1.4 Battery Cell Charge

Battery cell charging is a much more sensitive operation compared to discharging. Modern batteries, when discharging, can handle short bursts of high power output without severe consequences to battery life performance or chemical stability. In contrast, battery charging is a heavily monitored and controlled process to maximize safety and battery life. Many aircraft design studies limit the battery model to discharge only. The discharge only operation along with the reduced capacity and additional battery pack weight means that the effective specific energy of the battery is at least 30% lower than that of its cells.

To model battery charging without significant expansion of test data, discharge curves are used in reverse at an increased voltage of 1.5× the discharge voltage. This means that for the same power, the charging C-rate is slower than the discharging C-rate. This voltage increase is to artificially account for the power draw of charging monitors and regulators. Charging is also limited to 1C to model the battery with lifetime economics in mind.

A battery's main advantage over other energy storage systems is that it can be charged and thus is energy-reversible. This reversibility can superficially increase the specific energy of the battery, by harvesting energy which would otherwise be used un-economically and using it at a later time when economics are improved. If charging can increase the specific energy while de-rating conventional energy sources (*i.e.* reducing on-board fuel), a new system optimal may be possible. To date, aircraft design studies have not found a new optimal without battery charging. This should be completely expected, since Jet-A fuel is 61× the energy density of a battery cell (Jet-A being 18,400 BTU/lb [23] $\approxeq$ 42.8 MJ/kg = 11.9kWh/kg).

3.2.2 Electric Motor/Generator

The model for electric motors and generators used is adopted from McDonald [30] and shown in Equation 3.13 to 3.21. The model, shown in Figure 3.10, uses five constants to scale the maximum efficiency ($\eta_{\max}$), parasitic losses (k_0) and scalings of the motor limits in torque, power and speed (k_Q, k_P and k_ω). To reduce the motor sizing to a single input variable, a relation between nominal power and speed is derived for high-speed electric machines using data from Moghaddam [31]. The final model builds a complete motor map up

to the maximum power of the motor ($P_{\max}$), equivalent to P_{ssl} for a turboshaft engine.

$$C_0 = k_0 \frac{\omega_{\text{des}} Q_{\text{des}}}{6} \frac{1-\eta_{\max}}{\eta} \tag{3.13}$$

$$C_1 = \frac{-3C_0}{2\omega_{\text{des}}} + \frac{Q_{\text{des}}(1-\eta_{\max})}{4\eta_{\max}} \tag{3.14}$$

$$C_2 = \frac{C_0}{2\omega_{\text{des}}^3} + \frac{Q_{\text{des}}(1-\eta_{\max})}{4\eta_{\max}\omega_{\text{des}}^2} \tag{3.15}$$

$$C_3 = \frac{\omega_{\text{des}}(1-\eta_{\max})}{2Q_{\text{des}}\eta_{\max}} \tag{3.16}$$

$$Q_{\max} = k_Q Q_{\text{des}} \tag{3.17}$$

$$P_{\max} = k_P Q_{\text{des}} \omega_{\text{des}} \tag{3.18}$$

$$\omega_{\max} = k_\omega \omega_{\text{des}} \tag{3.19}$$

$$P_L = C_0 + C_1\omega + C_2\omega^3 + C_3 Q^2 \tag{3.20}$$

$$\eta = \frac{\omega Q}{\omega Q + P_L} \tag{3.21}$$

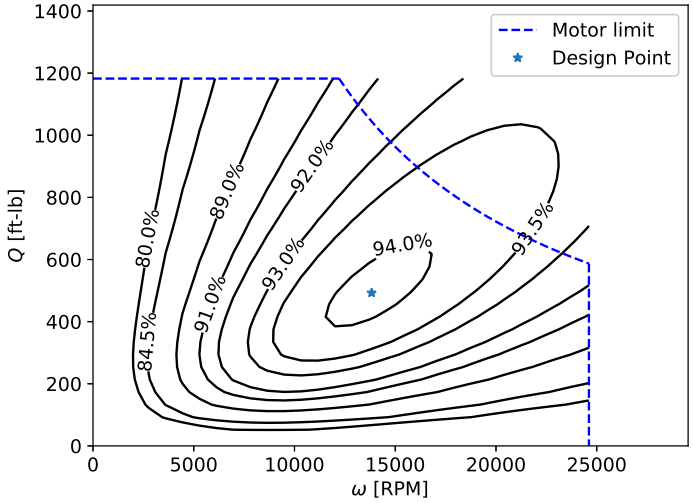

Figure 3.10: Electric motor model shown for $P_{\max} = 2750\,\text{shp}$, $\omega_{\text{des}} = 24\,612\,\text{rpm}$. Model settings: $\{k_0 = 0.95, k_Q = 2.4, k_P = 2.12, k_\omega = 1.78, \eta_{\max} = 0.941\}$

Series hybrid electric powertrains operate electric machines in solely motive or generator modes. When electric machines are used in motive modes for propulsion, operation efficiency is dependent on the efficiency islands in Figure 3.10. When electric machines are used as generators, it is assumed that the operation is performed at optimal speed, thus a constant of $\eta_{\max}$ is used.

The efficiency map of electric motors/generators having an upper bound efficiency of 94% implies that, independent of the number of propulsors or cable power losses, the series hybrid electric powertrain is at a maximum 88.5% efficient (the product of the maximum efficiency of two electric motors) from

turboshaft to reduction gearbox at the propulsor. As such to provide equivalent power at the gearbox, the turboshaft has to be rated for 11.5% more power in a hybrid electric system as compared to a turboprop engine. The losses of this power path have to be counter-acted by the capabilities of the battery system.

3.2.2.1 Geometric Model

To aid in geometric modelling of aircraft engine nacelles, an electric motor geometric model was developed from a review of the SOA electric motors, from supplier sales material and sources collated in Moghaddam [31]. The model is an approximation of the expected diameter (Equation 3.22), power density (Equation 3.23) and length (Equation 3.24) of electric motors. Aerospace electric motors may differ in their geometries significantly from their automotive equivalents. In contrast to automotive applications, aerospace will favour power density over torque density and may require additional convective cooling because of the increases in power and their operation in less dense air.

$$D[\text{in}] = 10^{(0.310 \log_{10}(P_{ssl}[\text{MW}])+1.338)} \tag{3.22}$$

$$\frac{V}{P}[\text{kW/in}^3] = 10^{(-0.359 \log_{10}(P_{ssl}[\text{kW}])+0.244)} \tag{3.23}$$

$$L[\text{in}] = \frac{\frac{V}{P} P[\text{kW}]}{(D/2)^2 \pi} \tag{3.24}$$

3.2.3 Power Management and Distribution

Power management in a HEAC manages the output of the turboshaft generator and the discharge/charge of the battery to meet the power demands of the propulsive system. The PMAD function is shown in Algorithm 1 shows how battery power is determined based on the output of the other power systems. The propulsion power requirements are determined by the electric motor at the propeller ($P_{\text{propulsive}}$), dependent on the operating conditions and the thrust throttle parameter (T_{set}). The power output of the turboshaft generator (P_{gen}) is similarly determined by the operating conditions and the generator throttle parameter (G_{set}). The power of the propulsion and power losses of the cable system ($P_{\text{propulsive}} + P_{\text{cable loss}}$) must be equal to the input power of the battery system and turboshaft generator ($P_{\text{battery}} + P_{\text{gen}}$). The power requirements of the battery are the difference between the power outputs and the power generation. If this difference is positive, the battery discharges. If

this difference is negative the battery charges. When discharging, the battery the battery power output is boosting the output of the generator to meet the propulsion requirements. When charging the battery the generator is creating more power than required for propulsion and charging the battery with the excess power. More details on how the PMAD system is used in aircraft performance analysis is provided in Section 4.3. A power cable model from Stückl [27] was used to determine cable weight and resistance. The cables modelled with an aluminum core, chosen for its balance of weight and resistivity performance. The cable system is nominally rated for 500 Vdc. A DC distribution is sufficient since the cable distance are not significant enough to incur large power losses in transmission.

Algorithm 1 Power management and distribution function

function PMAD($T_{\text{set}}, G_{\text{set}}, \text{SOC}_i, M, h, t$)
    $T, P_{\text{propulsive}} \leftarrow$ Electric Motor(T_{set}, M, h)
    P_{gen}, BSFC $\leftarrow$ Turboshaft(G_{set}, M, h)
    $I_{\text{cable}} \leftarrow P_{\text{propulsive}}/V_{\text{cable}}$
    $P_{\text{cable loss}} \leftarrow {I_{\text{cable}}}^2 R$
    $P_{\text{battery}} \leftarrow P_{\text{propulsive}} + P_{\text{cable loss}} - P_{\text{gen}}$
    $\text{SOC}_f \leftarrow$ Battery($P_{battery}, \text{SOC}_i, t$)
    return $T, \text{SOC}_f, \text{BSFC}$
end function

With a conventional turboprop propulsion systems modelled and validated against propulsion data, the added electric components and common subsystem components has built a series hybrid electric powertrain. The thrust and power requirements on the propulsion system vary with aircraft drag, weight and mission flight profile. Thus the entire aircraft system needs to be fully understood to design the propulsion system.

In the next chapter, the two propulsion systems will be integrated into regional aircraft models. The turboprop propulsion system can be further validated at the aircraft performance level using operational data. The integration of the hybrid electric system will require estimation of best design practices since there are no reference aircraft to base design decisions.

4 Regional Aircraft Design

In this chapter a regional, propeller-driven aircraft configuration is presented. This configuration model aims to be universal for aircraft utilizing conventional aero-propulsive designs (where propellers are mounted forward of the wing). The benefits of a new propulsion system, like hybrid electric, need to be considered from the perspective of aircraft performance. A new propulsion system that provides benefits at the propulsion system level but incurs costs in overall aircraft performance due to its integration has to be considered for the new system to be a viable concept for development.

This aircraft configuration presented has two propulsion system options, a conventional turboprop and a series hybrid electric powertrain. The modelling and analysis methods of these options is discussed in this chapter, with their system and aircraft design to be presented in Chapter 6. A blown-wing aero-propulsive model is used to increase maximum lift coefficient ($C_{L,max}$) of the aircraft wing. The weight models of the aircraft structure and components are presented. Weight and mission sizing methods are presented and validated against in-service turboprop aircraft using their design missions and payload-range diagrams.

4.1 Aircraft Configuration Model

The aircraft configuration model combines the individual sub-systems and structures together into one programmable object. The geometry can be seen in Figure 4.1. The unified configuration model includes payload, fuel tank and landing gear systems. Using the aircraft configuration model as input, aerodynamics, stability and control, and weight and balance analysis can be completed on the aircraft. The aircraft configuration can be calibrated against reference aircraft data and extended to novel configurations (structural and other system changes).

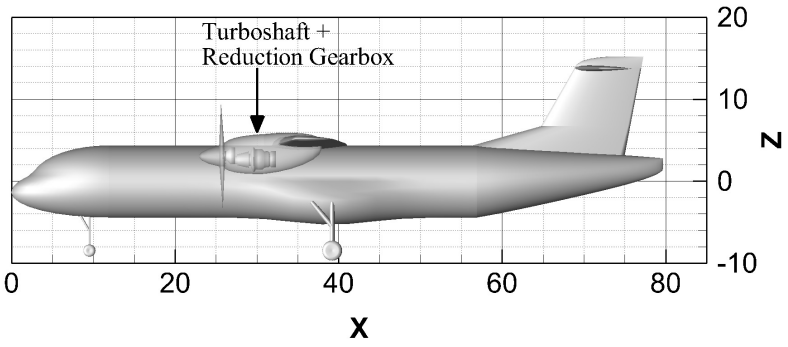

Figure 4.1: Conventional turboprop aircraft configuration. Transparent nacelles are used to visualize the internal geometries of the engine. Dimensions in feet.

4.1.1 Hybrid Electric Configuration

The series hybrid electric aircraft model inherits the structures, aerodynamics, propulsion and weights models from the turboprop aircraft model. The geometric model is modified at the nacelle to account for the change in engine geometry, otherwise the geometry model is identical. The generator is placed at the start of the tail section on the fuselage centreline. This design decision considers the future integration of air-inlets, volume and balance limitations. The generator consists of the turboshaft engine and an electric generator. The electric motor in the nacelle is connected to the propeller via a reduction gearbox, just as a turboprop engine would be. While electric motors do not need speed reduction to increase torque, the optimal operating speed of the motor is 10-11$\times$ of the optimal operating speed of the propeller. The hybrid electric aircraft model can be sized without a turboshaft engine, creating an all-electric aircraft, or without batteries creating a turboelectric aircraft model. Power cabling is not modelled geometrically but is included in weights and balance. The layout of the HEP within the aircraft is shown in Figure 4.2.

The batteries are not geometrically modelled but are included as a point mass in the weights and balances model. The longitudinal position of the batteries is between the MAC and the start of the tail section so as to satisfy the stability, weights and balance analysis of the constraints in Table 6.2, to be used in design studies in Chapter 6.

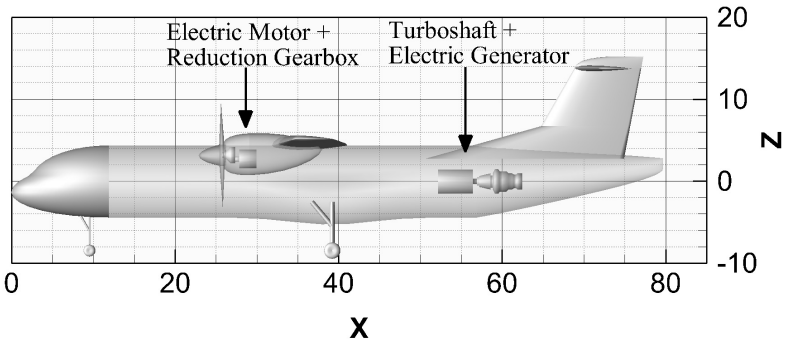

Figure 4.2: Hybrid electric aircraft configuration. Transparent structures are used to visualize the HEP components (Turboshaft generator and electric motor propulsors.

4.2 Blown-Wing Model

To analyze the takeoff and landing performance of propeller driven aircraft, the $C_{L,max}$ of the aircraft has to account for the increased dynamic pressure present on wing area in the streamtube of the propeller. Jameson [32] developed a lifting line model where an infinite wing segment is encapsulated by an elliptic streamtube from the propeller(s). This model was further expanded for wings with blown and unblown segments. Equation 4.1 to 4.4 shows the process of increasing overall $C_{L,max}$ of the wing based on the marginal increase in lift of blown-wing segment. The marginal velocity increase in the blown-wing flow due to thrust is shown as σ. The blown-wing span, aspect ratio and area are denoted as b_{bl}, $\mathit{A\!R}_j$ and S_{bl}. The blown-wing span accounts for the downstream contraction of the accelerated propeller flow. The aspect ratio of the elliptic propeller flow is shown as λ_j, for a wing with a single propeller this aspect ratio is 1 as the ellipse reduces to a circle.

$$\sigma^2 = 1 + \frac{T_a}{(1/2)\rho V^2 \left(D_p/2\right)^2} \tag{4.1}$$

$$b_{bl} = D_p \sqrt{\frac{1+\sigma^{-1}}{2}} \tag{4.2}$$

$$\left(\frac{C_{L,\max,bl}}{C_{L,\max,\text{clean}}}\right)_j = \frac{\mathit{A\!R}_j + 2}{\mathit{A\!R}_j + 2\frac{1+\sigma^2\lambda_j}{\sigma^2+\lambda_j}}\sigma^2 \tag{4.3}$$

$$\frac{C_{L,\max}}{C_{L,\max,\text{clean}}} = \left(1 - \frac{S_{bl}}{S}\right) + k_{bl}\left(\frac{S_{bl}}{S}\right) \sum_{j=1}^{nEng} \left(\frac{C_{L,\max,bl}}{C_{L,\max,\text{clean}}}\right)_j \tag{4.4}$$

The blown-wing model was further improved by Stoll *et al.* [33] who used CFD analysis to determine the correlation factor k_{bl} shown in Equation 4.5. k_{bl} was used to correlate the analytical model with CFD results.

$$k_{bl} = 0.302 \sum_{j=1}^{\text{nEng}} \frac{S_{bl,j}}{S} + 0.792 \tag{4.5}$$

4.3 Design Mission Profile

Aircraft design missions are divided into two phases: main and reserve. Each phase is made of segments which include a combination of warm up, taxi, takeoff, climb, cruise, descent, loiter or landing. The standard mission profile is outlined in Figure 4.3. The reserve mission meets FAR 25 contingency fuel requirements. Speed and altitude in cruise and climb segments are included as design variables.

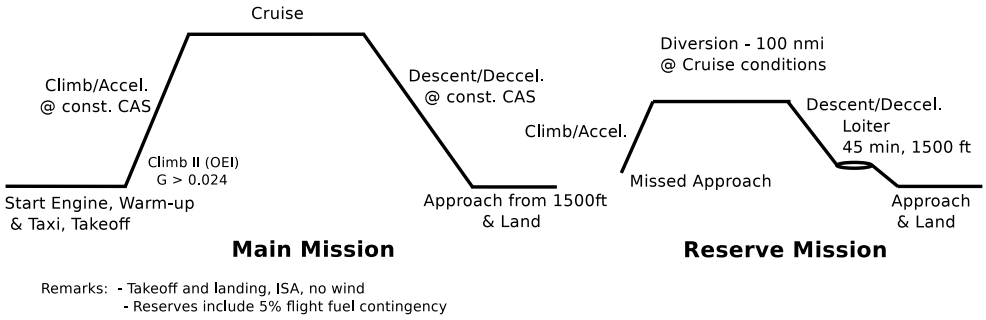

Figure 4.3: Standard Mission Profile

To validate aircraft and performance models against public data, aircraft climb and cruise profiles from BADA [26] are used to determine the design missions of in-service aircraft. Using the parametric engine model described in Section 3.1.1, the fuel consumption is sensitive to the throttle setting (T_{set}) used. A fixed set of T_{set} are assigned over the mission profile and are shown in Table 4.1. The T_{set} for each segment are fixed to reflect the typical inputs by pilots and so are driven by external human factors. Optimization of the T_{set} of each segment could add performance benefits, but is not indicative of the practical use of aircraft. As well, optimal settings are not likely to vary significantly from the fixed settings nor will optimal settings affect the optimal solution of other systems. By optimizing the propulsive power with these fixed settings, pseudo-optimal conditions can be found with the least number of variables.

Table 4.1: T_{set} settings for standard mission profile.

Segment	T_{set}
Ground	0.10
Taxi	0.15
Takeoff	1.00
Takeoff C34/obstacle clearance	1.00
Climb/level acceleration	0.88[1]
Cruise	$T(T_{\text{set}}, M, h) - D = 0$[2]
Descent	$T(T_{\text{set}}, M, h) - D = 0$ or 0.15[3]
Landing	0.15

[1] Climb occurs at a constant CAS. At the top of climb an acceleration transitioning from the climb CAS to cruise Mach occurs, must meet a minimum acceleration, meaning the T_{set} value may be increased to satisfy demands. This typically occurs with turboprop propulsion systems.
[2] In cruise unaccelerated flight is desired, T_{set} is the root solution.
[3] In descent a steady rate of descent (RoD) is desired, T_{set} can be a root solution or the assigned value depending on their RoD.

In accordance with FAR25 contingency fuel requirements, mission fuel is determined based on the requirements of the main and reserve missions plus an additional 5% of the main mission requirements as shown in Equation 4.6.

$$W_f = 1.05 W_{f,\text{main}} + W_{f,\text{reserve}} \tag{4.6}$$

4.4 Component Weight Models

The aircraft weight models already included in *pyACDT* are used for structures, systems, payload and fuel that have been combined from a selection of sources [34–37]. Unique components to turboprop and hybrid electric aircraft use the weight equations in Table 4.2.

4.5 Mission and Weight Sizing Method

In aircraft design, weight is the main metric to which all system requirements and performance are connected. Design mission performance requires an accurate estimation of take-off weight which requires an accurate understanding of the on-board fuel weight (W_f), payload weight (W_{pay}) and operational empty weight (OEW, the fixed structural and system weights of the aircraft). The design mission of a transport aircraft is typically defined by a design payload weight and design range (R), based on the business case of the aircraft.

Table 4.2: Turboprop and electric component weight models. Equations requiring multiple lines are included in the Appendix.

Component	Equation	Source
Electric Motor/Generator	$8.0\frac{kW}{kg}$	[38][1]
Turboshaft/Turboprop[2]	Appendix: Equation A.1	
Reduction Gearbox	$72({P_{\text{ssl}}}^{0.76})\frac{{\omega_{\text{eng}}}^{0.13}}{{\omega_{\text{prop}}}^{0.89}}$	[39]
Propeller[2]	Appendix: Equation A.2	
Battery Pack	$(n+m)w_{\text{cell}}(1+pmf)$	[18, 28]

[1] The latest in electric motor development, the Koenigsegg Quark achieves a peak power density of 8.3kW/kg.
[2] A review of in-service aircraft propellers datasheets. $R^2 = 0.97$

The aircraft weight method in *pyACDT* determines the maximum take-off weight (MTOW) based on the design payload and fuel weight (W_f). The aircraft OEW is determined by the sum of the component and structural weights, many of which the weight is estimated using regression with respect to MTOW, as such an initial MTOW guess is needed (MTOW_i). Using an initial MTOW guess, the OEW is determined and then combined with the W_f and W_{pay} to give a calculated MTOW. The weight methods are re-calculated with an updated MTOW_i based on the last calculated value, until the guess and calculated value are converged, giving a final MTOW value. The weight sizing process is illustrated in Figure 4.4b.

The weight sizing method is combined with a mission sizing method to define the aircraft weights. Similar to the weight sizing method, the mission sizing method uses an initial fuel weight guess ($W_{f,i}$) which is passed to the weight sizing to determine the MTOW and then to the mission performance method. The mission performance method determines the fuel required for the mission. The fuel weight guess is updated and the combined weight sizing and mission performance is re-calculated. When the fuel weight guess and the mission fuel requirements converge, the mission sizing is converged. The mission sizing process is illustrated in Figure 4.4a. The combined weight and mission sizing of the aircraft at the design mission define all the weights of the aircraft based on the design mission requirements.

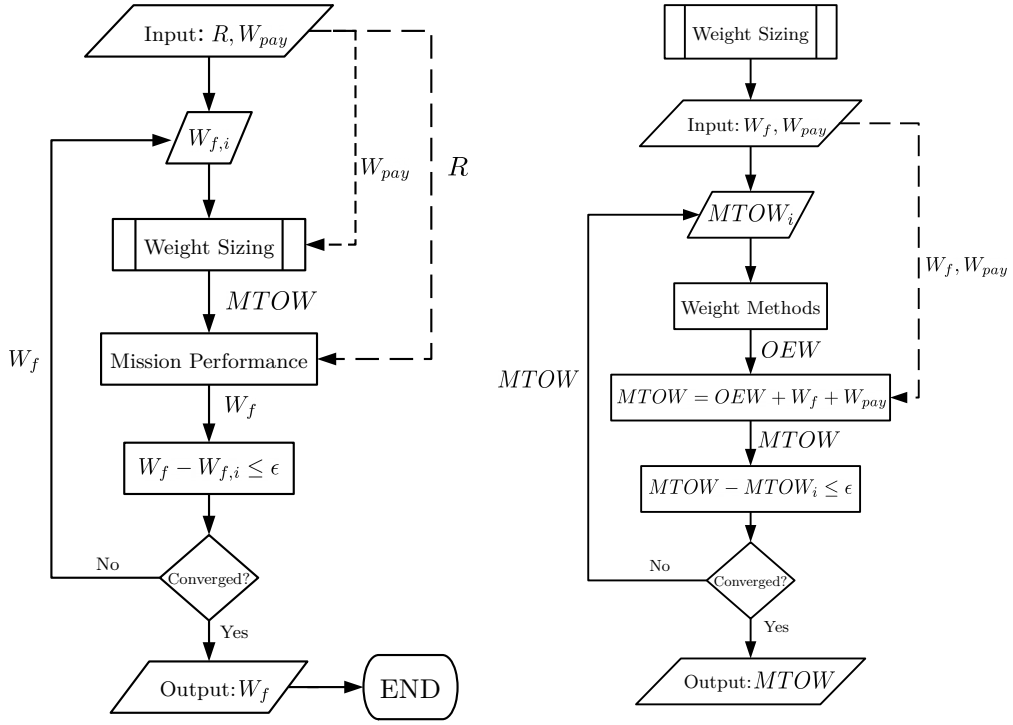

(a) Mission Sizing (b) Weight Sizing

Figure 4.4: Sizing method including design mission performance and weight convergence. Dashed lines denote data-only connectors.

4.6 Weight & Field Length Model Validation

The turboprop aircraft model was tuned and validated by matching performance data for field performance, payload-range and weights of three in-service aircraft (DHC-8 Q400, ATR 72-600 and SAAB 2000) using their publicly available data. The propulsion model was validated using engine specific data in Section 3.1.3 and the aerodynamic models were tuned so that the aircraft system performance matched. Take-off field length ($TOFL$) was determined using the Powers method [40]. Landing Field Length (LFL) was determined based on the summation of approach, flotation, flare and ground run distances. $C_{L,max}$ was determined using method in Section 4.2. Table 4.3 denotes the aircraft model outputs for weight, field length and $C_{L,max}$ for the three in-service aircraft, the model data is compared to published data for these aircraft.

Table 4.3: Comparison of aircraft model to aircraft specifications. Weights shown in pounds and lengths in feet. No aircraft data available for $C_{L,max}$.

	ATR72-600		DHC-8 Q400		SAAB 2000	
	Model	Δ[%][1]	Model	Δ[%]	Model	Δ[%]
MTOW [lb]	52 807	+5.11	62 281	+6.21	47 558	−2.90
OEW [lb]	31 425	+7.08	37 635	−0.45	28 540	−10.73
W_{pay} [lb]	15 753	−4.72	17 492	+1.72	11 970	−1.24
$W_{f,\text{max}}$ [lb]	9 131	−17.16	11 821	−0.09	10 761	+14.85
W_f [lb]	5 629	−0.48	7 154	−23.83	7 048	−19.16
R [nmi]	490	0.0	580	0.0	840	0.0
TOFL [ft]	5 477	+25.25	3 969	−6.96	2 788	−30.39
LFL [ft]	2 931	−16.01	3 072	−26.15	2 653	–
$C_{L,max}$@ TO	2.223		2.115		2.118	

[1] Difference is model relative to aircraft specification.

For the more modern aircraft (The ATR and Q400) the aircraft weight model is well within acceptable agreement for a conceptual design study, with the exception of maximum fuel weight (MFW) where wing tank geometry dominates the weight sizing. Between the three in-service aircraft there is not good agreement on how far along the wingspan that wing tanks should go. The chosen design rule aims to minimize the impact on all aircraft compared to, as such the SAAB design has a comparatively large fuel tank and the ATR a comparatively small fuel tank.

4.7 Payload-Range Model Validation

Payload-range diagrams are used by transport aircraft manufacturers to market the utility of their aircraft to customers. Operators use payload-range diagrams for flight planning. For a complete performance model, matching aircraft performance to the payload-range diagrams means that the summation of aerodynamic and propulsion system performance matches the in-flight performance of aircraft.

A payload range has four data points as range increases, the first two points are at zero and the design range (DR), each at the design payload weight (W_{pay}). Along this section, the takeoff weight (TOW) is increasing, starting from the maximum zero fuel weight (MZFW) and ending at the maximum

takeoff weight (MTOW). The third point on the diagram is the maximum fuel-payload range (MFPR), between the DR and MFPR the aircraft increases the onboard fuel from the design fuel weight (DFW) to the maximum fuel weight (MFW) and decreases the W_{pay} as shown so that the overall aircraft weight stays at the MTOW. The fourth and final point on the diagram is the ferry range (FR), the absolute maximum distance the aircraft can cover with no payload.

In Figure 4.5 the key weight values of the aircraft are fixed to the values in aircraft data sheets. When these values are fixed, the aircraft performance matched very well for all aircraft. When aircraft weight sizing models are used, producing the values shown in Table 4.3, the payload-range values in Figure 4.6 are produced. The W_{pay} values are still in agreement for all aircraft. The slope (dW_{pay}/dR) between the DR and $MFPR$ agrees well for the ATR and Q400. The oversized fuel tank for the SAAB leads to an extended $MFPR$ and FR.

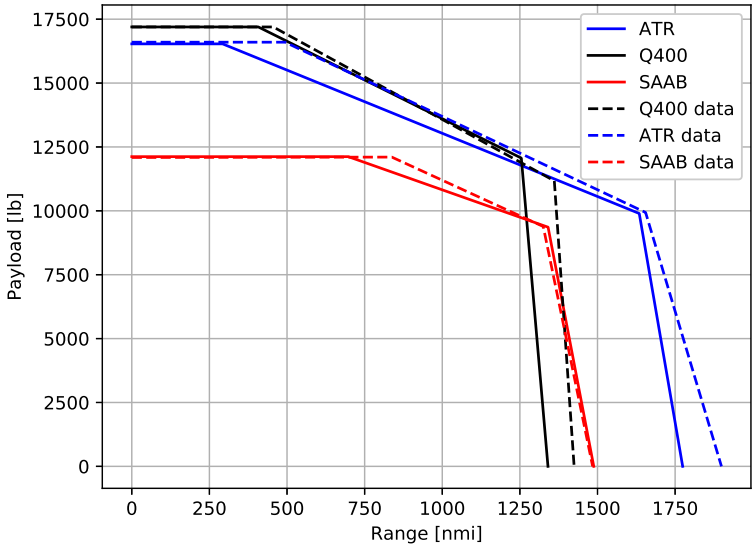

Figure 4.5: Payload-range diagram with fixed OEW,MTOW,MPLW,MFW to aircraft specification

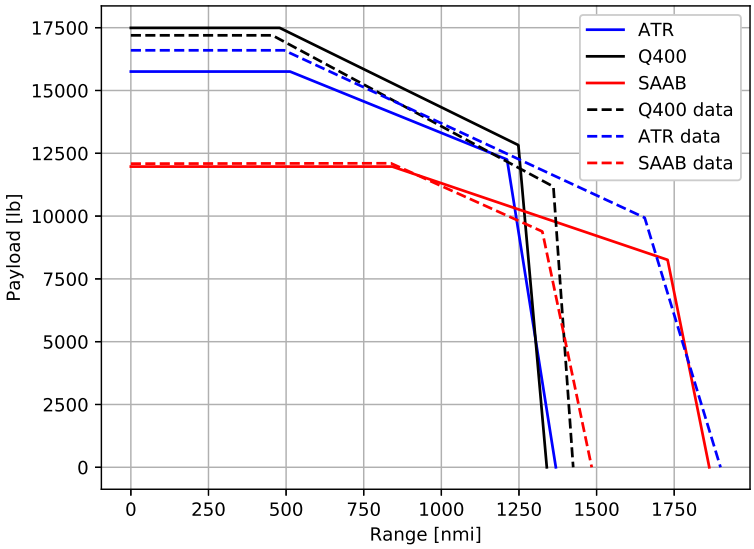

Figure 4.6: Payload-range diagram with *pyACDT* weight method

4.8 Regional Design Mission Requirements

The weight and performance methods shown in this chapter allow aircraft geometries along with their design missions to define the weights of aircraft systems and structures. These methods still need to be provided with a design payload and range (as shown in the flowchart in Figures 4.4a) as input to begin the sizing methods. For transport aircraft and especially passenger aircraft, the design payload is inherently dependent on the route network that the aircraft is operating and the performance of the family of aircraft operated in the fleet and the propulsion technologies used. The thorough analysis of the couplings between aircraft design and route networks was investigated previously [41–46], which includes matching design payload to the requirements of the route network. This coupling is computationally expensive and would be overburdensome on design evaluation times to be included on top of the requirements for complete analysis of hybrid electric mission performance (to be discussed in Chapter 5). The simple conclusions from research on aircraft design for route networks suggests the following:

- Design payloads are complemented by the propulsion design in the aircraft. A combination of payload and propulsion sizing which leads to maximized payload-range fuel efficiency (PRE) [47, 48] at the design range, generally leads to the best PRE at all mission ranges. PRE being a mission performance metric of:

$$\mathrm{PRE} = \frac{R\, W_{\mathrm{pay}}}{W_{f,\mathrm{main}}} \tag{4.7}$$

  where $W_{f,\mathrm{main}}$ is the fuel consumption in the main mission phase.
- Regional aircraft, generally having the shortest design range in the aircraft fleet, are well suited when this performance is focused on short mission ranges and does not attempt to make trade-offs in performance to improve extended range capability. At these short ranges, larger aircraft are hindered by the high height and speed of their climb profiles and do not get the benefits of their cruise performance.

Given these conclusions as a qualitative assessment baseline, the design payload will be included as a design variable in the aircraft design (design variables to be discussed later in Section 6.1). Design range can be assessed by a statistical assessment of regional networks data. Figure 4.7 shows the distribution of daily passenger demand over route ranges within the Qantas domestic route network in 2019. The cumulative distribution function (cdf) of the network data shows the percentage of passenger demand below that design range. At 500nmi, 58% of the passenger demand is included, as well as the highest density range bin (200-400nmi).

Using this statistical assessment of a regional route network, 500nmi was chosen as the design range for the subject of this work. This mission range allows comparative analysis of different aircraft designs, with different propulsion systems, payloads and OML's. The comparison of different aircraft designs is also made possible by the PRE metric which gauges fuel consumption to the payload weight. This design mission range and performance metric in addition to aircraft design constraint analysis sets the stage to determining higher efficiency and feasible regional aircraft designs.

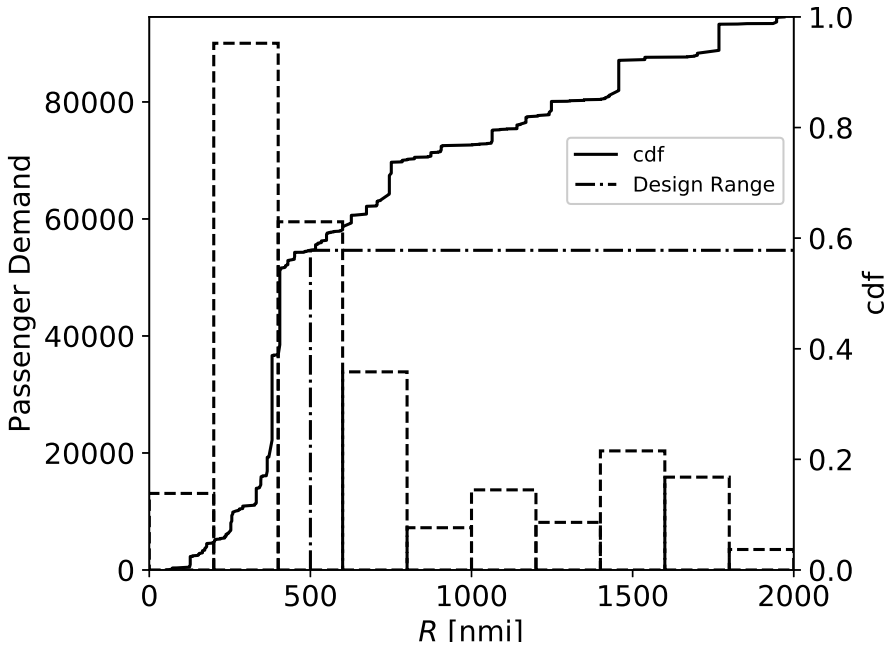

Figure 4.7: Qantas regional route network daily passenger demand data from 2019. Route passenger demand is binned every 200nmi in range using the left-hand axis. Cumulative distribution of passenger demand in the network on right-hand axis.

5 Hybrid Electric Mission Performance Analysis

Hybrid powertrain performance is more dependent on the design case than conventional powertrains due to the increased variability that comes with two power and energy sources. Power requirements vary throughout the design case and the optimal use of the two power sources is crucial to maximizing the performance of a powertrain design. The optimal use or power management of the hybrid powertrain can employ different strategies depending on the power and capacity of the electric and combustion components in the powertrain. The power management in the test case should reflect the optimal capabilities of that design.

In HEV design, the power requirements over the design mission change quickly and frequently since city driving includes many stops and starts, accelerations and deceleration. While HEV have the benefit of regenerative braking to harvest energy during deceleration, the unpredictability of power requirements leads to a HEV powertrain which is sized to have capacity and power available for many future power requirements. The design implications of power management means that real-world fuel consumption improvements are limited.

A HEAC has the benefit of predictable power requirements in a standard transport mission. A HEAC also has significant and often compounding penalties, including no regenerative braking, a 30-60$\times$ the power requirements and increased performance sensitivity to weight. However, if power management can use the predictability of power to downsize conventional components, then a HEAC can achieve fuel consumption improvements that a HEV could not.

In this chapter an optimization problem is formulated to analyze mission performance with the ability to design and to optimize the power management. The optimization of this problem will be shown for two test cases and results analyzed. These test cases will show the necessity for power management solutions that are specific to each aircraft design and test case.

5.1 Power Management Optimization Problem

To maximize the performance of a hybrid electric powertrain, the power management strategy is an essential component of the design. Optimizing the power management requires all mission segments to be considered and optimized in unison. Battery power and capacity at any segment is dependent on the battery usage in previous segments. An optimal power management strategy considers the opportunity costs of battery usage at each segment considering future power requirements. This opportunity cost is further complicated when the battery can be charged and discharged. The objective for the power management strategy chosen is the minimization of fuel weight (W_f).

An optimal solution to W_f will provide the mission and weight sizing methods (described in Section 4.5) with the minimum W_f for the aircraft design. The added fixed weights of the hybrid powertrain components will increase the OEW. In conventional aircraft sizing, increases in OEW compound into increases in W_f from lower aero-propulsive performance, as shown in Figure 5.1 where wing-loading, drag and thrust connect increases in OEW to increases in W_f. This positive feedback loop is the main reason why OEW/MTOW stays relatively constant throughout aircraft design. The challenge in this design will be to find reductions in W_f so that increases in OEW lead to limited increases in MTOW, effectively breaking the cycle in Figure 5.1 between step 4 and 5. If the power management cannot find W_f reductions, the increases in OEW and the positive feedback loop illustrated in Figure 5.1 will induce performance penalties just as it does in conventional aircraft sizing.

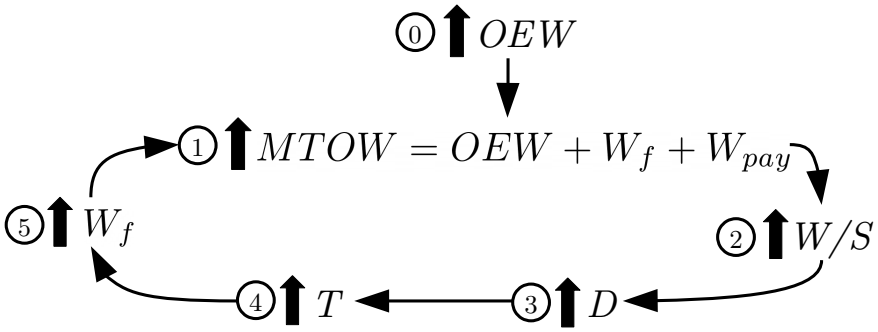

Figure 5.1: Positive feedback loop caused by increases in OEW

For a conventional aircraft, the mission performance uses fixed thrust settings

(T_{set}) for takeoff, climb and descent while in cruise the T_{set} is trimmed such for constant aircraft speed (For a conventional aircraft these settings are outlined in Table 4.1). In the mission sizing method the range is fixed and the MTOW is converged using the mission performance, as shown in Figure 4.4. For a HEAC, the thrust and generator settings (T_{set} and G_{set} respectively) can differ when advantageous for fuel consumption. The disassociation of thrust and fuel consumption increases the variability in HEAC mission sizing, now MTOW and power management must converge for complete sizing. Using the mission sizing method in Figure 4.4, the power management will be optimized during the "Mission Performance" block, determining an optimized W_f and using the same method for converging MTOW as a conventional sizing method. The power management optimization problem is shown more formally in Equation 5.1 where $G_{set,i}$ is the power setting of the turboshaft engine at n distributed points along the design mission. The objective function is chosen as it is the required output for the sizing loop.

$$\begin{aligned} \min \quad & W_f && (5.1)\\ \text{w.r.t} \quad & G_{set,i} \quad i = 1, \ldots, n \\ \text{s.t.} \quad & 1 - g_{\text{mission complete}} \leq 0 && (5.2) \end{aligned}$$

Mission performance analysis can fail to evaluate the mission when either the batteries are discharged beyond their practical bounds or more battery power is demanded than available. These failures are specific to the G_{set} inputs chosen. To reduce performance analysis failure and improve optimizer efficiency, failed mission performance evaluations are captured and are assigned a completeness score ($g_{\text{mission complete}}$) based on how far through the mission the failure occurred. Complete and feasible mission performance evaluations are assigned a $g_{\text{mission complete}}$ of 1.

To determine if feasible solutions exist before starting optimization, an initial solution is evaluated where all segments are set to a G_{set} of 1.00. For a given HEAC, this mission should be feasible. If this mission is infeasible, then the powertrain will, most likely, always be infeasible. The initial solution feasibility is important when the powertrain sizing is also being optimized and the generator maybe under-sized for the aircraft.

Table 5.1 shows the chosen distribution of G_{set} power management points along the design mission. Shorter segments with less operating condition variation like takeoff and landing are allocated fewer points. The emphasis of the

allocation is on climb and cruise, where segment time is longer and therefore total energy higher. The climb and cruise segments also have higher variation in operating conditions (atmosphere, speed, battery SOC) throughout their segments. The idle throttle setting of the generator is set at 0.10 which provides the lower bound for low power segments, whereas high power segments have a lower bound of 0.50 to improve the design space search. A different allocation of points or more points may achieve better performance. The allocation was chosen based on a trade-off of optimization speed and solution optimality, with a larger emphasis on optimization speed since in further reformulations, the power management problem will be a nested optimization problem within the aircraft design problem.

Table 5.1: G_{set} settings for HEAC mission profile. For a single stop mission there are 24 points in total.

Segment	Discretization	# of G_{set} points	Bounds
Main Phase			
Warm Up/idle	0.06hr	-	[0.10]
Taxi	0.15hr	1	[0.10,1.00]
Takeoff	[1]	1	[0.50,0.10]
Obstacle Clearance	300ft	1	[0.50,0.10]
Climb	1500ft	6[2]	[0.50,1.00]
Level acceleration	10ft/s	-[2]	[0.50,1.00]
Cruise	≈75nmi[3]	4	[0.50,1.00]
Descent	1500ft	2	[0.10,1.00]
Landing	[1]	1	[0.10,1.00]
Reserve Phase			
Climb	1500ft	6[2]	[0.50,1.00]
Level acceleration	10ft/s	-[2]	[0.50,1.00]
Cruise	≈75nmi[3]	1	[0.50,1.00]
Loiter	0.1hr	1	[0.50,1.00]
Descent	1500ft	2	[0.10,1.00]

[1] Takeoff and landing methods are discretized by events (e.g. ground, rotation, transition, etc.)

[2] Climb and level acceleration are grouped together into the climb segment.

[3] Main cruise segment discretized into 4 steps, step size is subject to change as cruise range changes.

5.2 Power Management Test Cases

A test case of the power management optimization is shown for an ATR 72 aircraft with a generic hybrid electric powertrain retrofitted to the aircraft (Geometry shown in Figure 4.2). The mission profile closely matches the current operation of the aircraft. The design mission range is 500nmi and optimized first as a single cycle mission (origin→destination) and then as a double cycle mission (origin→destination→origin). The hybrid electric powertrain and mission design parameters are outlined in Table 5.2.

Table 5.2: Hybrid electric powertrain and mission design parameters for test case.

Parameters	Value
Electric motor propulsor power	2750shp
Turboshaft generator power	6300shp
Battery n	50
Battery m	50
Flight Range	500nmi
Climb CAS	170kts
Cruise altitude	15,000ft
Cruise Mach	0.45

The power management problem is optimized using a Feasible Directions Particle Swarm Optimization (FDPSO) [49]. The sizing of each test case required two sizing loop iterations to converge the MTOW of the aircraft. The power management problem optimization for each test case and sizing iteration is shown in Figure 5.2.

The optimization in the first sizing iteration uses the maximum power generation solution as the initial solution. The second optimization is initialized with the previous optimization solution and the maximum power generation solution. In Figure 5.2a, the single cycle mission history shows that in the second sizing iteration, the power management solution from the previous optimization solution was not completely feasible with the updated MTOW. In this case the best solution of the early function evaluations is the maximum power generation solution. As the previous optimization solution is modified and becomes feasible once again, it is now the best solution and further refinement and optimization of the solution continues.

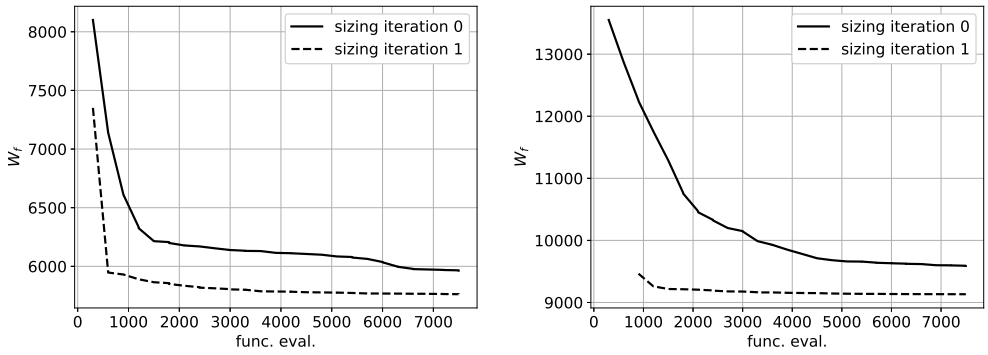

(a) Single cycle mission

(b) Double cycle misison

Figure 5.2: Optimization history for power management test cases.

In the double cycle mission in Figure 5.2b, the previous power management solution does not require modification to be feasible. Refinement of the solution happens earlier in the double cycle mission compared to the single cycle mission. Ultimately the difference in power management solutions is small between the two sizing loop iterations, but there is an improvement in fuel consumption of the power management solution with the updated MTOW.

5.2.1 Single Stop Design Mission

To characterize the power management solution Figure 5.3 shows the generator and battery use over the mission time. The G_{set} data shows the how the design variables are allocated throughout the mission and the timings and intensity of the generator use. The generator use and propulsion power requirements determines the battery use as calculated by the PMAD. The state of charge (SOC) of the battery indicates the available battery energy charge throughout the mission. The G_{set} and SOC are indicated by the left-hand y-axis. The C-rate is the normalized current of the battery, discharging and charging the battery have a positive and negative C-rate respectively.

The data shown in Figure 5.3 shows a few trends of optimal power management that will continue throughout the results:

1. Battery discharge through take-off and climb which boosts the power of the generator. At the end of climb the battery is close to the minimum charge (SOC_{min}).

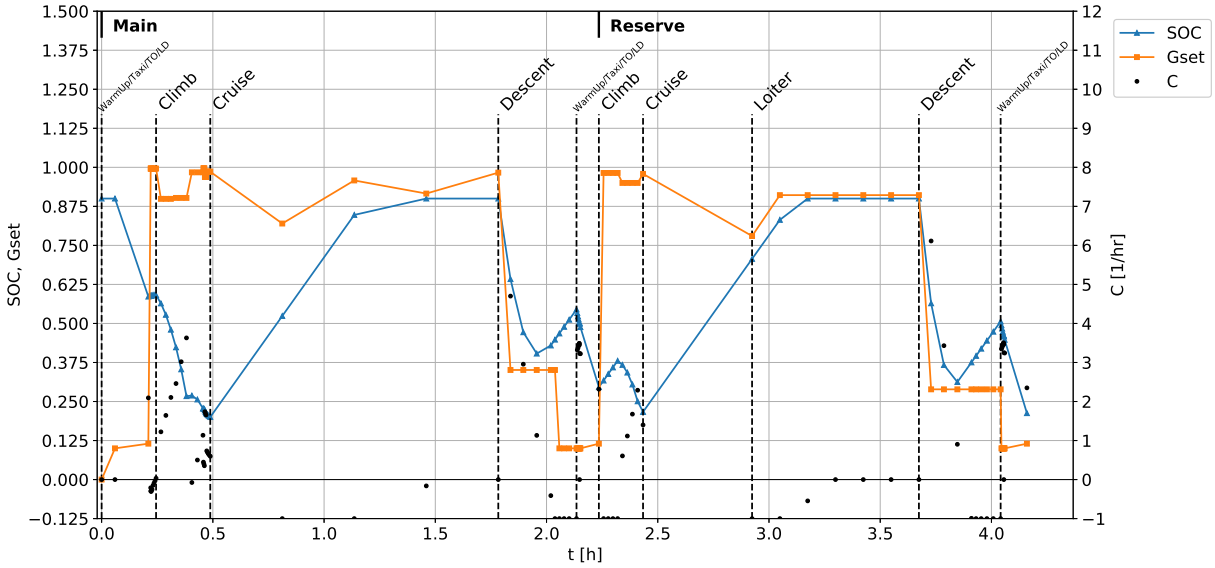

Figure 5.3: Power management solution for an ATR 72 aircraft on a single-stop design mission. Design mission is at a range of 500nmi carrying the design payload.

2. Battery charge through the first half of cruise. The generator produces slightly more power than required by the propulsion system to charge the battery.
3. No battery use in the second half of cruise as the battery is close to the maximum charge (SOC_{max}) and the powertrain operates in an almost complete turbo-electric state. The generator operates as close to the optimal fuel consumption while meeting propulsion power requirements.
4. Battery discharge through descent when thrust is still required and propeller is not feathered/wind-milling. In this segment the BSFC of the generator is far from optimal, so minimum power output is desired to reduce overall consumption. In the final stages of descent when the aircraft is effectively gliding and the generator is idling some charging occurs, in preparation for the reserve segment.
5. In the reserve climb segment, the battery is discharged but used less aggressively as there is less battery power and charge available.
6. In the reserve cruise/diversion segment a similar strategy to the main cruise segment is used, where the battery is charged by the generator operating at a slightly higher power setting than required by propulsion.
7. In the reserve loiter segment the powertrain is operating completely turbo-electric as the battery is at SOC_{max}.

8. In the reserve descent segment the battery is discharged heavily and the generator is operated at a lower power setting than the main descent segment.

The weight sizing and mission performance resulting from the power management is shown in Table 5.3. The baseline shows the performance of an identical aircraft in a turboprop configuration. The additional and re-configured components that make up the hybrid electric powertrain increase the OEW considerably, which leads to a relative increase of MTOW of just over half compared to the OEW increase. The fuel weight and mission time are reduced by 1-2% even with the increased MTOW, which is partially due to the small reduction in fuel consumption over the mission.

Table 5.3: Comparison of single-stop weight sizing and mission performance

Variable	Baseline	Hybrid Electric	Δ
MTOW [lb]	52 169	56 226	+7.8%
OEW [lb]	30 566	34 687	+13.5%
W_f [lb]	5 834	5 762	-1.2%
W/S [lb/ft^2]	79.48	85.56	+7.6%
t [hr]	2.27	2.24	-1.3%

Figure 5.4 breaks down the mission performance by segment of the power management solution in comparison to the baseline turboprop aircraft. This breakdown is considered in terms of the range of each segment (totalling to 500nmi for the main mission as per the design mission requirements), fuel consumption of each segment and finally the PRE of each segment (where the payload weight is equivalent for the hybrid electric and turboprop aircraft).

The comparison of segment range in Figure 5.4a most notably shows that the climb segment is performed over a shorter range for the HEAC. This range is then transferred to the cruise segment range. The fuel reduction is achieved mostly by improvements in fuel consumption in climb where there is the largest relative change. The fuel consumption of this segment is partially transferred to the cruise segment due to changes in segment range and battery re-charging in cruise. Fuel use during the reserve segments is similar, with matched improvements in climb as in the main climb segment.

The cumulative changes in segment range and fuel consumption manifest in the segment PRE comparison, shown in Figure 5.4c. The reduced range and fuel consumed in climb of the HEAC result in a lower PRE in climb, but a

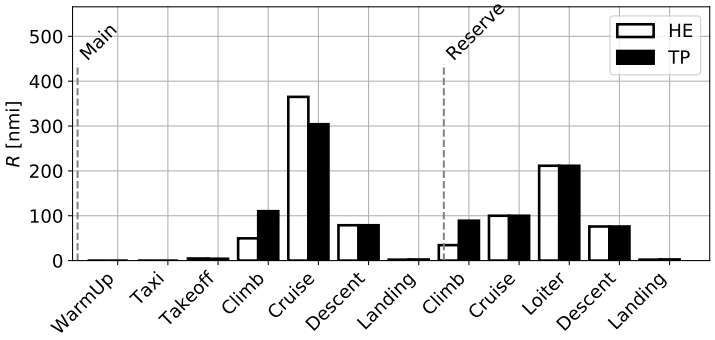

(a) R

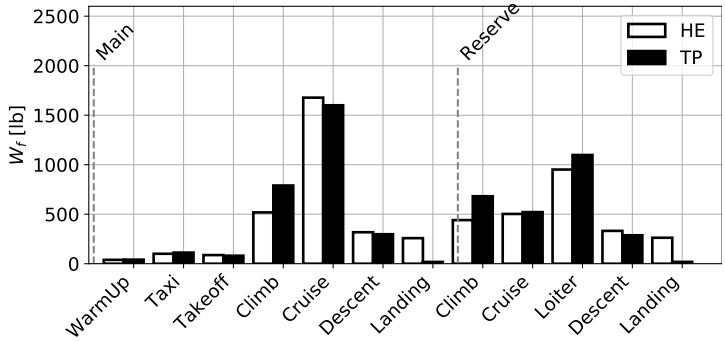

(b) W_f

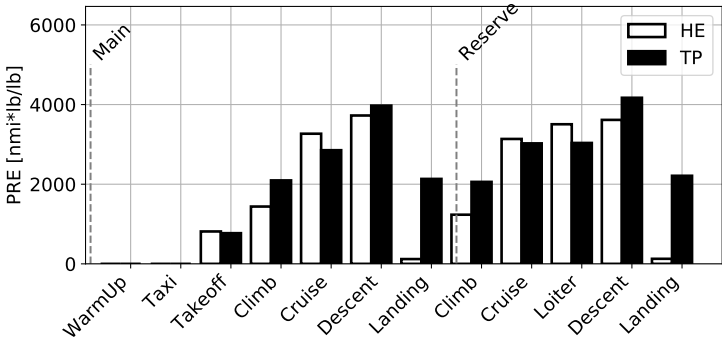

(c) PRE

Figure 5.4: Segment performance comparison of power management solution of the single stop mission to the baseline turboprop aircraft.

larger PRE in cruise. This ultimately leads to an overall improvement in PRE due to climb being a larger segment in terms of both time and range.

5.2.2 Double Stop Design Mission

Regional aircraft are typically used in spoke routes in hub-and-spoke route networks. They feed larger international hub airports from smaller regional airports. Typically, the turn-around time at these regional airports is shorter and servicing capabilities limited. As such, aircraft are not refuelled at these locations and the fuel weight of both missions must be included. Multiple stop missions as design missions are common for regional aircraft designs because of these economic and logistical factors. To investigate a HEAC's potential using this design mission in Section 5.2.1 was repeated with a double stop design mission. Figure 5.5 shows the power management solution to this design misssion for the same aircraft design as detailed in Table 5.2.

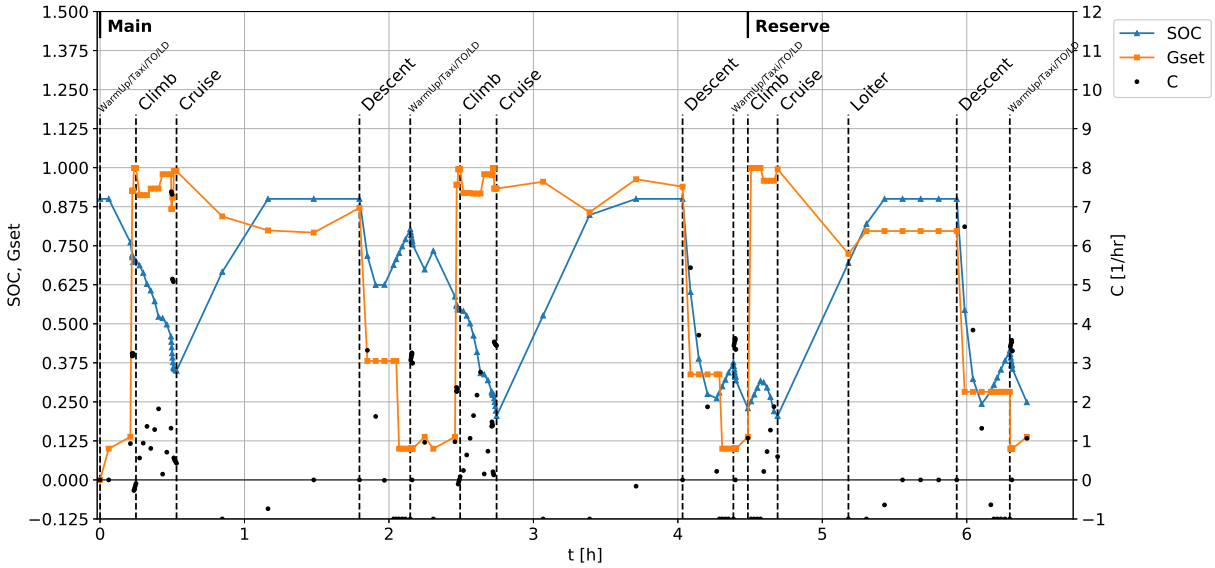

Figure 5.5: Power management solution for an ATR 72 aircraft on a double-stop design mission. Design mission is at a range of 500nmi carrying the design payload.

Similar power management strategies can be seen in the double-stop design mission as seen in single stop mission prior. The descent segment prior to the first stop uses less battery charge as shown in the single stop mission and is kept for use in the next climb segment. This means that over the first stop of the mission, the SOC only drops from SOC_{max} to 80%. This shows that the productive utility of the battery is not as an alternative fuel storage but as

temporary energy storage solution to minimize the overall fuel.

Table 5.4 shows the weight sizing and mission performance results of the multi-stop design mission comparing the HEAC to a turboprop. The multi-stop design mission shows similar increases in MTOW and OEW as found in the single stop mission. The fuel consumption and mission time show 3-5% improvement over the baseline, compared to 1-2% in the single stop mission.

Table 5.4: Comparison of double-stop sizing mission performance

Variable	Baseline	Hybrid Electric	Δ
MTOW [lb]	56 615	60 186	+6.3%
OEW [lb]	31 238	35 276	+12.9%
W_f [lb]	9 609	9 133	-5.0%
W/S [lb/ft^2]	86.25	91.69	+6.3%
t [hr]	4.63	4.49	-3.0%

As in the single stop mission, the range fuel consumption and PRE are compared in Figure 5.6. The range distribution shows similar transfer of range from the climb to cruise segment and decreases and increases in fuel consumption in climb and cruise respectively. The changes in range and fuel consumption lead to recognizable trends in segment PRE with similar relative differences between segment. The increased fuel consumption benefits of the HEAC in the single stop mission *vs.* double stop mission can be simplified down to more battery discharge cycles in the double stop mission (3 cycles) *vs.* single stop mission (2 cycles). More cycles of the battery in the double stop mission allow more opportunities for the power management method to reduce the strain on the generator in both high and low power segments.

Over both single and double stop missions, HEAC have shown potential to change the power profile of regional aircraft. While the double stop showed larger fuel consumption reductions than the single stop mission, it came at the cost of doubling the power management design variables. In the macroscopic view of both test cases, their results were within error of each other and within parity of the baseline test case. The hybrid electric powertrain showed parity performance to a turboprop engine even with more energy conversion steps (Mechanical→Electrical→Mechanical) leading to lower powertrain efficiency and higher overall powertrain weight. The increased powertrain weight also resulted in aerodynamics penalties due to an increase in wing loading.

The powertrain designs in single and double stop missions were chosen as feasible solutions, not necessarily optimal solutions. These feasible powertrain designs showed slightly improved fuel consumption over the turboprop aircraft equivalent. It remains to be shown if an optimally designed powertrain, an optimally designed aircraft can achieve significant fuel consumption improvement.

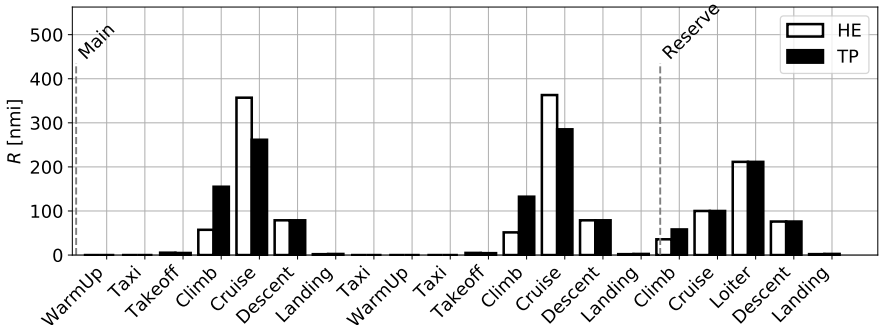

(a) R

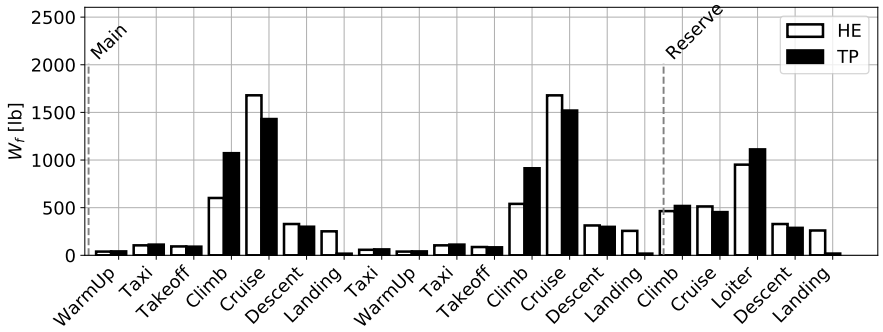

(b) W_f

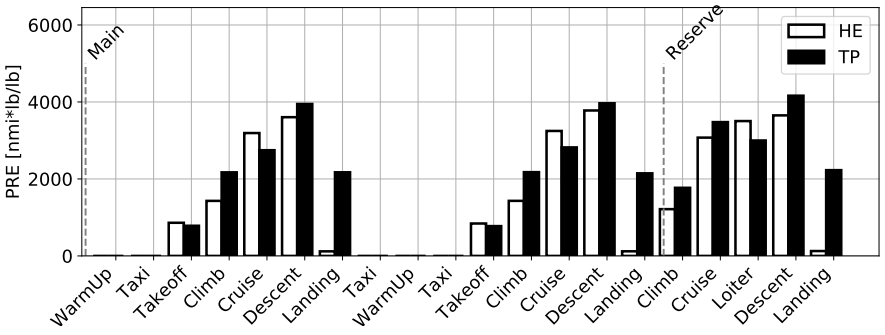

(c) PRE

Figure 5.6: Segment performance comparison of double stop power management solution to the baseline turboprop aircraft.

6 Aircraft Design Optimization

To use the capabilities of the aircraft configuration model and the mission performance model, a nested optimization problem is formulated. This problem is solved under different scenarios based on potential implementations of hybrid electric aircaft based on manufacturer's previous capabilities and future development limitations. In this chapter the problem formulation of the nested design optimization is introduced and solutions analyzed with different design variable sets. As shown in Section 4.1, a turboprop aircraft configuration model was developed. The optimized turboprop aircraft design solution, as well as the in-service aircraft modelled, are compared on their performance and design philosophies.

6.1 Aircraft Design Variables and Constraints

The aircraft configuration model has many (> 100) settings, the aircraft design variables use here are a limited subset of these settings which covers the fuselage, wing, control surfaces and propulsion sizing. Other configuration settings are fixed at default values based on common commercial aircraft practices (for example, seat pitch is set to 30in). Mission design variables are included with the geometric design variables. The configuration of HEAC requires additional design variables for the hybrid electric powertrain (HEP). The geometric, propulsion, powertrain and mission design variables are listed in Table 6.1. The aircraft design variables are a mix of continuous, integer and binary types, all of which can be handled by the optimizer (FDPSO).

A set of constraints are used to base the aircraft design on common design principles and Federal Aircraft Regulations Part 25 (FAR25). These constraints include geometric limitations for airport operations, take-off and landing performance, one engine inoperative control authority and operation and center of gravity forward and aft limits. Some control surface geometric constraints are implemented based on weight and aerodynamic model limitations. These constraints limit the tail geometries, relative to the geometries of the wing. Table 6.2 quantifies the constraint limits.

Table 6.1: Aircraft design variables

Discipline	Name	Symbol	Type[1]	Bounds
Cabin	Single Class Capacity	cap	I	[15,120]
	Seats Abreast	$seats$	I	[2+1,3+3]
Wing	Wing-Fuselage Connection	$wing\_loc$	B	[High,Low]
	Semi-Span, [ft]	$b_w/2$	C	[25,40]
	LE Sweep [deg]	$\Lambda_{LE,w}$	C	[10,40]
	Root Chord, [ft]	$c_{r,w}$	C	[18.0,45.0]
	Crank Location, [% Semi-Span]	b_{crank}	C	[20.0,40.0]
	Inner Segment Taper [%]	$\lambda_{i,w}$	C	[0.4,0.8]
	Inner Segment Tip Thickness [%]	$t_{i,w}$	C	[0.11,0.14]
	Outer Segment Taper [%]	$\lambda_{o,w}$	C	[0.2,0.6]
	Outer Segment Tip Thickness [%]	$t_{o,w}$	C	[0.08,0.11]
	Dihedral, [deg]	Γ_w	C	[−2.0,7.5]
	Root Leading Edge Location, [%]	x_w	C	[0.25,0.75]
Horizontal Tail	Horizontal Tail Semi-Span [ft]	$b_{ht}/2$	C	[16.0,35.0]
	Root Chord [ft]	$c_{r,ht}$	C	[12.0, 28.0]
	Taper Ratio	λ_{ht}	C	[0.2, 0.7]
	LE Sweep [deg]	$\Lambda_{LE,ht}$	C	[15.0,50.0]
	Dihedral [deg]	Γ_{ht}	C	[−3.0,8.0]
Vertical Tail	Vertical Stabilizer Configuration	VT_type	I	[Conventional, T-Tail]
	Semi-Span [ft]	$b_{vt}/2$	C	[10.0,40.0]
	Root Chord[ft]	$c_{r,vt}$	C	[11.0,30.0]
	Taper Ratio	λ_{vt}	C	[0.2 ,0.9]
	LE Sweep [deg]	$\Lambda_{LE,vt}$	C	[15.0,50.0]
Landing Gear	Main LG Mounting Points	MLG	B	[Nacelle, Fuselage]
Propulsion	Propulsor Power[2] [eshp]	P_{prop}	C	[1800, 6000]
	Propeller Diameter [ft]	D_p	C	[10, 15]
	Number of Engines	$nEng$	I	[2,6]
	Engine Incidence Angle [deg]	eng_{ia}	C	[−3.0,3.0]
	Engine Toe–in Angle [deg]	eng_{ta}	C	[−3.0 ,3.0]
Hybrid Electric Powertrain[3]	Generator Power[2] [eshp]	P_{gen}	C	[1800, 6000]
	Battery pack n Dimension[2]	n	C	[10, 15]
	Battery pack m Dimension[2]	m	C	[2, 6]
Operation	Cruise Mach Number	M_{cruise}	C	[0.43, 0.65]
	Initial Cruise Altitude [×1000 ft]	h_{cruise}	I	[15, 27]
	Constant Climb CAS [knots]	V_{climb}	I	[150, 230]

[1] C=Continuous, I=Integer, B=Binary.
[2] In a turboprop configuration the propulsor is a turboshaft engine and in a hybrid electric configuration it is an electric motor.
[3] Design variables apply to HEAC only, all other design variables are universal between turboprop and HEAC.

Table 6.2: Aircraft design constraints

Discipline	Constraint	Value
Geometry	Wing Span, [ft]	≤ 95
	HT Quarter Chord Sweep, [deg]	Wing $\Lambda_{c/4} \leq \Lambda_{c/4} \leq 6 \times$ Wing $\Lambda_{c/4}$
	VT Quarter Chord Sweep, [deg]	Wing $\Lambda_{c/4} \leq \Lambda_{c/4} \leq 15 \times$ Wing $\Lambda_{c/4}$
	HT Aspect Ratio,	$\mathcal{AR} \leq 0.6 \times$ Wing $\mathcal{AR}$
	VT Aspect Ratio,	$\mathcal{AR} \leq 0.10 \times$ Wing $\mathcal{AR}$
	Tip–back Angle, [deg]	$\geq 15.0^\circ$
	Rotation Angle, [deg]	$\geq 10.0^\circ$
	Available Wing Fuel Volume, [cubic ft]	$\geq$ Required Fuel Volume
Weights	Forward Center of Gravity Location, [% MAC]	≥ 0
	Aft Center of Gravity Location, [% MAC]	≤ 60
Stability and Control	Minimum Static Margin, [%]	≥ 10
	Trim HT Lift Coefficient	≤ 0.85
	Maximum Aileron Deflection (OEI TO), [deg]	$\leq 15^\circ$
	Maximum Rudder Deflection (OEI TO), [deg]	$\leq 24^\circ$
	Maximum Roll Angle (OEI TO), [deg]	$\leq 5^\circ$
	Static Roll Stability, [1/rad]	$-0.20 \leq C_{l_\beta} \leq 0.05$
	Static Yaw Stability, [1/rad]	$0.03 \geq C_{n_\beta}$
Performance	Takeoff Field Length, [ft]	≤ 6500
	Engine-Out Climb Gradient II	≥ 0.024
	Landing Field Length, [ft]	≤ 5000

6.2 Nested Hybrid Electric Aircraft Design Problem Formulation

Combining the aircraft design problem and power management problem requires a nested formulation of the two optimization problems. This nested formulation also has to size and converge the aircraft weights. Figure 6.1 illustrates the nesting of the outer aircraft design optimization with the inner power management optimization. For each outer optimization iteration, the mission sizing using the inner problem typically converge within two sizing iterations, meaning the inner problem is also typically done twice.

The outer loop is prescribed a mission range, the outer problem optimizes aircraft and mission design variables. The aircraft configuration and design mission are passed to weight sizing for an initial MTOW and OEW estimate. The aircraft configuration, design mission profile and weight estimate are then passed to the power management problem which optimizes the fuel

consumption over the design mission profile, as shown in Chapter 5. The fuel consumption of a weight-resolved mission is then passed back to the outer aircraft design mission. The PRE is then determined, based on the aircraft design payload, prescribed mission range and optimized fuel consumption of the main mission.

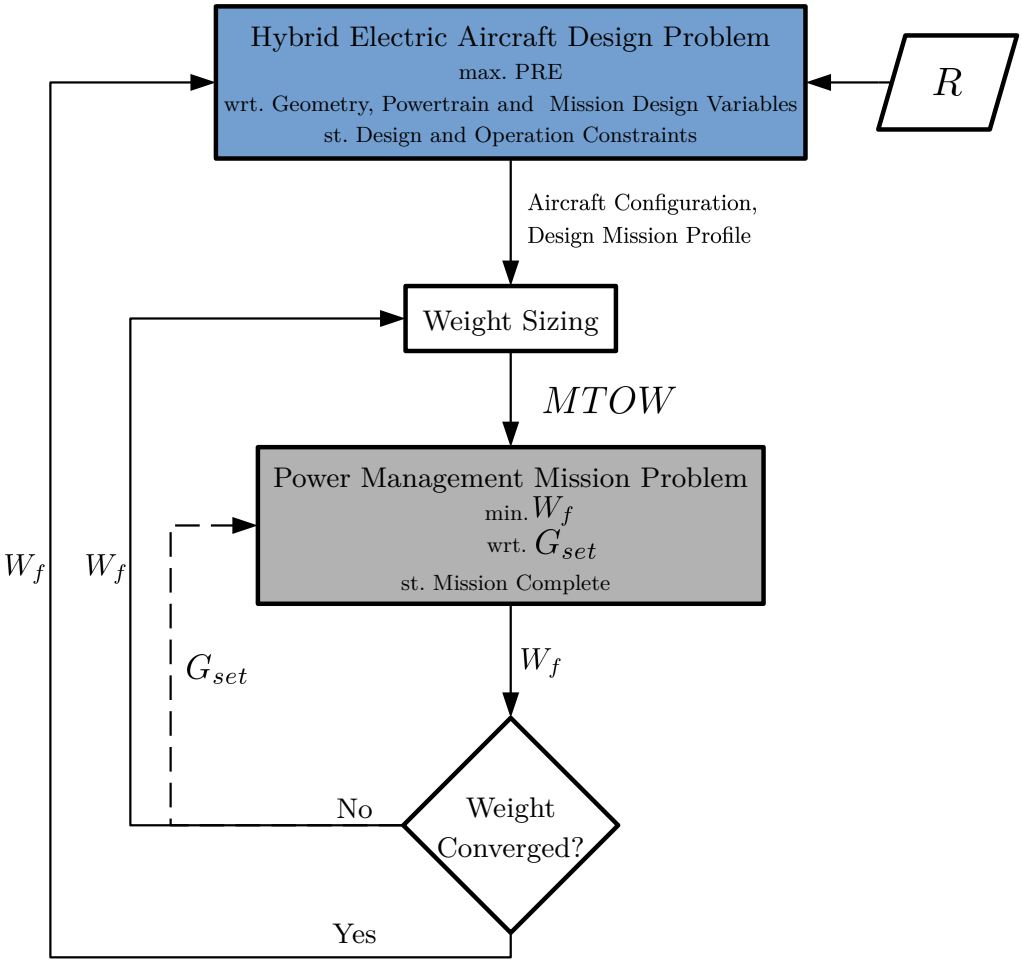

Figure 6.1: Nested optimization of HEAC sizing. Dashed line denotes a data-only connector.

6.3 Next-Gen Turboprop Aircraft

A novel turboprop design to compare against HEAC resolves two questions of aircraft design:

1. How much of the performance is due to the bias', calibration or fidelity limitations in the analysis methods (aerodynamics, propulsion, weight, etc.) used?
2. Is the technology jump (hybrid electric) absolutely necessary to achieve the proposed performance? Or is there a smaller technology step that could produce most, all or more of the same benefits?

This turboprop aircraft named as a Next-Gen turboprop aircraft (NG-TP) is a clean sheet design based on modern turboprop engine performance and in-service airline route network data (see Section 4.8). The aircraft was optimized for the same objectives and mission range as the HEAC (maximum PRE for a design mission range of 500nmi). In-service aircraft solutions, namely the ATR 72, DHC-8 Q400 and SAAB 2000 were seeded into the optimizer as initial solutions. The optimizer used is the Feasible Directions Particle Swarm Optimizer [49], as used for the inner power management problem. The optimization solution is specified in Table 6.3 and geometry shown in Figure 6.2.

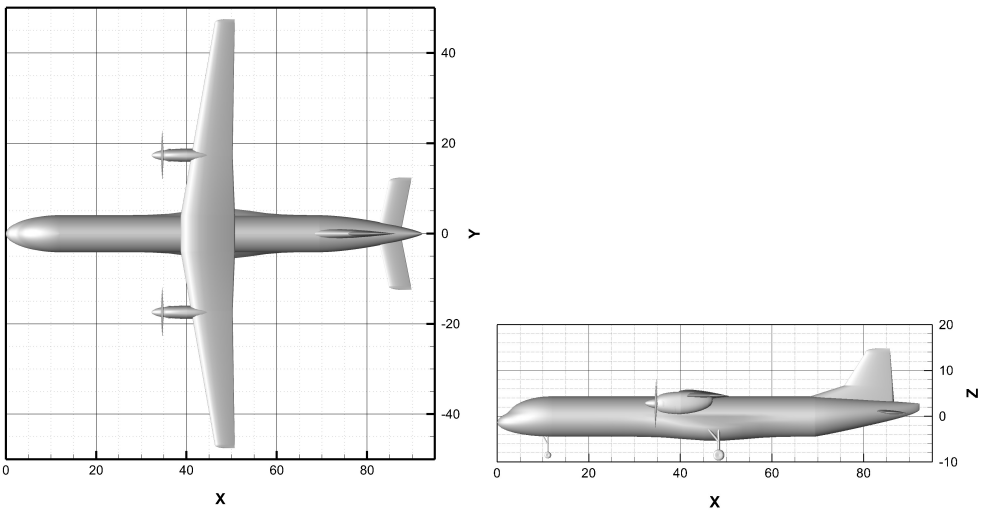

(a) (b)

Figure 6.2: Next-Gen turboprop

The Next-Gen turboprop aircraft incorporates the high-wing, fuselage-podded main landing gear design of the ATR 72. The wing is swept slightly more than the seed solutions. The cabin seats 90 passengers in a "2+2" seat configuration, this is significantly more capacity than the initial cabin designs of the seed aircraft solutions, but notably is close to the configuration that the DHC-8 Q400 is currently marketed with (with the exception that seat pitch is larger in this solution, creating a longer cabin section and fuselage). The tail control surface are in a conventional layout aligning with the SAAB 2000 design and diverging from more modern aircraft that institute a T-tail. The horizontal tail has a high $\mathcal{AR}$ to improve aerodynamic efficiency, in-line with newer transport aircraft design. The horizontal tail has a slight anhedral angle, this is likely to avoid the down-wash effects of the main wing.

Table 6.3: Next-Gen turboprop aircraft solution

Variable	Value	Variable	Value	Variable	Value	Variable	Value
cap	90	$t_{i,w}$	0.13	$\Lambda_{LE,ht}$	12.4	P_{prop}	3790
$seats$	2+2	$\lambda_{o,w}$	0.48	Γ_{ht}	-2.73	D_p	10.8
$wing\_loc$	High	$t_{o,w}$	0.13	VT_type	Conventional	$nEng$	2
$b_w/2$	42.7	Γ_w	0.02	$b_{vt}/2$	11.17	eng_{ia}	1.00
$\Lambda_{LE,w}$	1.00	x_w	0.42	$c_{r,vt}$	10.6	eng_{ta}	0.12
$c_{r,w}$	12.0	$b_{ht}/2$	11.43	λ_{vt}	0.51	M_{cruise}	0.45
b_{crank}	0.31	$c_{r,ht}$	5.13	$\Lambda_{LE,vt}$	32.8	h_{cruise}	26,000
$\lambda_{i,w}$	0.76	λ_{ht}	0.95	MLG	Fuselage	V_{climb}	177

The turboprop engines are sized to 3 790 shp with a 10.8ft propeller disk. This engine is significantly de-rated compared to the DHC-8 Q400 but the aircraft mission profile is slower to account for this. The design mission climbs at 177kts. akin to an ATR 72 to a cruise altitude of 26 000 ft which is similar to the SAAB 2000 cruise altitude. This combination of slow climb speed and higher altitude cruise reduces the time spent in level acceleration to the cruise mach number as the cruise altitude is moved closer to the crossover altitude of the climb speed and cruise Mach. Level acceleration for the turboprop aircraft is a noted weak point in the design mission due to high thrust requirements and low thrust available. This weak point causes the climb range to extend much further than what is required to climb to the cruise altitude. Table 6.4 summarizes the key performance indicators (KPI) of three in-service aircraft where their design mission was changed to 500 nmi compared the Next-Gen turboprop aircraft solution. The power to weight ratio and wing loading are close to the those of the ATR 72 and SAAB 2000 respectively.

Table 6.4: Turboprop aircraft KPI comparison. All aircraft sized to 500 nmi design range. Equal design range may force sub-optimal performance and/or weights of in-service aircraft.

	ATR 72	DHC-8 Q400	SAAB 2000	NG-TP
MTOW [lb]	52 168	61 628	44 609	63 542
OEW [lb]	30 566	36 550	27 029	37 676
Seats	72	78	53	90
W_{pay} [lb]	15 768	17 492	11 981	20 273
W_f [lb]	5 834	7 586	5 599	5 594
PRE [nmi×lb/lb]	2 625	2 315	2 283	3 695
W/S	79.46	92.17	81.27	81.54
P_{prop} (x2) [hp]	5 500	10 200	8 304	7 580
P_{prop}/W	0.11	0.17	0.19	0.12
V_{climb} [kts]	170	230	210	177
M_{cruise}	0.45	0.52	0.62	0.45
h_{cruise}[ft]	15 000	20 000	25 000	26 000
t[hr]	2.27	1.87	1.85	2.33

In breaking down the Next-Gen turboprop aircraft performance by segment and comparing these results to the in-service aircraft, the changes to the climb and cruise of the aircraft are apparent. In Figure 6.3a, the range covered in climb by the Next-Gen turboprop aircraft is almost equal to the range covered in the cruise segment. The cost of this transfer of range from cruise to climb results in a small increase in climb segment fuel consumption and a large decrease in cruise fuel consumption, as shown in Figure 6.3b. Figure 6.3c shows the PRE performance of the aircraft over its design mission. The combination of the fuel consumption and range distribution in the design mission, as well as a 16-69% increase in design payload over its competitors, culminates in a superior PRE performance in all mission segments.

The Next-Gen turboprop aircraft designed here show that significant performance improvement gains are possible without the inclusion of technology leaps. The PRE optimization shows an improvement of 41-62% over the current market competitors. The cost of this efficiency is flight time and field length performance. The flight time of the design mission increases by 3-26% over competitors. The field performance of the DHC-8 Q400 and SAAB 2000 are 39% and 57% lower TOFL than the design constraint respectively (see Table 4.3 for field length data, Table 6.2 for design constraints).

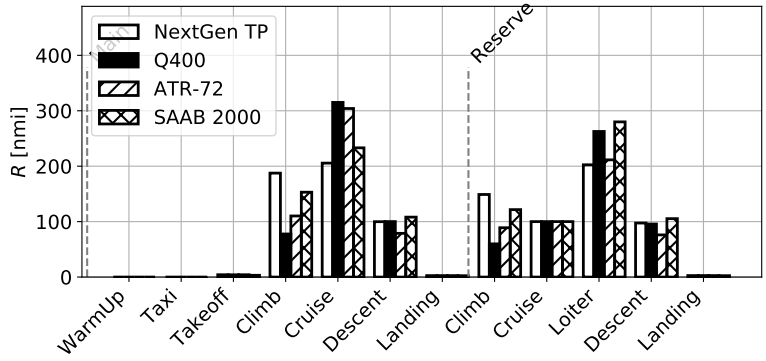

(a) R

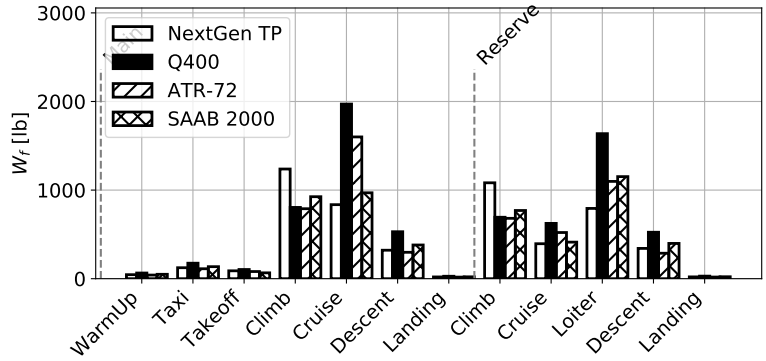

(b) W_f

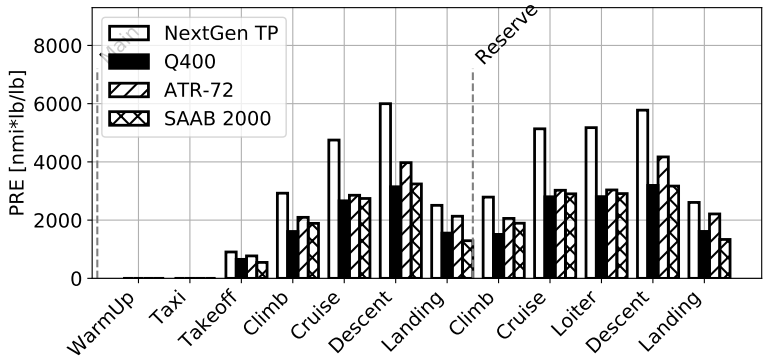

(c) PRE

Figure 6.3: Comparison of turboprop aircraft by segment for KPI.

6.4 Retro-fit Powertrain Design

To begin analyzing the potential for HEAC, the most simple design case should be considered. For propulsion technologies, often a retrofit of current aircraft is the chosen design strategy. A retro-fitted aircraft design reduces the flight envelope testing requirements and overall development time and costs at the expense of maximizing the system efficiency gains of new technologies. This also provides an intermediate sized problem to aid in development of the design code, so that HEP design could be tested within an aircraft and mission systems. The nested optimization formulation presented in Figure 6.1 is modified at the outer problem design variables. The outer aircraft design problem is limited to only the design variables associated with the HEP and the design mission variables.

Retrofit solutions were found for all three in-service turboprop aircraft, their KPI are shown in Table 6.5. The retrofitted ATR 72 had minor changes to its design mission, climbing slightly faster and to a higher cruise altitude. The retrofit engine sizing was increased by 22% over the combined power of its two turboprop engines and 17% increase in propulsive power. With power loading staying constant and wing loading increasing 15%, performance improvements proved difficult even with an optimal power management. The negligible improvements in W_f sizing thus the OEW increases of 18% lead to MTOW increases of 10%. Ultimately the ATR 72 airframe design does not have excess performance to be spared for the added systems weight of hybrid powertrains. The optimizer did not choose to eliminate batteries all together, they are inevitably necessary to overcome the increased power losses in the longer power path of hybrid powertrains. Without the batteries the generator would have to be even further oversized to account for increased weight and matching all mission power demands.

The DHC-8 Q400 is on the other end of the spectrum to the ATR 72. This aircraft is built with significant STOL performance requirements that drove the design of its predecessors, producing high lift and power at low speeds. The aircraft is also a fuselage extension of its predecessors, extending the cabin to 78 passengers at 30in. seat pitch in a 2+2 seat configuration. The addition of a hybrid powertrain increased OEW of the Q400 by 3% more than the OEW increase seen in the ATR 72. The hybrid electric Q400 was able to de-rate power leading to power loading reductions of 13% and 15% in generation and propulsion. A 13% increase in wing loading, leading to reductions in climb speed and cruise mach increases mission time by 16% and W_f increase

Table 6.5: Comparison of in-service aircraft and their hybrid electric retrofit equivalents.

	ATR 72			DHC-8 Q400			SAAB 2000		
	TP	HE	Δ	TP	HE	Δ	TP	HE	Δ
MTOW [lb]	52 168	57 582	+10.4%	61 628	69 645	+13.0%	44 609	44 274	−0.8%
OEW [lb]	30 566	35 987	+17.7%	36 550	43 919	+20.2%	27 029	27 578	+2.0%
Seats	72	72	+0.0%	78	78	+0.0%	53	53	+0.0%
W_{pay} [lb]	15 768	15 777	+0.1%	17 492	17 502	+0.1%	11 981	11 987	+0.1%
W_f [lb]	5 834	5 817	−0.3%	7 586	8 224	+8.4%	5 599	4 710	−15.9%
PRE [nmi×lb/lb]	2 625	2 583	−1.6%	2 315	2 049	−11.5%	2 283	2 477	+8.5%
W/S [lb/ft^2]	79.46	87.72	+10.4%	92.17	104.15	+13.0%	81.27	80.66	−0.8%
P_{prop} (x2)	5 500	6 450	+17.3%	10 200	9 996	−2.0%	8 304	4 138	−50.2%
P_{gen}	5 500	6 708	+22.0%	10 200	9 746	−4.5%	8 304	5 106	−38.5%
P_{prop}/W	0.11	0.11	+6.2%	0.17	0.14	−13.3%	0.19	0.09	−49.8%
P_{gen}/W	0.11	0.12	+10.5%	0.17	0.14	−15.4%	0.19	0.12	−38.0%
n	-	84	–	–	197	–	–	103	–
m	–	154	–	–	103	–	–	113	–
Total cells	–	12 936	–	–	20 291	–	–	11 639	–
V_{climb} [kts]	170	181.1	+6.5%	230	200	−13.0%	210	173.5	−17.4%
M_{cruise}	0.45	0.45	+0.0%	0.52	0.46	−11.5%	0.62	0.455	−26.6%
h_{cruise} [ft]	15 000	18 000	+20.0%	20 000	21 000	+5.0%	26 000	23 000	−11.5%
t [hr]	2.27	2.23	−1.8%	1.87	2.17	+16.0%	1.85	2.31	+24.9%

of 8%. Even though the STOL performance of the Q400 allows for larger OEW increases compared to the increases in the ATR, this does not lead to fuel consumption benefits over the baseline turboprop aircraft. The Q400 has 56% more battery cells in its battery pack than the ATR 72. An increase in battery size is to be expected, as the turboprop Q400 has 18% higher MTOW but the battery pack size increases is three times higher than the increase in MTOW. The battery pack cell dimensions show that the pack design favours voltage/power density by increasing n or current/energy density by increasing m. The ATR favours energy density, having 83% more cells in m than n. In contrast the Q400 favours power density, as it has 91% more cells in n than m. This suggests that the HEP of the Q400 is limited by magnitude of the power demands by the Q400 compared to the power density of hybrid electric cells. The HEP of the ATR is less limited by the power demands and thus is able to put more cells in the m dimensions for improved energy density.

The SAAB 2000 is a low-wing aircraft that uses a Rolls-Royce AE 2100 engine which is a 4 100 shp engine developed from the Allison T56. The design mission of the SAAB 2000 is a relatively fast and long range due to its design and the market philosophy taken in its development, direct route competition with larger turbofan aircraft. In the SAAB 2000 retrofit, the design range is

500nmi, which is shorter than its original 800nmi design mission. The reduction in range leads to a reduction in all design mission variables by 11-27%. The reduction in cruise Mach by 27% closely correlating with an increase in mission time of 25%. This reduction in design mission scale leads to reductions in power loading of 38% and 50% in generation and propulsion respectively. The combination of the mission and power de-rate, as well as the power management of the hybrid powertrain culminates in a 16% reduction in W_f. The hybrid powertrain design for the SAAB 2000 leads to a 2% increase in OEW and a minor reduction in MTOW and wing loading due to the W_f reductions. The similar wing loading of the retrofit means that the HEP along with its optimal power management was able to negate the aerodynamic penalty by counteracting the OEW increase with decrease in W_f.

The effect of a HEP retrofit was different for each aircraft, depending on how the hybrid powertrain affected the design mission and the scale of the power requirements of the aircraft to the power capabilities of batteries. This shows that a HEP is not guaranteed to be effective and provide system-wide benefits. The weight effects on wing-loading and the powertrain augmentation of the definition of power loading likely necessitates the need for a new aircraft, designed around higher OEW as a proportion of MTOW, but potentially lower W_f

6.5 Next-Gen Hybrid Electric Aircraft design

A Next-Gen aircraft configuration is designed with a hybrid powertrain (Next-Gen Hybrid Electric or NG-HE), using the sizing and optimization formulation shown in Figure 6.1. The variables include the mission, geometric (used in Section 6.3) and powertrain (used in Section 6.4) design as well as optimal power management. The solution to this design optimization is specified in Table 6.6 and geometry in Figure 6.4. The optimization history shown in Figure **??** shows the convergence of the result.

The HEAC solution uses a slightly shorter fuselage than the turboprop aircraft in Section 6.3. The cabin layout is 71 seats in a 2+1 seat configuration as opposed to the 90 seats in a 2+2 configuration of the turboprop aircraft solution. The wing has increased sweep by 9° and inner segment taper to create a more pronounced wing Yehudi. The wing longitudinal location is at a similar location in both aircraft. The HEAC is using a longer distribution of payload weight to balance the aft weight of the HEP. The HEAC design

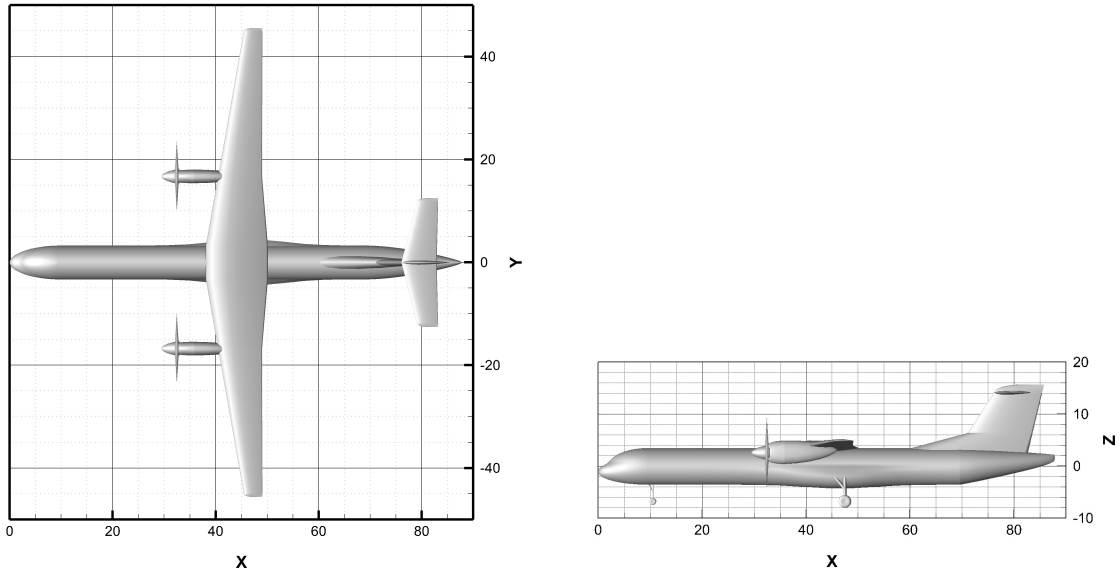

(a) (b)

Figure 6.4: Next-Gen HEAC geometry

mission climbs faster and cruises faster than the turboprop aircraft design due to the improved altitude performance of electric motors. The power management solution for the aircraft can be seen in the Appendix in Figure C.7. The overall strategy of the power management solution has not qualitatively changed since the results shown and discussed in Section 5.2.1.

Table 6.6: Next-Gen HEAC solution

Variable	Value	Variable	Value	Variable	Value	Variable	Value
cap	71	$t_{i,w}$	0.15	$\Lambda_{LE,ht}$	14.47	P_{prop}	2772
$seats$	2+1	$\lambda_{o,w}$	0.42	Γ_{ht}	0.89	D_p	13.57
$wing\_loc$	High	$t_{o,w}$	0.13	VT_type	T-Tail	$nEng$	2
$b_w/2$	41.8	Γ_w	1.9	$b_{vt}/2$	12.01	eng_{ia}	0
$\Lambda_{LE,w}$	10	x_w	0.43	$c_{r,vt}$	12.46	eng_{ta}	0.1
$c_{r,w}$	12.05	$b_{ht}/2$	12.55	λ_{vt}	0.75	M_{cruise}	0.53
b_{crank}	0.32	$c_{r,ht}$	6.84	$\Lambda_{LE,vt}$	33	h_{cruise}	25 000
$\lambda_{i,w}$	0.71	λ_{ht}	0.59	MLG	Fuselage	V_{climb}	180
P_{gen}	6124	n	107	m	101		

The KPI shown in Table 6.7 show the similarities and contrasts in the performance of a Next-Gen turboprop (NG-TP) and hybrid electric (NG-HE) aircraft for the same mission range. The OEW and MTOW of the aircraft are within 10% of each other even though the HEAC is carrying 21% less payload. The HEAC, carrying less weight requires 7% more W_f for the same mission range, leading to a 29% difference in PRE.

Table 6.7: KPI comparison of Next-Gen turboprop and HEAC.

	NG-TP	NG-HE	Δ
MTOW [lb]	63 542	57 425	−9.6%
OEW [lb]	37 676	35 376	−6.1%
Seats	90	71	−21.1%
W_{pay} [lb]	20 273	16 057	−20.8%
W_f [lb]	5 594	5 992	+7.1%
PRE [nmi×lb/lb]	3 695	2 641	−28.5%
W/S [lb/ft^2]	81.54	78.43	−3.8%
P_{prop} (x2) [shp]	7 580	5 544	−26.9%
P_{prop}/W [shp/lb]	0.12	0.10	−19.5%
P_{gen} [shp]	7 580	6 124	−19.2%
P_{gen}/W [shp/lb]	0.12	0.11	−11.1%
V_{climb} [kts]	177	180	+1.7%
M_{cruise}	0.45	0.53	+17.8%
h_{cruise} [ft]	26 000	25 000	−3.8%
t [hr]	2.33	2.07	−11.2%

The HEAC has a similar wing loading to the Next-Gen turboprop aircraft and a 20% and 10% reduction in propulsion (P_{prop}/W) and generation (P_{gen}/W) power loading respectively. In conventional aircraft sizing the power loading reduction would be a significant improvement. In this sizing method, where more details in performance analysis are considered, the improvement of the result is much more diluted. The HEAC is capable of the power loading reduction only with the inclusion of other HEP components, namely the battery, cabling and electric generator. This increased number of components and their weight is included in the detailed OEW estimation in this sizing. While the power management method is able to extract the best fuel consumption out of the HEP, when compared to the Next-Gen turboprop aircraft, the performance is inferior.

The only performance metric which is superior for the HEAC solution is that it completes the mission in 11% less time, mostly through increases in cruise Mach. It is possible that a turboprop aircraft with an identical payload and constrained to the same mission time as the HEAC, could achieve superior fuel consumption performance to the HEAC.

The speed of the HEAC solution is apparent in Figure 6.5, which breaks down the turboprop and HEAC designs range, fuel and PRE performance by segment. The HEAC completes the climb segment in less distance and with less fuel and a longer cruise with a proportionally small increase in fuel. The turboprop aircraft is however carrying 21% more payload, which means that these changes in mission performance do not lead to PRE improvement in any segment and thus the mission overall.

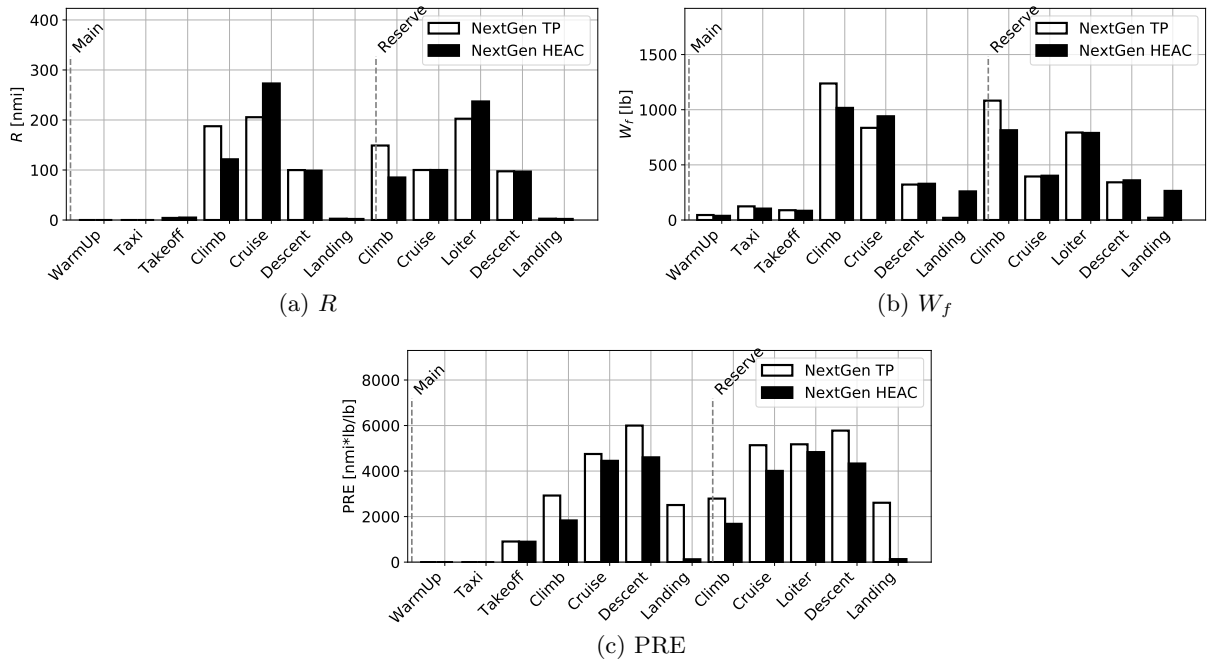

(a) R

(b) W_f

(c) PRE

Figure 6.5: Comparison of Next-Gen aircraft solutions as a turboprop and hybrid electric propulsion, by segment for key performance metrics.

6.6 Next-Gen Hybrid Electric Aircraft with Generator Redundancy

The results presented up to this point have compared HEAC (one engine generator) to turboprop aircraft, (two engines). This was done intentionally to see if the weight economies of scale of turboshaft engines would perform favourably in a HEAC with only one engine.

This configuration would prove difficult to certify as all commercial aircraft have two engines for redundancy. As well, new aircraft which rely on electrical energy generation for flight critical systems, like the Boeing 787 and Airbus A350, have twin-pack APU's to provide electric power generation redundancy as well as propulsion engine redundancy. To provide a thorough assessment of HEAC, single-engine and twin-engine performance must be considered. The HEAC design method utilized in Section 6.5 was re-examined considering the generator sizing as a twin-pack. Figure 6.6 shows the twin-pack generator configuration considered in the tail section of the design.

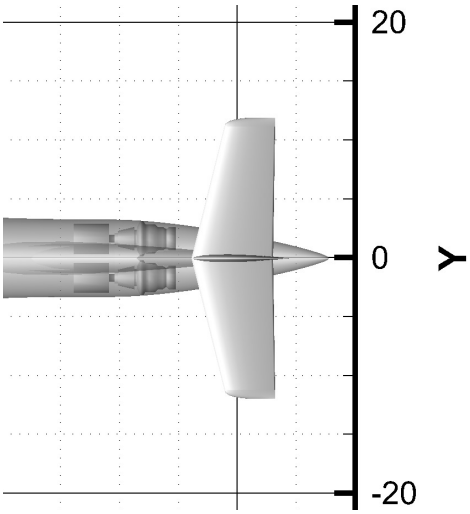

Figure 6.6: Redundant generator geometry in the tail section. Each turboshaft engine has its own electric generator.

The resulting aircraft design for a HEAC with redundant generators (NG-HERG) was very similar to the hybrid electric aircraft design in Section 6.5. The KPI comparison of the two aircraft is shown in Table 6.8. The design payload of the aircraft is identical, with the same seating capacity and layout.

The key weights of the aircraft are all similar (W_f, OEW and MTOW). The only significant difference between the KPI is the generator sizing. The twin-pack generator had 35% more power than the single-engine generator and 11% more battery cells.

Table 6.8: KPI comparison of HEAC with and without redundant generators.

	NG-HE	NG-HERG	Δ
MTOW [lb]	57 425	58 464	+1.8%
OEW [lb]	35 376	36 440	+3.0%
Seats	71	71	+0.0%
W_{pay} [lb]	16 057	16 082	+0.2%
W_f [lb]	5 992	5 941	−0.9%
PRE [nmi×lb/lb]	2 641	2 666	+0.9%
W/S [lb/ft^2]	78.43	79.68	+1.6%
P_{prop} (x2) [shp]	5 544	5 857	+5.6%
P_{prop}/W [shp/lb]	0.10	0.10	+5.6%
P_{gen} [shp]	6 124	8 270	+35.0%
P_{gen}/W [shp/lb]	0.11	0.14	+32.6%
n	120	115	−4.2%
m	103	119	+15.5%
Total cells	12 360	13 685	+10.7%
V_{climb} [kts]	181	183	+1.1%
M_{cruise}	0.53	0.52	−1.9%
h_{cruise} [ft]	25 000	22 000	−12.0%
t [hr]	2.07	2.09	+1.0%

The negligible impact of the redundant generators can most easily be shown in the weight sizing of turboshaft engines and electric motors. Electric motors are sized with a constant specific power (typically in kW/kg), so there is no difference between the weight of 2 electric generators at half the rating compared to one electric generator at the full rating. Turboshaft engines use statistical methods based on historical precedent to determine weight, the weight model is shown in Figure 6.7. The statistical methods provide increasing specific power as engine ratings increase. This specific power increase is very strong below 4 000shp and is less significant between a twin-pack at 4135 shp each and a single engine at 5 544shp.

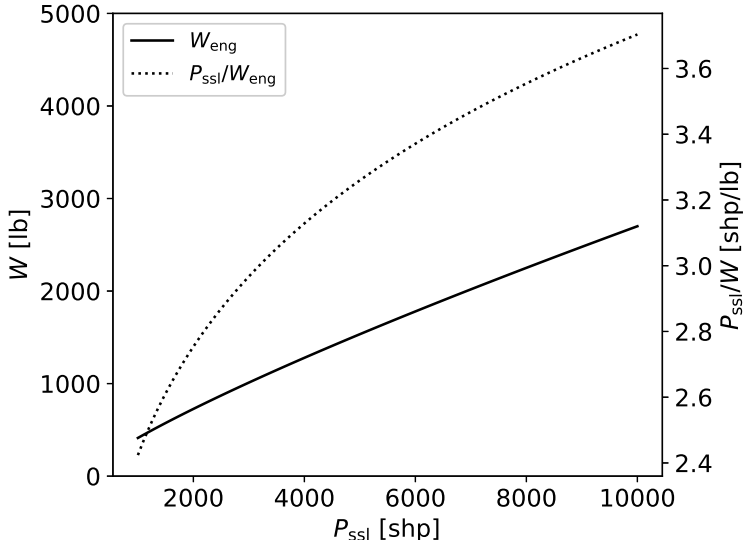

Figure 6.7: Turboshaft weight sizing, specific power included.

6.7 Results Overview

The design scenarios presented in Chapter 6 present the performance potential of regional turboprop aircraft and regional HEAC with hybrid. The scenarios reflect both clean-sheet designs and retro-fit designs, showing the design and performance implications of wider and narrower design spaces respectively. The KPI of the in-service aircraft, the Next-Gen turboprop aircraft, Next-Gen HEAC and the in-service aircraft with HEP retro-fits are shown together in Table 6.8.

The in-service aircraft each have different characteristics in their design mission. Some of these characteristics limit the PRE of the aircraft but deliver wider operational capabilities of the aircraft. The constraints used in the optimization capture the basic requirements of transport aircraft for typical operation feasibility and certification. The constraints do not require feasibility of wider operational capabilities, like the one included in the design of in-service aircraft, since constraint analysis needs to provide a more generalized transport aircraft design than one tailored to specific requirements. This provides an expanded design space for a new solution. Given this expanded design space, it is not surprising that the solutions designed with one objective function metric can achieve superior performance in that metric. What the solutions do provide is a concept aircraft, a new direction for further design.

Figure 6.8: Overview of regional aircraft solutions.

	ATR 72-600	DHC-8 Q400	SAAB 2000	NG-TP[1,2]	ATR-HE[3]	Q400-HE	SAAB 2000-HE	NG-HE	NG-HERG[4]
MTOW [lb]	52 168	61 628	44 609	63 542	57 582	69 645	44 274	57 425	58 464
OEW [lb]	30 566	36 550	27 029	37 676	35 987	43 919	27 578	35 376	36 440
Seats	72	78	53	90	72	78	53	71	71
W_{pay} [lb]	15 768	17 492	11 981	20 273	15 777	17 502	11 987	16 057	16 082
W_f [lb]	5 834	7 586	5 599	5 594	5 817	8 224	4 710	5 992	5 941
PRE [nmi×lb/lb]	2 625	2 315	2 283	3 695	2 583	2 049	2 477	2 641	2 666
W/S [lb/ft^2]	79.46	92.17	81.27	81.54	87.72	104.15	80.66	78.43	79.68
P_{prop}[5][shp]	5 500	10 200	8 304	7 580	6 450	9 996	4 138	5 544	5 857
P_{prop}/W [shp/lb]	0.11	0.17	0.19	0.12	0.11	0.14	0.09	0.10	0.10
P_{gen} [shp]	5 500	10 200	8 304	7 580	6 708	9 746	5 106	6 124	8 270
P_{gen}/W [shp/lb]	0.11	0.17	0.19	0.12	0.12	0.14	0.12	0.11	0.14
n	N/A	N/A	N/A	N/A	84	197	103	120	115
m	N/A	N/A	N/A	N/A	154	103	113	103	119
Total cells	N/A	N/A	N/A	N/A	12 936	20 291	11 639	12 360	13 685
V_{climb}	170	230	210	177	181.1	200	173.5	180	183
M_{cruise}	0.45	0.52	0.62	0.45	0.45	0.46	0.455	0.52	0.52
h_{cruise}	15 000	20 000	26 000	26 000	18 000	21 000	23 000	25 000	22 000
t [hr]	2.27	1.87	1.85	2.33	2.23	2.17	2.31	2.07	2.09

[1] NG=Next-Gen/Clean Sheet Design.
[2] TP=Turboprop.
[3] HE=Hybrid Electric.
[4] RG=Redundant Generators.
[5] Sum of 2 propulsors for all aircraft.

The new direction for a Next-Gen turboprop aircraft is a high-capacity aircraft which climbs for a larger proportion of the mission to a higher altitude. This design concept shows potential for improving fuel efficiency.

Hybrid electric retrofit aircraft can make for a lower cost integration of HEP and will likely provide a platform to learn economic and operational lessons about hybrid electric aviation. Hybrid electric retrofits will however likely only ever achieve fuel efficiency parity with their predecessor turboprop aircraft, with electric components at their current technology level. The retro-fit is too costly on OEW which cannot be counteracted with fuel weight savings, this leads to a higher MTOW, wing loading and drag.

A Next-Gen aircraft, which is designed around a HEP can achieve higher PRE than in-service turboprop aircraft. Unlike the Next-Gen turboprop aircraft, the Next-Gen HEAC keeps capacity similar to predecessors. The aircraft sizes the HEP and wing design in tandem to keep weight comparable to predecessors. This alleviates the wing loading which hampered performance of the retro-fit designs. The current technology level of HEP could not compete with the PRE performance of a Next-Gen turboprop aircraft but could deliver PRE improvements while decreasing mission time, rather than increasing it.

Overall, the aircraft designs presented show that a HEAC design process that includes power management is advantageous to extract the best design mission performance out of current technology level, producing competitive results and in the right conditions, superior results. This will provide an important foundation for the aircraft analysis of future technologies and operational applications.

6.8 Weight Sizing in Hybrid Electric Propulsion Design

The first aim of this design study was to find sizing reductions in the power management efficiency gains which would overcome the 11.5% power conversion losses in the hybrid electric powertrain and improve upon current powertrains. The second aim of this design study was to downsize power generation and propulsion components which would make the hybrid powertrain competitive on weight. Figure 6.9 illustrates qualitatively the outcomes of the

investigation into the second aim. The lines show the weight sizing equation of each component, the markers show the typical value of each component and error bars show the variation in sizing of each component dependent on the aircraft into which it is integrated. The variation on the turboshaft generator is wide but the weight will always be greater than the weight of two turboprop engines. The sum of the weights of the entire hybrid electric powertrain including the generator, motors, cables and batteries dwarfs the weight of the turboprop propulsion system.

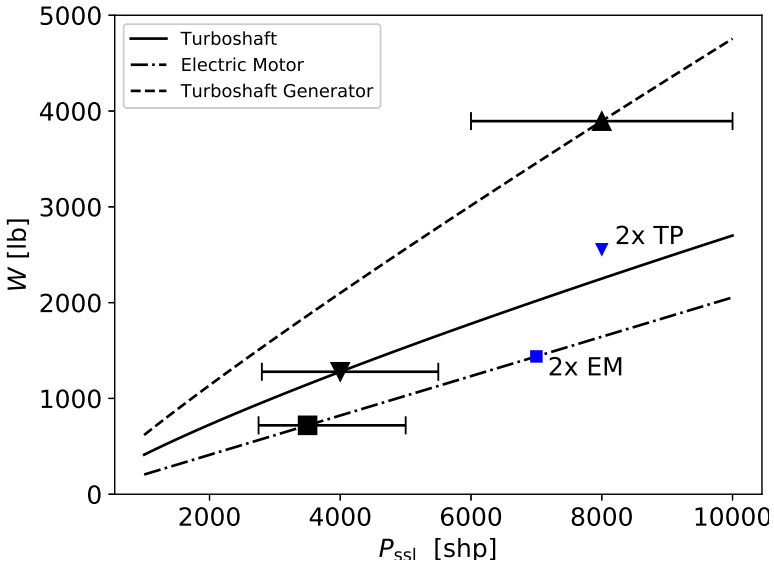

Figure 6.9: Propulsion components weight sizing. Error bars show variation in sizing due to design factors including payload weight, mission profile and aircraft configuration.

The series hybrid electric powertrain causes the OEW/MTOW of the HEAC to be higher than a turboprop aircraft (optimized or in-service) by approximately 0.02 to 0.025. Even with full sizing and operational variability to change the HEAC design and improve performance, the power management cannot overcome this difference in weight.

6.9 Results Comparison to Hybrid Electric Design Literature

The uniqueness and value of the HEAC sizing methods presented in this research is most notable when the aircraft design results are compared to the SOA in literature to date. Table 6.9 shows the HEAC design studies for different hybrid electric architectures and aircraft classes. The studies design the hybrid electric either in the limited scope of a propulsion retrofit or Next-Gen aircraft which also adjusts the aircraft OML to compensate for the HEP weight. The sizing methods have similar but not always identical metrics which are noted in Table 6.9. The classifications of design int this study are also shown at the top of the table showing the Next-Gen HEAC and SAAB 2000 retrofit design cases respectively. No design studies include battery charging, this difference will be noticeable in the following results.

Table 6.9: Comparable HEAC design studies

Author	Architecture	Aircraft Class	Design Type	Objective
Reid	Series	Regional	Next Gen	Max. PRE
	Series	Regional	Retrofit	Max. PRE
Finger [18]	Parallel	MALE UAV	Retrofit	Min. MTOW
Pornet [16]	Parallel	Short-Medium Haul	Next-Gen	Min. COSAR
	Partial Parallel	Short-Medium Haul	Next-Gen	Min. COSAR
Isikveren [50]	Parallel	Regional	Retrofit	Min. W_f
Voskujil [51]	Parallel	Regional	Retrofit	Min. W_f
Zamboni [19]	Series-distributed	Regional	Retrofit	Min. Energy
	Partial Hybrid	Regional	Retrofit	Min. Energy
	Parallel	Regional	Retrofit	Min. Energy

The results of the studies summarized in Table 6.9 are shown in Table 6.10. The table also notes the specific energy and power of batteries and electric motors used in the study. The proportion of OEW and W_f to MTOW is shown for all studies, as well as the proportion of battery weight (W_{batt}) as a proportion of OEW. While the classification of battery cell *vs.* pack and whether W_{batt} is included in OEW varies between studies, it would not account for the contrasts in sizing shown.

The specific energy of batteries used in this study are at least 61% lower than those used in any other study. The HEPs proposed in other studies use unproven battery chemistries, high temperature super conductors in motors or cryogenic cooling to enable high specific energy and power, as well as high

Table 6.10: Electric component sizing inputs and HEAC weight ratios

Author	E^*_{batt} [Wh/kg]	P^*_{batt} [kW/kg]	P^*_{EM} [kW/kg]	PRE [Δ%]	$\frac{\text{OEW}}{\text{MTOW}}$ [-]	$\frac{W_f}{\text{MTOW}}$ [-]	$\frac{W_{\text{battery}}}{\text{OEW}}$ [-]
Reid	**196**	1.6	8	1	0.62	0.10	**0.04**
	196	1.6	8	8	0.62	0.11	**0.05**
Finger [18]	500	10	10	1	-	0.14	-
Pornet [16]	1500	-	15	13	0.57	0.06	0.21
	1500	-	15	8	0.54	0.08	0.21
Isikveren [50]	500	1	9	-64	0.57	0.25	0.34
Voskujil [51]	1000	-	15	39	0.53	0.06	0.22
Zamboni [19]	750	0.8	9	0	0.56	0.07	0.14
	750	0.8	9	0	0.52	0.05	0.32
	750	0.8	9	0	0.52	0.05	0.31

transmission and conversion efficiency in the powertrain. The sizing methods in this study designed the battery pack such that its weight was proportionally lower than in any other study. The battery packs in this study made up 4-5% of OEW whereas other battery packs, with higher energy densities, ranged from 14-34% of OEW.

The aircraft OEW/MTOW varies with the aircraft class considered in each study. However, the results of this study show the highest OEW/MTOW due to the conservative technology assumptions in the HEP sizing. The power management methods included in the sizing method counteract the increase in OEW/MTOW by improving fuel consumption and reducing W_f/MTOW relative to other methods. The resulting PRE improvement over baseline is similar to other methods but is achieved with much less battery energy and more realistic technology levels.

The results shown here do not show that HEPs, at their current technology level, are ready for adoption in regional aircraft but they do show that current technology performs closer to parity with current aircraft than has been shown in previous work. The results show how battery charging can be implemented to maximize the utility of a battery in an aircraft propulsion system. The optimal power management has shown how battery pack design shows that batteries are neither unnecessary weight nor cause OEW weights to multiply.

7 Conclusions and Recommendations

Electrification of aircraft propulsions systems is being considered as current aviation technologies reach maturity and cease to improve efficiency at the industry goal of 2%/year. Implementing new aviation technologies has to balance the sub-system performance benefits with the multi-disciplinary effects of their inclusion. Design changes to sub-systems often implicate additional weight to the aircraft and while other systems can be re-designed to match this change, large architectural changes like aircraft propulsion electrification are more difficult to overcome.

This research was focused on the multi-disciplinary design implications of HEAC. Series HEP was chosen based on the lack of research in the current state-of-the-art, electric motors being used in single-mode operation and the sizing freedom provided to the conventional components in the powertrain.

Regional transport aircraft were chosen as the potential application of series HEPs as these missions have varying power requirements over the mission which is where prior hybrid electric applications have shown promise. Regional aircraft are also an under-developed part of the aviation sector due to low passenger demand and profits. As fuel prices trend upward with reducing oil exploration, carbon pricing schemes and social pressure, regional aircraft markets may see an increase in demand and market growth.

Additionally, this research developed methods to analyze HEAC mission performance in conceptual design. These methods allowed for analysis of the power management over the mission and quickly determine the approximate optimal management strategy and approximate performance potential for a given powertrain. This analysis showed that there are distinct discharge and charge cycles in regional aircraft missions.

The combination of HEAC design and power management were proposed as a way to find sufficient performance benefits to overcome the weight additions of HEPs. The HEAC design were compared to lower technology development al-

ternatives including new turboprop aircraft design and hybrid electric retrofits to current aircraft. While current design regulations are not well suited to non-mechanical power sources, attempts were made to consider certification requirements in the design including power generation redundancy.

7.1 Conclusions

The energy conversions and component weights proved to be challenging limitations to achieving HEAC performance improvement over both in-service and new turboprop aircraft. The process of converting fuel energy to propeller power requires conversions from chemical energy to heat, to mechanical, to electrical and finally to mechanical power. This chain of conversions is significantly longer than the chain in a turboprop engine. Not accounting for the negligible losses in cable transmission, the additional electrical conversion step costs at least 13% in efficiency. Additionally, the more complex architecture requires at least 3 electric motors and one turboshaft engine, as opposed to a turboprop aircraft with two turboshaft engines.

The HEAC designed (NG-HE and NG-HERG) achieved a competitive $MTOW$ by reducing seats and payload weight. At this weight, the HEAC achieved similar PRE performance to the best in-service aircraft for efficiency, the ATR 72-600. The electric propulsors, showing improved climb performance over turboprop engines completed the same design mission in 8% less time. Turboshaft generator redundancy, expected to be a certification requirement of HEAC, was not a significant impairment on performance.

The most significant performance result in the aircraft designed in this study was the capabilities of the optimized baseline case, a Next-Gen turboprop aircraft design. The Next-Gen turboprop aircraft design (NG-TP) was able to find the best PRE performance in the design mission of all the aircraft analyzed. The trade-offs for this performance are longer mission times and longer field performance.

7.2 Recommendations for Future Work

Using the design methods for HEAC developed in this work, multiple avenues of further exploration are exposed for future research. The main benefit of the component-based powertrain design approach is that changes in aircraft

performance due to performance changes of any component can be realized. The two most notable examples in the powertrain are electric motor/generator and battery performance. The electric motor/generators can be updated for different weight and efficiency map models. The battery charge and discharge curves, as well as operating limits can be updated and the aircraft performance re-assessed.

Powertrain components can also be re-organized into different architectures, the series HEP used in this study is not only the only possible architecture for aircraft. Parallel HEP, where the turboshaft and electric motor drive a common shaft and the electric motor serves as a motor and generator, may improve powertrain weight. A parallel HEP will need to include turboshaft speed as a part of the performance map so that electric motors can be integrated. Thorough parallel hybrid electric design analysis may require full engine cycle analysis, rather than the parametric performance model used in this research.

The analysis presented in this research was limited to the design mission and building sizing methods around the design mission. Hybrid electric aircraft with power management have the capability to tune power consumption to off-design ranges better than turboprop aircraft, leading to route network performance benefits.

The aircraft analysis performed here was purely physics-based. The basis for any viable aircraft concept has to have sound physics and economics. Including economics methods into HEAC design would further solidify the case for its development. Recent fluctuations in oil price, coupled with increased carbon pricing will further pressure aircraft economics towards maximum fuel efficiency. The difficulty with HEAC economics will be in estimating the research and development of both the electrical components, their integration into aircraft and flight testing for certification and infrastructure costs. The wide variation in potential research and development costs will lead to wide variations in profitability of the aircraft for manufacturers. Charging infrastructure and rate will impact economics and will have to be split amongst the manufacturers and local airport authorities. Charging infrastructure has already shown to be a limiting factor for plug-in HEV and EV adoption. Regional aircraft in particular, which fly to smaller regional airports, will have to plan their operation and build the economics of the aircraft around available charging infrastructure.

Bibliography

[1] V. Masson-Delmotte, P. Zhai, H.-O. Pörtner, D. Roberts, J. Skea, A. Pirani P.R. Shukla, W. Moufouma-Okia, C. Péan, R. Pidcock, S. Connors, J. B. R. Matthews, Y. Chen, X. Zhou, M. I. Gomis, E. Lonnoy, T. Maycock, M. Tignor, and T. Waterfield, editors. *Global Warming of 1.5˚C. An IPCC Special Report on the impacts of global warming of 1.5˚C above pre-industrial levels and related global greenhouse gas emission pathways, in the context of strengthening the global response to the threat of climate change, sustainable development, and efforts to eradicate poverty.* IPCC, 2018.

[2] Aircraft Technology Roadmap to 2050. Technical report, IATA, 2019.

[3] Fact sheet 3: Tracking aviation efficiency. Technical report, Air Transport Action Group, February 2021.

[4] 2019 Environmental Report: Aviation and Environment. Technical report, ICAO, 2019.

[5] Patrick W. Wheeler, Jon C. Clare, Andrew Trentin, and Serhiy Bozhko. An overview of the more electrical aircraft. *Proceedings of the Institution of Mechanical Engineers, Part G: Journal of Aerospace Engineering*, 227(4):578–585, December 2012.

[6] Report 6 - Civil Aviation Infrastructure in the North - Transport Canada. Technical report, Auditor General of Canada, 2017.

[7] Mehrdad Ehsani. *Modern electric, hybrid electric, and fuel cell vehicles.* CRC Press, Taylor & Francis Group, Boca Raton, 2018.

[8] *Commercial Aircraft Propulsion and Energy Systems Research.* The National Academies Press, Washington, DC, 2016.

[9] R. E. Perez and J. R. R. A. Martins. pyACDT: An Object-Oriented Framework for Aircraft Design Modelling and Multidisciplinary Optimization. In *12th AIAA/ISSMO Multidisciplinary Analysis and Optimization Conference*, Victoria, BC, September 2008.

[10] A. F. Burke. Hybrid/Electric Vehicle Design Options and Evaluations. In *SAE Technical Paper Series.* SAE International, February 1992.

[11] K.T Chau and Y.S Wong. Overview of power management in hybrid electric vehicles. *Energy Conversion and Management*, 43(15):1953–1968, October 2002.

[12] Transportation Research Center at Argonne National Labratory. U.S. HEV Sales by model. Online, January 2020.

[13] Alparslan Emrah Bayrak, Namwoo Kang, and Panos Y. Papalambros. Decomposition-Based Design Optimization of Hybrid Electric Powertrain Architectures: Simultaneous Configuration and Sizing Design. *Journal of Mechanical Design*, 138(7), June 2016.

[14] C. Pornet, S. Kaiser, A.T. Isikveren, and M. Hornung. Integrated fuel-battery hybrid for a narrow-body sized transport aircraft. *Aircraft Engineering and Aerospace Technology*, 86(6):568–574, September 2014.

[15] A.T. Isikveren, S. Kaiser, C. Pornet, and P.C. Vratny. Pre-design strategies and sizing techniques for dual-energy aircraft. *Aircraft Engineering and Aerospace Technology*, 86(6):525–542, September 2014.

[16] Clément Pornet. *Pornet, Clément. Conceptual design methods for sizing and performance of hybrid-electric transport aircraft.* phdthesis, Technische Universität München, April 2018.

[17] Joachim Kurzke. Gasturb 12: Design and off-design performance of gas turbines. *Aachen: GasTurb GmbH*, 2007.

[18] Felix Finger. *Methodology for Multidisciplinary Aircraft Designunder Consideration of Hybrid-Electric Propulsion Technology.* phdthesis, RMIT University, September 2020.

[19] J. Zamboni. A method for the conceptual design of hybrid electric aircraft. mathesis, Delft University of Technology, August 2018.

[20] HyunKi Lee, Caleb M. Harris, Jonathan C. Gladin, and Dimitri N. Mavris. A Method for Simultaneous Optimization of Power Split and Flight Path Trajectories for Hybrid Electric Aircraft. In *AIAA Scitech 2021 Forum*. American Institute of Aeronautics and Astronautics, January 2021.

[21] Tyler J. Wall and Richard T. Meyer. Hybrid electric aircraft switched model optimal control. *Journal of Propulsion and Power*, 36(4):488–497, July 2020.

[22] Sai Krishna Sumanth Nakka and Michael J. Alexander-Ramos. Simultaneous combined optimal design and control formulation for aircraft hybrid-electric propulsion systems. *Journal of Aircraft*, 58(1):53–62, January 2021.

[23] J.D. Mattingly, W.H. Heiser, and Pratt D.T. *Aircraft Engine Design*. AIAA Educational Series. AIAA, 2nd edition, 2002.

[24] Dieter Scholz. Der Propellerwirkungsgrad – einfache berechnungen. Lecture notes, HAW Hamburg, April 2020.

[25] Hamilton Standard. Generalized method of propeller performance estimation. Technical Report PDB 6101A, Windsor Locks, CT, 1963.

[26] Angela Nuic, Damir Poles, and Vincent Mouillet. BADA: An advanced aircraft performance model for present and future ATM systems. *International Journal of Adaptive Control and Signal Processing*, 24(10):850–866, August 2010.

[27] Stefan Stückl. *Methods for the Design and Evaluation of Future Aircraft Concepts Utilizing Electric Propulsion Systems*. 2016, Technische Universität München, April 2016.

[28] Patrick Vratny, Corin Gologan, Clément Pornet, Askin Isikveren, and Mirko Hornung. Battery Pack Modeling Methods for Universally-Electric Aircraft. In *4th CEAS Air & Space Conference*, September 2013.

[29] Heather M. Barkholtz, Armando Fresquez, Babu R. Chalamala, and Summer R. Ferreira. A database for comparative electrochemical performance of commercial 18650-format lithium-ion cells. *Journal of The Electrochemical Society*, 164(12):A2697–A2706, 2017.

[30] Robert McDonald. Electric Motor Modeling for Conceptual Aircraft Design. In *51st AIAA Aerospace Sciences Meeting including the New Horizons Forum and Aerospace Exposition*. American Institute of Aeronautics and Astronautics, January 2013.

[31] Reza Rajabi Moghaddam. High speed operation of electrical machines, a review on technology, benefits and challenges. In *2014 IEEE Energy Conversion Congress and Exposition (ECCE)*. IEEE, September 2014.

[32] A Jameson. The analysis of propeller-wing flow interaction. *Analytical Methods in Aircraft Aerodynamics*, 1970.

[33] Alex M. Stoll and Gregor Veble Mikic. Design Studies of Thin-Haul Commuter Aircraft with Distributed Electric Propulsion. In *16th AIAA Aviation Technology, Integration, and Operations Conference*. American Institute of Aeronautics and Astronautics, June 2016.

[34] Daniel Raymer. *Aircraft design : a conceptual approach*. American Institute of Aeronautics and Astronautics, Inc, Reston, Virginia, 2018.

[35] Jan Roskam. *Airplane design Part V: Component Weight Estimation*. DARcorporation, Lawrence, Kan, 1986.

[36] Egbert Torenbeek. *Synthesis of Subsonic Airplane Design*. Springer Netherlands, 1982.

[37] B. H. Oman. Vehicle design evaluation program (vdep). techreport NASA-CR-145070, General Dynamics, January 1977.

[38] Melissa Zhuo. Quark and terrier: Koenigsegg's first in-house e-motor and ev-drive unit with pioneering 'raxial flux' topology. techreport, Koenigsegg, January 2022.

[39] N. E. Anderson, S. H. Loewenthal, and J. D. Black. An analytical method to predict efficiency of aircraft gearboxes. *Journal of Mechanisms, Transmissions, and Automation in Design*, 108(3):424–432, September 1986.

[40] Sidney A. Powers. Critical field length calculations for preliminary design. *Journal of Aircraft*, 18(2):103–107, February 1981.

[41] P. W. Jansen and R. E. Perez. Coupled Optimization of Aircraft Family Design and Fleet Assignment for Minimum Cost and Fuel Burn. In *12th AIAA Aviation Technology, Integration, and Operations (ATIO) Conference and 14th AIAA/ISSMO Multidisciplinary Analysis and Optimization Conference*, Indianapolis, Indiana, September 2012. AIAA.

[42] P. W. Jansen and R. E. Perez. Coupled Optimization of Aircraft Design and Fleet Allocation with Uncertain Passenger Demand. In *2013 Aviation Technology, Integration, and Operations Conference*, Los Angeles, California, August 2013. AIAA.

[43] P. W. Jansen and R. E. Perez. Robust Coupled Optimization of Aircraft Design and Fleet Allocation for Multiple Markets. In *AVIATION 2014, AIAA/3AF Aircraft Noise and Emissions Reduction Symposium*, number AIAA 2014-2735, Atlanta, GA, June 2014.

[44] P. W. Jansen and R. E. Perez. Coupled optimization of aircraft families and fleet allocation for multiple markets. *Journal of Aircraft, In Press*, 2016.

[45] Peter W. Jansen and Ruben E. Perez. Integrated Design and Optimization of Aircraft Families and Air Transport Network. In *16th AIAA Aviation Technology, Integration, and Operations Conference*. American Institute of Aeronautics and Astronautics, June 2016.

[46] Stewart J. Reid, Ruben E. Perez, Peter W. Jansen, and Cees Bil. Influence of Carbon Pricing on Regional Aircraft and Route Network Design.

In *AIAA Scitech 2021 Forum*. American Institute of Aeronautics and Astronautics, January 2021.

[47] JE Green. Greener by design—the technology challenge. *The Aeronautical Journal*, 106(1056):57–113, 2002.

[48] R. K. Nangia. Efficiency parameters for modern commercial aircraft. *The Aeronautical Journal*, 110(1110):495–510, aug 2006.

[49] Peter W. Jansen and Ruben E. Perez. Multi–Objective Design Optimization of an MoM Aircraft using an Asynchronous Constrained PSO. In *AIAA Scitech 2019 Forum*. American Institute of Aeronautics and Astronautics, January 2019.

[50] A. T. Isikveren, Y. Fefermann, C. Maury, C. Level, K. Zarati, J.-P. Salanne, C. Pornet, and B. Thoraval. Pre-design of a commuter transport utilising voltaic-joule/brayton motive power systems. *The Aeronautical Journal*, 122(1248):205–237, December 2017.

[51] Mark Voskuijl, Joris van Bogaert, and Arvind G. Rao. Analysis and design of hybrid electric regional turboprop aircraft. *CEAS Aeronautical Journal*, 9(1):15–25, October 2017.

Appendices

A Additional Component Data

A.1 Propeller Data

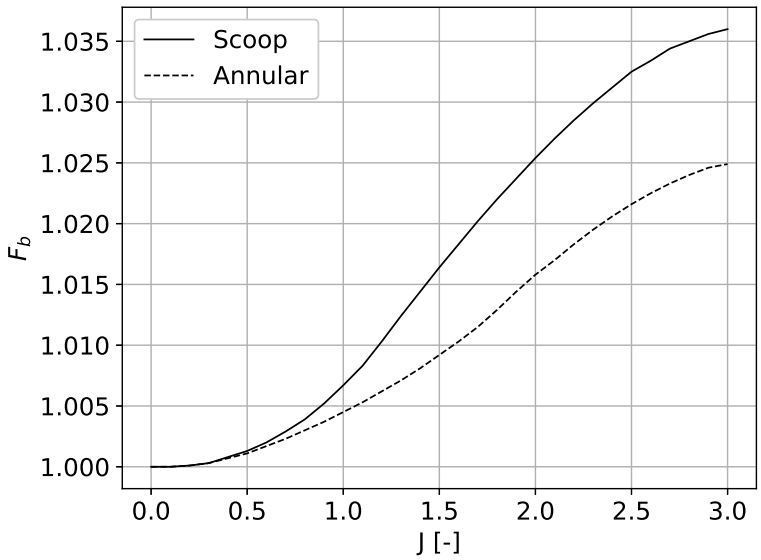

Figure A.1: Turboprop inlet blockage correction [25].

A.2 Battery Data

A.3 Component Weight Equations

$$\begin{aligned} w_{eng} &= 1.4716{P_{ssl}}^{0.8159} \\ w_{starter} &= 12.05\left(\frac{w_{eng}}{10^3}\right)^{1.458} \\ w_{oil\&cool} &= 0.07 w_{eng} \\ w_{GT} &= w_{eng} + w_{starter} + w_{oil\&cool} \end{aligned} \tag{A.1}$$

Table A.1: LCO battery details. Prices current as of June 2017. [29]

Anode	Cathode	Nominal Capacity (Ah)
Graphitic carbon	$LiCoO_2$	2.5
Nominal Voltage (V)	Measured Capacity (Ah)	Measure Energy (Wh)
3.6	2.44±0.03	8.8±0.1
Maximum Discharge Current (A)	Operating Temperature Range ($°C$)	Nominal Volume (ml)
20	$[0, 50]$	16.5
Measured Mass (g)	Cost per cell ($)	Energy Density (Wh/kg)
44.9	7.50	533.3
Specific Energy (Wh/kg)	Cost per Capacity ($/kWh)	
195.8	852.3	

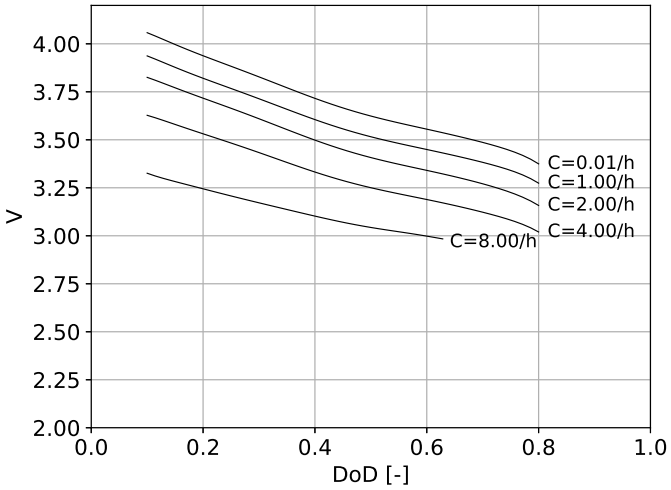

Figure A.2: Polynomial fit model. Model extended to $C = 0.01$/h.

$$
\begin{aligned}
N_b &= 6 \text{ (assumed constant)} \\
w_{blades} &= 1.1 \left(D_p P_{ssl} {N_b}^{0.5} \right)^{0.52} \\
w_{control} &= 0.322 {N_b}^{0.589} \left(\frac{D_p P_{ssl}}{10^3} \right)^{1.178} \\
w_{prop} &= w_{blades} + w_{control}
\end{aligned}
\tag{A.2}
$$

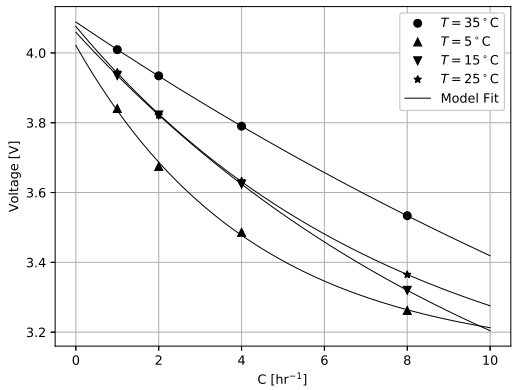

Figure A.3: Voltage curve fit for discharge rates at $SOC = 90\%$. Curve fitting using $f(x) = ae^{-\frac{x}{b}+c}$. Used to determine voltage shift for low C-rates.

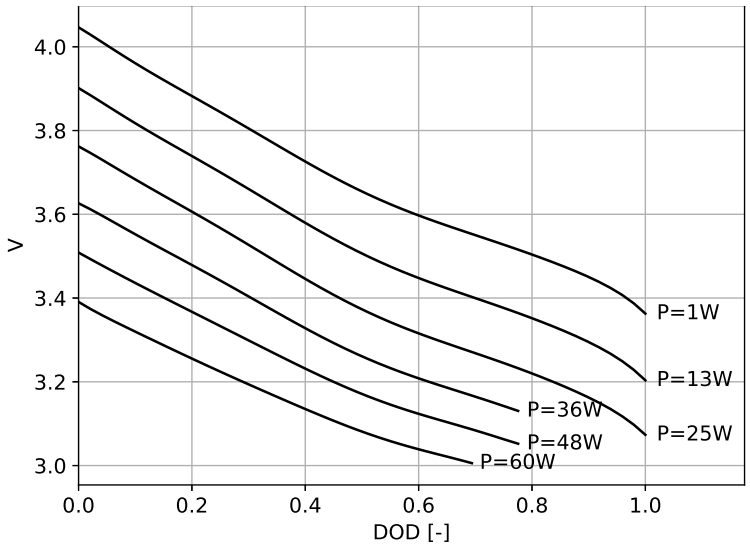

Figure A.4: Voltage at constant power discharge in the battery model

B Additional Regional Aircraft Model Data

B.1 Feasible Wing & Landing Gear Combinations

Turboprop aircraft differ from turbofan aircraft in the possible locations of the main landing gear (MLG). In-service turboprop aircraft have MLG in pods in the underbelly of the fuselage (ATR 42/72, A400M, C-130 and many other MIL transports) or also in the aft section of the engine nacelle (DHC-8, SAAB340/2000). Table B.1 shows the possible combinations of wing and MLG location for the configuration model.

MLG \ Wing	High	Low
Nacelle	✓	✓
Fuselage	✓	×

Table B.1: Feasible wing and landing gear combinations

B.2 In-Service Aircraft Model Data

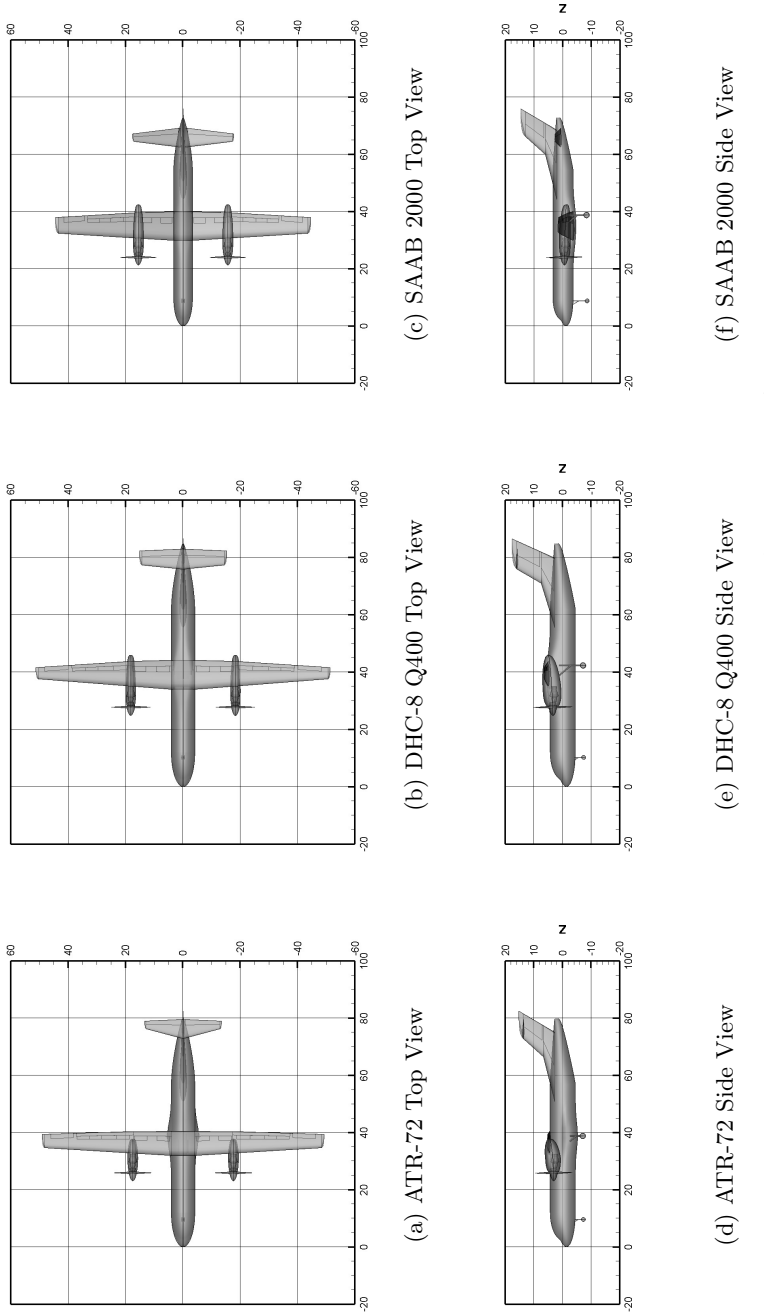

(a) ATR-72 Top View (b) DHC-8 Q400 Top View (c) SAAB 2000 Top View

(d) ATR-72 Side View (e) DHC-8 Q400 Side View (f) SAAB 2000 Side View

Figure B.1: In-service regional turboprop configurations. All dimensions in feet.

B.3 Regional Aircraft Weight Modelling

Weight statements are taken at the original design range of each in-service aircraft, correlating with the performance results shown in Section 4.6 and 4.7.

Listing B.1: ATR72-600 weight and balance statement

		Weights [lbf]	xCG(FWD)	xCG(AFT)	yCG	zCG
Maximum Takeoff Weight (MTOW)	:	52925.6	33.048	36.521	0.059	1.646
Maximum Landing Weight (MLW)	:	48862.4	32.859	36.621	0.064	1.387
Maximum Empty Weight (MEW)	:	27590.2	32.792	39.455	0.114	2.639
Operational Empty Weight (OEW)	:	31444.2	32.020	37.866	0.100	2.250
Zero Fuel Weight (ZFW)	:	47197.7	32.773	36.667	0.067	1.268
Zero Payload Weight (ZPW)	:	37172.2	32.528	37.473	0.085	2.637
AMPR Weight	:	18932.5				
Fuel	:	5727.9	35.316	35.316	4.762	4.762
Furnishings	:	4651.0	27.078	43.006	0.000	0.000
Operational Items	:	3854.0	26.493	26.493	−0.536	−0.536
Payload	:	15753.4	34.275	34.275	−0.693	−0.693
Propulsion	:	2944.0	28.809	29.803	3.195	3.195
Structures	:	12909.3	37.426	44.268	3.122	3.122
Fuselage	:	4089.6	31.856	47.785	0.000	0.000
Wing	:	5679.4	35.069	37.870	0.000	4.749
Horizontal Tail	:	522.8	75.639	77.591	0.000	13.842
Vertical Tail	:	882.1	65.412	70.311	0.000	5.612
Nacelle	:	495.0	31.277	33.025	17.546	3.195
Nacelle	:	495.0	31.277	33.025	−17.546	3.195
Landing Gear	:	745.6	34.191	34.481	4.217	−2.704
Systems	:	6024.8	34.996	38.063	3.836	3.836
Anti−Ice	:	700.9	34.018	36.119	0.000	4.749
Air Conditioning	:	952.0	36.119	38.920	0.000	4.397
Avionics	:	1148.7	7.168	8.761	0.000	0.000
Auxiliary Power Unit	:	493.7	59.731	78.048	0.000	2.188
Electrical	:	1244.0	35.769	37.870	0.000	4.397
Flight Controls	:	785.0	51.908	51.908	0.000	6.595
Fuel System	:	407.2	35.419	37.519	0.000	4.749
Hydraulics	:	293.3	51.908	51.908	0.000	6.595

Listing B.2: DHC-8400 weight and balance statement

		Weights [lbf]	xCG(FWD)	xCG(AFT)	yCG	zCG
Maximum Takeoff Weight (MTOW)	:	62344.2	35.548	39.143	0.292	2.007
Maximum Landing Weight (MLW)	:	57383.2	35.343	39.248	0.317	1.743
Maximum Empty Weight (MEW)	:	33537.3	35.139	41.821	0.542	3.076
Operational Empty Weight (OEW)	:	37644.9	34.473	40.425	0.483	2.681
Zero Fuel Weight (ZFW)	:	55137.3	35.238	39.302	0.330	1.609
Zero Payload Weight (ZPW)	:	44851.7	35.027	40.023	0.406	3.062
AMPR Weight	:	21812.3				
Fuel	:	7206.9	37.922	37.922	5.052	5.052
Furnishings	:	5149.4	28.778	45.706	0.000	0.000
Operational Items	:	4107.6	29.028	29.028	−0.549	−0.549
Payload	:	17492.4	36.885	36.885	−0.698	−0.698
Propulsion	:	4751.1	30.815	31.862	3.475	3.475
Structures	:	15579.4	40.465	47.500	3.771	3.771

Fuselage	:	4566.3	33.856	50.785	0.000	0.000
Wing	:	6294.5	37.641	40.821	0.000	5.267
Horizontal Tail	:	727.3	78.175	80.521	0.000	16.066
Vertical Tail	:	1033.4	69.523	74.543	0.000	6.133
Nacelle	:	918.0	36.250	39.039	18.240	3.475
Nacelle	:	918.0	36.250	39.039	−18.240	3.475
Landing Gear	:	1121.8	38.891	39.134	16.212	1.059
Systems	:	6767.5	37.454	40.756	4.124	4.124
Anti−Ice	:	796.7	36.449	38.834	0.000	5.267
Air Conditioning	:	1060.8	38.834	42.013	0.000	4.397
Avionics	:	1337.6	7.618	9.311	0.000	0.000
Auxiliary Power Unit	:	540.4	63.481	82.948	0.000	2.188
Electrical	:	1373.6	38.436	40.821	0.000	4.397
Flight Controls	:	896.5	56.604	56.604	0.000	7.779
Fuel System	:	426.9	38.039	40.423	0.000	5.267
Hydraulics	:	335.0	56.604	56.604	0.000	7.779

Listing B.3: SAAB 2000 weight and balance statement

		Weights [lbf]	xCG(FWD)	xCG(AFT)	yCG	zCG
Maximum Takeoff Weight (MTOW)	:	47569.8	31.082	33.994	0.225	−0.984
Maximum Landing Weight (MLW)	:	43993.5	30.869	34.019	0.243	−0.888
Maximum Empty Weight (MEW)	:	25235.4	30.718	36.208	0.423	−0.448
Operational Empty Weight (OEW)	:	28375.5	30.063	34.946	0.376	−0.517
Zero Fuel Weight (ZFW)	:	40345.7	30.614	34.048	0.265	−0.772
Zero Payload Weight (ZPW)	:	35599.5	30.800	34.692	0.300	−0.852
AMPR Weight	:	17264.5				
Fuel	:	7224.1	33.693	33.693	−2.168	−2.168
Furnishings	:	3591.9	24.714	39.251	0.000	0.000
Operational Items	:	3140.1	24.804	24.804	−1.070	−1.070
Payload	:	11970.2	31.919	31.919	−1.377	−1.377
Propulsion	:	4002.3	26.993	28.019	−0.457	−0.457
Structures	:	11234.9	35.479	41.398	−0.331	−0.331
Fuselage	:	2874.1	29.075	43.613	0.000	0.000
Wing	:	4748.4	33.326	36.632	0.000	−1.254
Horizontal Tail	:	658.3	64.569	66.429	0.000	1.647
Vertical Tail	:	648.9	58.876	63.775	0.000	5.001
Nacelle	:	747.4	32.536	35.340	15.586	−0.457
Nacelle	:	747.4	32.536	35.340	−15.586	−0.457
Landing Gear	:	810.4	33.876	34.390	13.179	−1.744
Systems	:	5435.7	33.072	35.967	−1.059	−1.059
Anti−Ice	:	743.3	32.086	34.565	0.000	−1.254
Air Conditioning	:	720.8	34.565	37.871	0.000	−3.514
Avionics	:	1040.3	6.542	7.996	0.000	0.000
Auxiliary Power Unit	:	391.0	54.516	71.234	0.000	1.749
Electrical	:	968.6	34.152	36.632	0.000	−3.514
Flight Controls	:	833.3	48.395	48.395	0.000	0.841
Fuel System	:	427.1	33.739	36.218	0.000	−1.254
Hydraulics	:	311.3	48.395	48.395	0.000	0.841

C Regional Aircraft Design Solution Data

C.1 Retrofit Supplemental Data

Table C.1: ATR Retrofit Hybrid Electric Aircraft Solution

Variable	Value	Variable	Value	Variable	Value	Variable	Value
P_{prop}	3225	P_{gen}	6708	n	84	m	154
M_{cruise}	0.45	h_{cruise}	18 000	V_{climb}	181.1		

Table C.2: Q400 Retrofit Hybrid Electric Aircraft Solution

Variable	Value	Variable	Value	Variable	Value	Variable	Value
P_{prop}	4998	P_{gen}	9746	n	197	m	103
M_{cruise}	0.463	h_{cruise}	21 000	V_{climb}	200.48		

Table C.3: SAAB 2000 Retrofit Hybrid Electric Aircraft Solution

Variable	Value	Variable	Value	Variable	Value	Variable	Value
P_{prop}	2069	P_{gen}	5106	n	103	m	113
M_{cruise}	0.455	h_{cruise}	23000	V_{climb}	173.5		

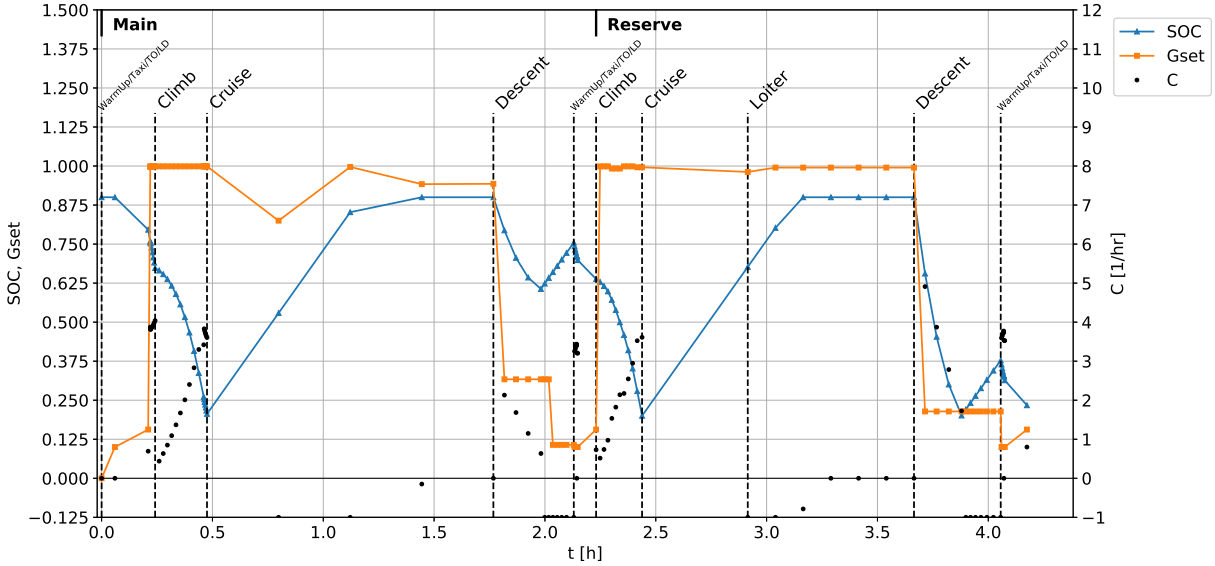

Figure C.1: ATR 72 retro-fit power management

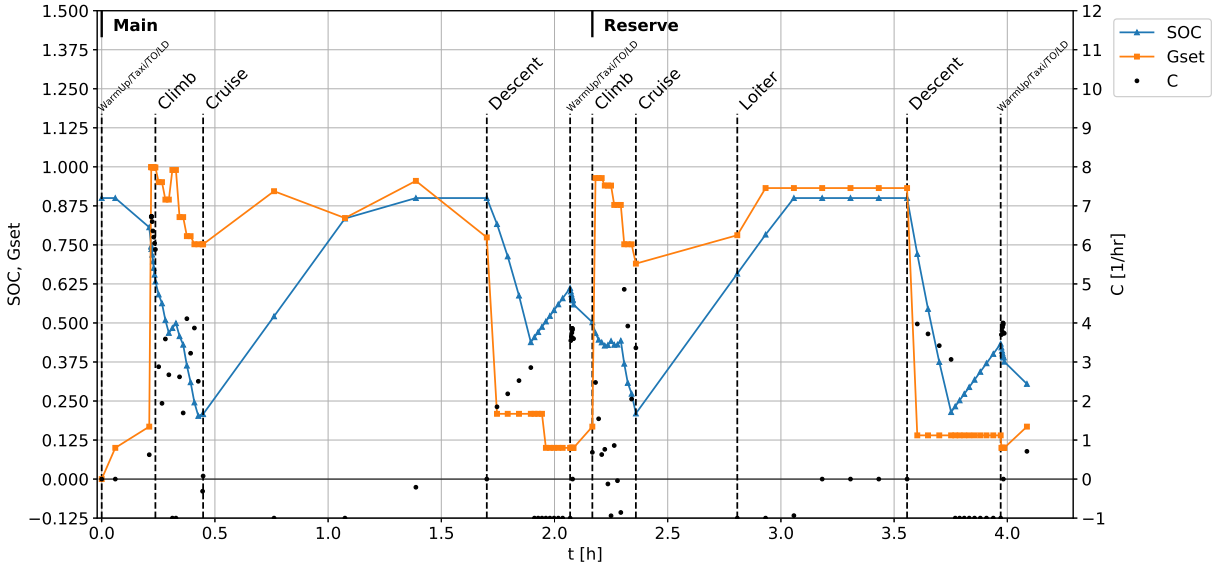

Figure C.2: Q400 retro-fit power management

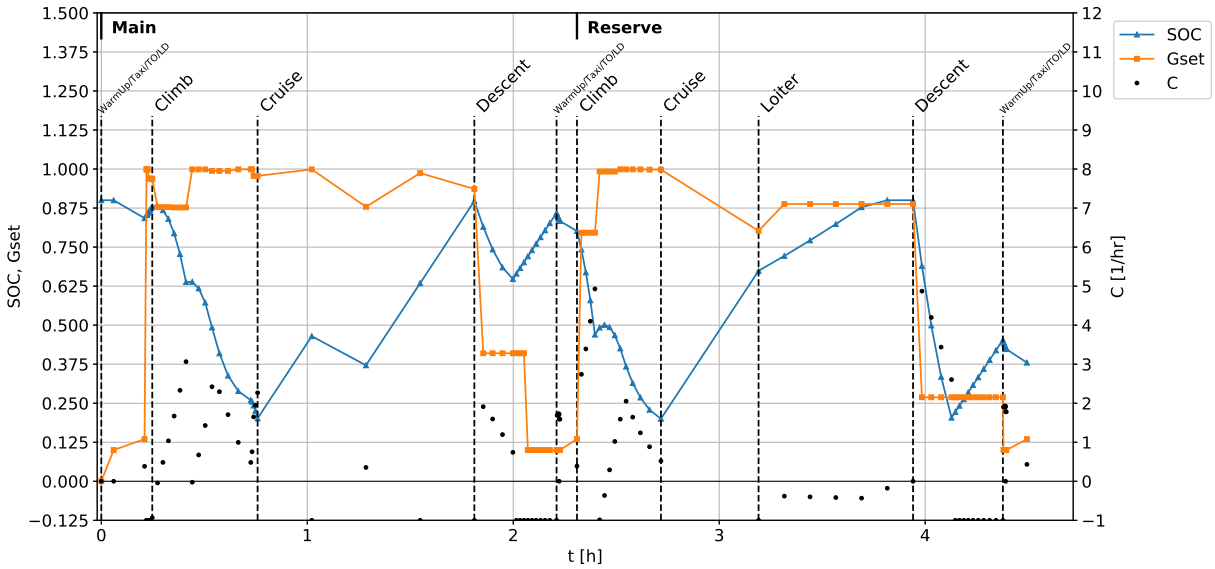

Figure C.3: SAAB retro-fit power management

C.2 Next-Gen Hybrid Electric Aircraft Power Management Data

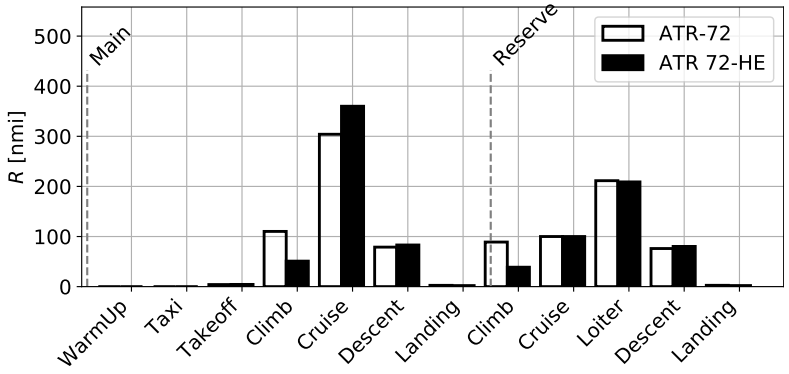

(a) R

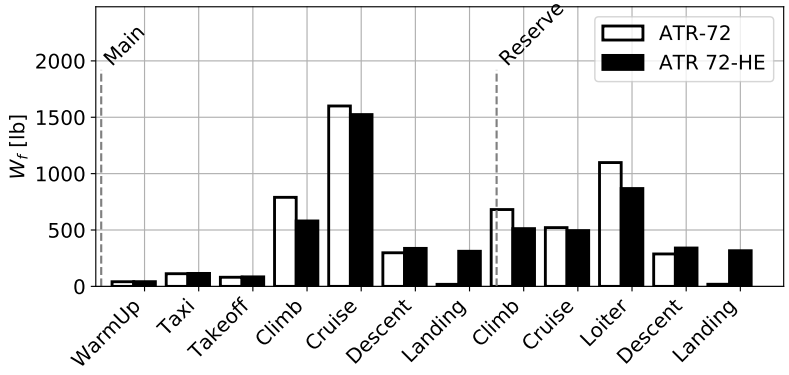

(b) W_f

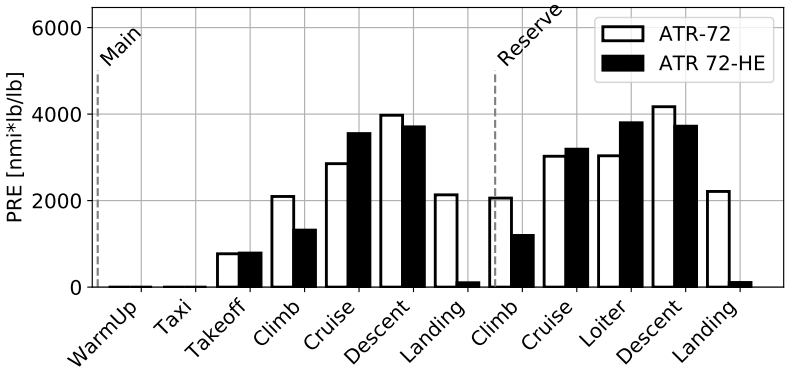

(c) PRE

Figure C.4: Comparison of ATR 72 aircraft configuration as a turboprop and hybrid electric propulsion by segment for key performance metrics.

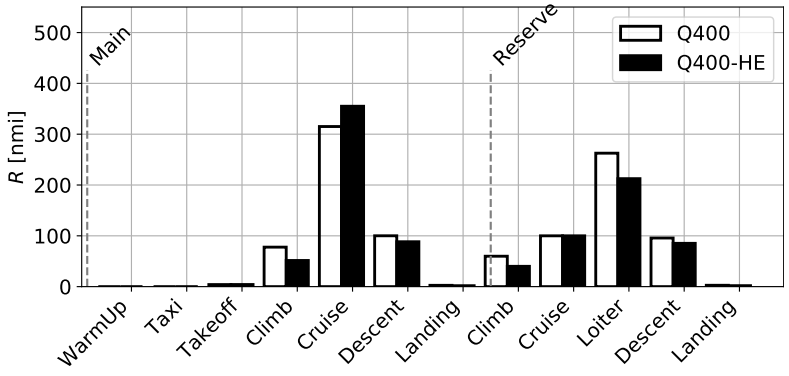

(a) R

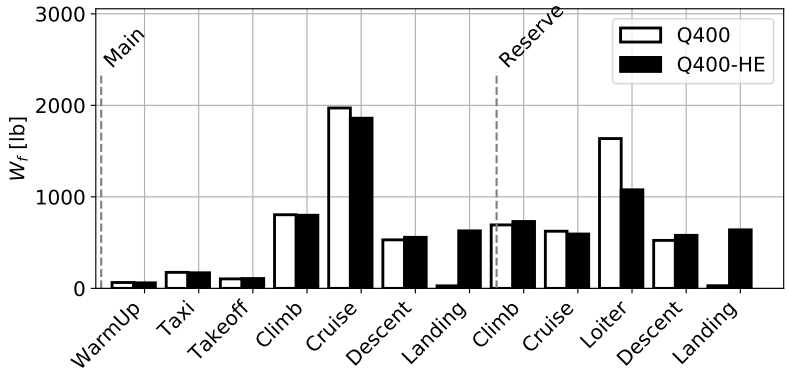

(b) W_f

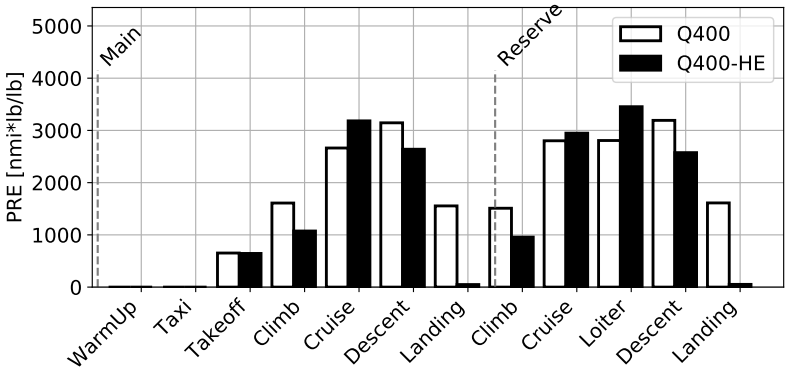

(c) PRE

Figure C.5: Comparison of Q400 aircraft configuration as a turboprop and hybrid electric propulsion by segment for key performance metrics.

C.3 Next-Gen Hybrid Electric Aircraft With Redundant Generators Supplemental Data

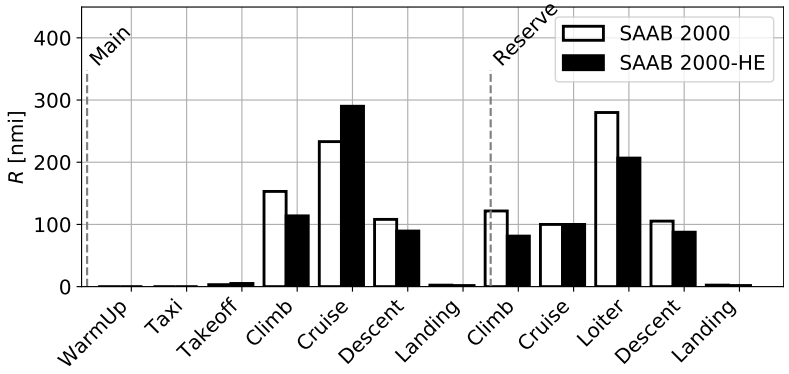

(a) R

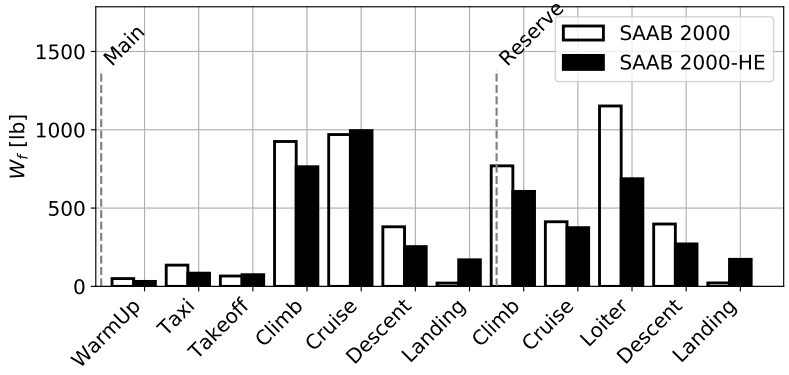

(b) W_f

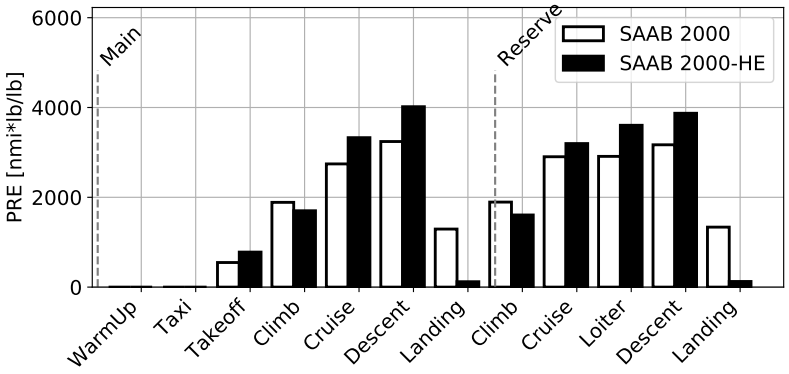

(c) PRE

Figure C.6: Comparison of SAAB 2000 aircraft configuration as a turboprop and hybrid electric propulsion by segment for key performance metrics.

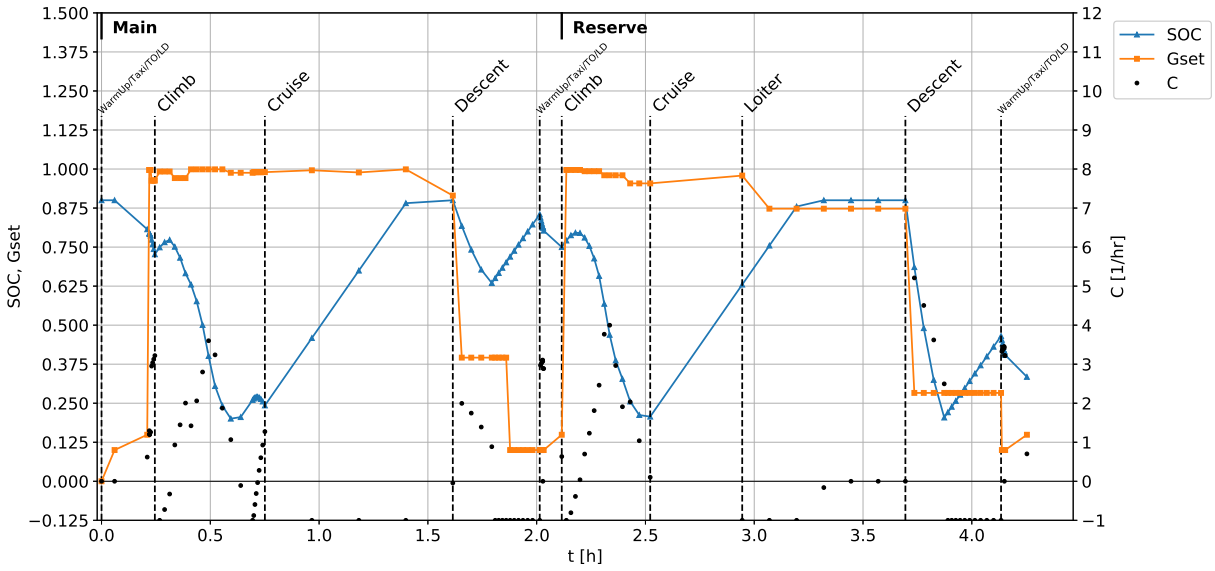

Figure C.7: HEAC power management solution

Table C.4: Next-Gen hybrid electric aircraft solution with generator redundancy

Variable	Value	Variable	Value	Variable	Value	Variable	Value
cap	71	$t_{i,w}$	0.15	$\Lambda_{LE,ht}$	14	P_{prop}	2928
$seats$	2+1	$\lambda_{o,w}$	0.47	Γ_{ht}	1.25	D_p	14.26
$wing\_loc$	High	$t_{o,w}$	0.13	VT_type	T-tail	$nEng$	2
$b_w/2$	41.2	Γ_w	1.67	$b_{vt}/2$	11.41	eng_{ia}	0.03
$\Lambda_{LE,w}$	11.1	x_w	0.43	$c_{r,vt}$	11.69	eng_{ta}	0.07
$c_{r,w}$	12	$b_{ht}/2$	11.95	λ_{vt}	0.7	M_{cruise}	0.52
b_{crank}	0.32	$c_{r,ht}$	6.94	$\Lambda_{LE,vt}$	32.59	h_{cruise}	22 000
$\lambda_{i,w}$	0.76	λ_{ht}	0.62	MLG	Fuselage	V_{climb}	183
P_{gen}	4135	n	115	m	119		

C.4 Final Results Table

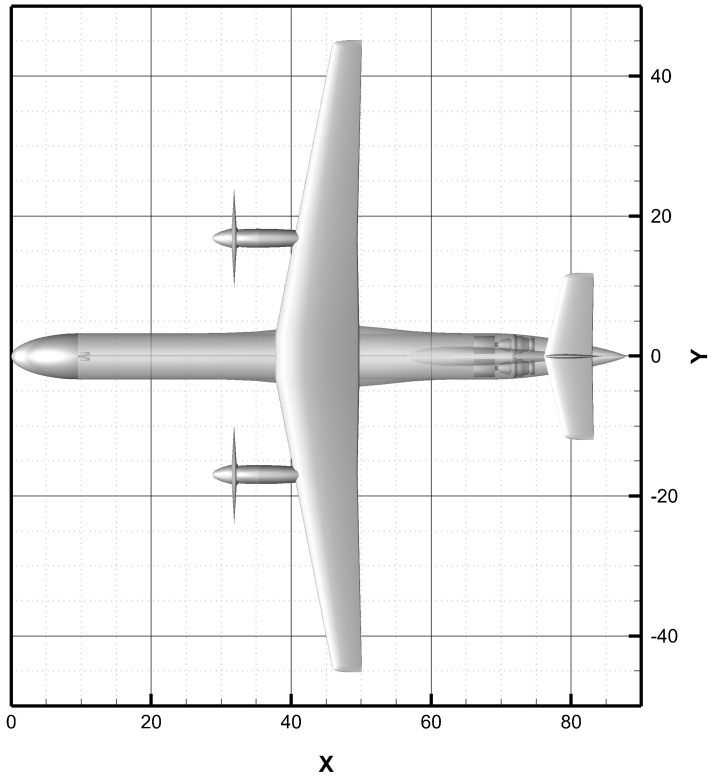

(a)

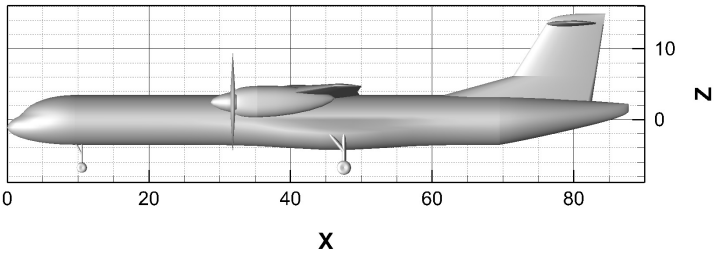

(b)

Figure C.8: Hybrid electric aircraft with redundant generators geometry.

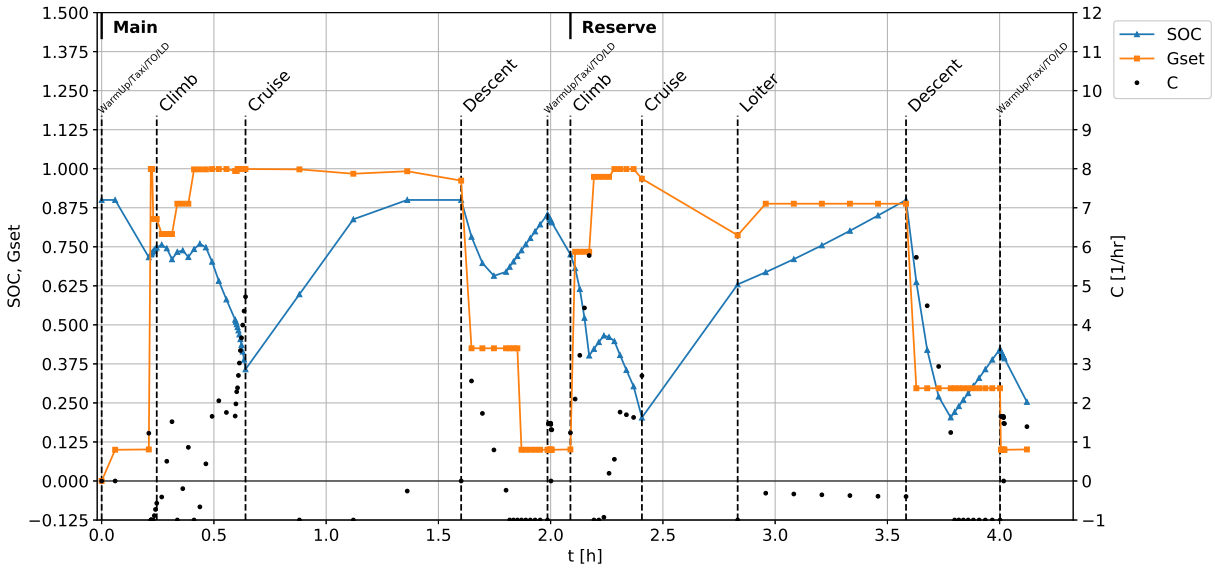

Figure C.9: HEAC-RG power management solution

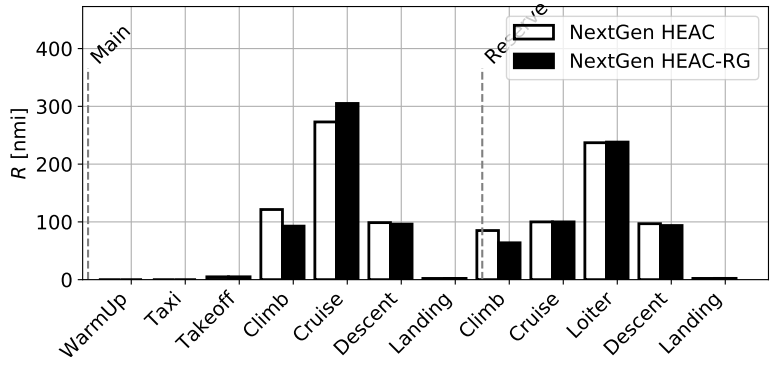

(a) R

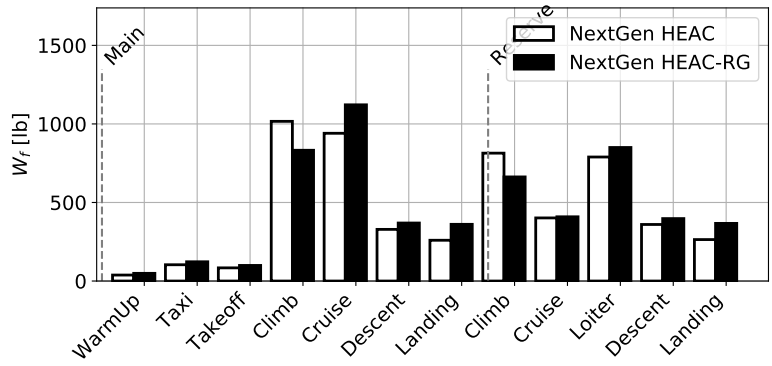

(b) W_f

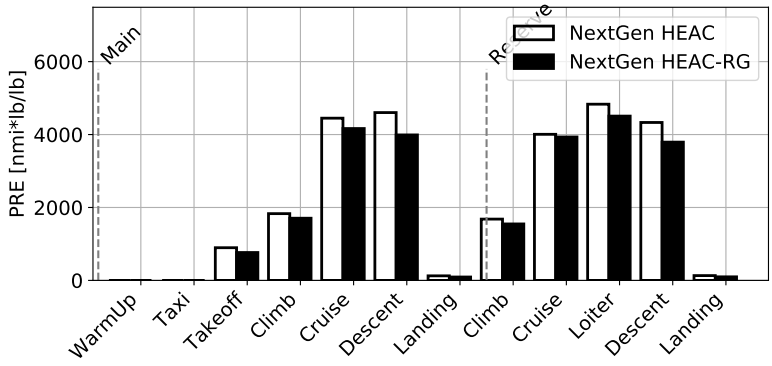

(c) PRE

Figure C.10: Comparison of hybrid electric aircraft solutions with and without redundant generators by segment for key performance metrics.

Figure C.11: Overview of regional aircraft solutions.

	ATR 72-600	DHC-8 Q400	SAAB 2000	NG-TP[1,2]	ATR-HE[3]	Q400-HE	SAAB 2000-HE	NG-HE	NG-HERG[3]
$MTOW$ [lb]	52 168	61 628	44 609	63 542	57 582	69 645	44 274	57 425	58 464
OEW [lb]	30 566	36 550	27 029	37 676	35 987	43 919	27 578	35 376	36 440
Seats	72	78	53	90	72	78	53	71	71
W_{pay} [lb]	15 768	17 492	11 981	20 273	15 777	17 502	11 987	16 057	16 082
W_f [lb]	5 834	7 586	5 599	5 594	5 817	8 224	4 710	5 992	5 941
PRE [nmi×lb/lb]	2 625	2 315	2 283	3 695	2 583	2 049	2 477	2 641	2 666
W/S [lb/ft^2]	79.46	92.17	81.27	81.54	87.72	104.15	80.66	78.43	79.68
P_{prop}[5][shp]	5 500	10 200	8 304	7 580	6 450	9 996	4 138	5 544	5 857
P_{prop}/W [shp/lb]	0.11	0.17	0.19	0.12	0.11	0.14	0.09	0.10	0.10
P_{gen} [shp]	5 500	10 200	8 304	7 580	6 708	9 746	5 106	6 124	8 270
P_{gen}/W [shp/lb]	0.11	0.17	0.19	0.12	0.12	0.14	0.12	0.11	0.14
n	N/A	N/A	N/A	N/A	84	197	103	120	115
m	N/A	N/A	N/A	N/A	154	103	113	103	119
Total cells	N/A	N/A	N/A	N/A	12 936	20 291	11 639	12 360	13 685
V_{climb}	170	230	210	177	181.1	200	173.5	180	183
M_{cruise}	0.45	0.52	0.62	0.45	0.45	0.46	0.455	0.52	0.52
h_{cruise}	15 000	20 000	26 000	26 000	18 000	21 000	23 000	25 000	22 000
t [hr]	2.27	1.87	1.85	2.33	2.23	2.17	2.31	2.07	2.09

[1] NG=Next-Gen/Clean Sheet Design.
[2] TP=Turboprop.
[3] HE=Hybrid Electric.
[4] RG=Redundant Generators.
[5] Sum of 2 propulsors for all aircraft.